The Dissertation Committee for Ahmet Yigit Ozcelik Certifies that this is the approved version of the following dissertation:

SEISMIC BEHAVIOR AND DESIGN OF STEEL PLATE SHEAR WALLS WITH BEAM-CONNECTED PLATES

Committee:

Patricia M. Clayton, Supervisor

Michael D. Engelhardt

Todd A. Helwig

Cem Topkaya

Eric B. Williamson

SEISMIC BEHAVIOR AND DESIGN OF STEEL PLATE SHEAR WALLS WITH BEAM-CONNECTED PLATES

by

Ahmet Yigit Ozcelik, B.S., M.S.

Dissertation

Presented to the Faculty of the Graduate School of

The University of Texas at Austin

in Partial Fulfillment

of the Requirements

for the Degree of

Doctor of Philosophy

The University of Texas at Austin

May 2017

Dedication

babama...

Acknowledgements

I would like to express my appreciation to my supervisor Dr. Patricia M. Clayton for her effort and patience throughout this study. Further thanks go to Drs. Michael D. Engelhardt, Todd A. Helwig, Cem Topkaya, and Eric B. Williamson for serving on my dissertation committee.

The scholarship provided by the Fulbright Foreign Student Program is gratefully acknowledged.

I am thankful to my family and my friends back home for their never-ending love and unconditional support.

SEISMIC BEHAVIOR AND DESIGN OF STEEL PLATE SHEAR WALLS WITH BEAM-CONNECTED PLATES

Ahmet Yigit Ozcelik, Ph.D.

The University of Texas at Austin, 2017

Supervisor: Patricia M. Clayton

Steel plate shear walls (SPSW) are a reliable lateral force-resisting system with high ductility, stable hysteretic response, and high lateral stiffness. The main lateral force-resisting elements of a SPSW are thin steel infill plates (web plates) that are connected to columns and beams on four edges. Due to a mechanism called tension field action, web plates pull in columns and induce significant flexural demands in columns when the system undergoes a lateral sway. Steel plate shear walls with beam-connected web plates (B-SPSW) are an alternative configuration to conventional SPSWs where columns are detached from web plates to eliminate column flexural demands resulting from tension field action. Due to the difference in the boundary conditions of web plates, the behavior of B-SPSWs is different than conventional SPSWs.

A three-phase numerical study has been undertaken to investigate the seismic behavior of B-SPSWs. In the first phase, a parametric study was conducted to characterize beam-connected web plate behavior using validated finite element models and a simplified model was proposed to simulate cyclic behavior of beam-connected web plates under lateral loading. In the second phase, web plate and beam design equations were proposed and eighteen B-SPSWs possessing different geometric characteristics were designed for a low-seismic site using these equations. The B-SPSWs were subjected

to ground motions to assess their seismic performance. The results of the proof-of-concept study indicated that B-SPSWs would be an attractive alternative lateral force-resisting system for low- and moderate-seismic regions. The third phase focused on the behavior of B-SPSW columns. The columns of the B-SPSWs considered in the second phase of the study were remodeled adopting more sophisticated modeling techniques to study the column behavior in detail. The results indicated that column flexural demands resulting from column rotations at floor levels due to differential interstory drifts caused column stability problems for some cases even if the axial load demands were below the design axial loads. Then a parametric study was conducted on isolated columns to quantify the effect of these flexural demands on column buckling strength. An empirical equation was proposed to estimate the reduction in the column buckling strength due to the moment demands associated with differential lateral drifts that are not considered in the design stage.

Table of Contents

List of Tables

List of Figures

Chapter 1: Introduction

1.1 BACKGROUND

Steel plate shear walls (SPSWs) are recognized as an efficient lateral-force resisting system owing to their high lateral stiffness, stable hysteresis characteristics, and high ductility. The lateral resistance of SPSWs mainly stems from infill plates called web plates that are typically connected to surrounding boundary frames (i.e., beams and columns) on all four sides. An example of a SPSW is given in Figure 1.

In earlier designs, web plates were proportioned to avoid shear buckling when SPSWs were loaded laterally, which required thick web plates or use of stiffeners. More recent studies revealed that unstiffened, thin web plates have a substantial lateral stiffness, strength, and ductility after shear buckling due to a mechanism called tension field action (TFA) provided that surrounding boundary frames have sufficient stiffness and strength to anchor the inclined pull-in web plate forces resulting from TFA.

Figure 1. A typical SPSW (Courtesy of Louis Crepeau and Jean-Benoit Ducharme, Groupe Teknika, Montreal, Canada)

The contribution of TFA to the shear strength of the web plate is dependent on the boundary conditions of web plates. When, web plates are connected to beams and columns on all four edges (i.e., fully-connected web plate), the entire web plate is engaged in TFA and contributes to the shear strength of the web plate (i.e., full TFA). A test photo of a fully-connected web plate is given in Figure 2. When web plates are connected to beams only and the columns are released from web plates (i.e., beam-connected web plate), the columns do not anchor the inclined tensile forces of TFA. Hence, a partial TFA (PTF) forms over some portion of the web plate between the beams. The portion of the web plate within the PTF contributes to the shear strength of the web plate, whereas the remaining portion of the web plate provides no contribution to the shear strength of the web plate. A test photo of a beam-connected web plate is given in Figure 3. Note that fully-connected web plates are adopted for conventional SPSWs.

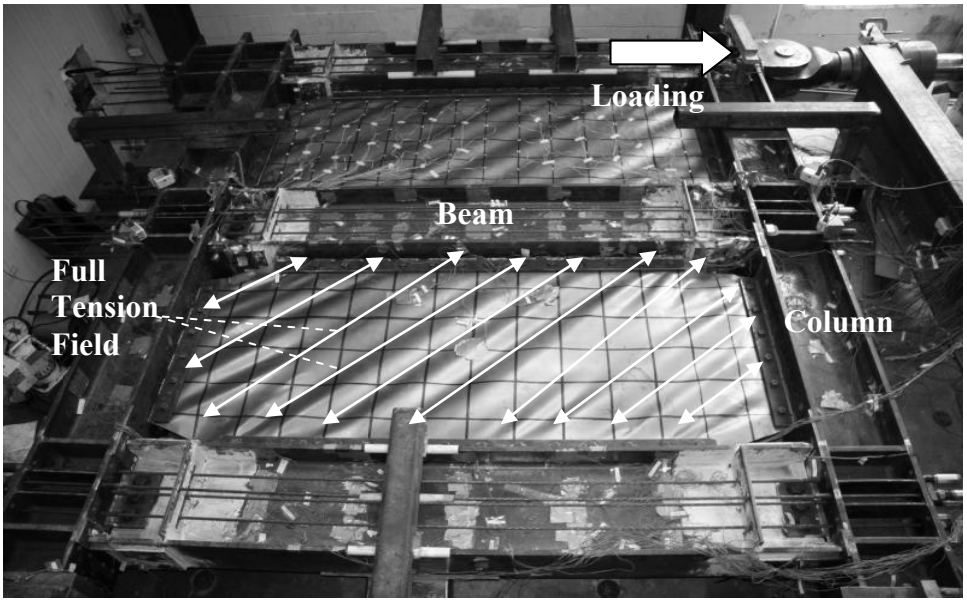

Figure 2. Full tension field (Clayton et al. 2013)

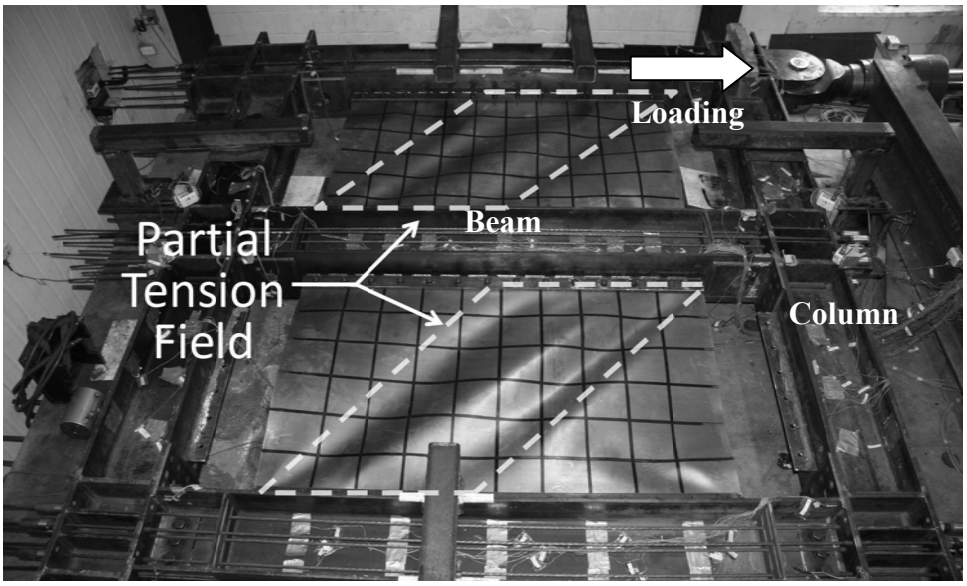

Figure 3. Partial tension field (Clayton et al. 2015)

Owing to the high lateral strength and stiffness of thin web plates resulting from the TFA, SPSWs provide many advantages over other lateral-force resisting systems that can be listed as follow (Sabelli and Bruneau 2012): (1) Thin webs plates provide more architectural flexibility compared to reinforced concrete shear walls. (2) With the same or less plan area dedicated for braced frames, comparable strength and stiffness can be provided. Despite these advantages over other lateral-force resisting systems, use of SPSWs is limited to high-seismic regions since the *AISC Seismic Provisions* (AISC 341-10) (AISC 2010a) cover only special SPSWs that are suitable for high-seismic applications. Their use in low- and moderate-seismic regions is not common in practice due to several factors such as stringent detailing and capacity design requirements given for special SPSWs in AISC 341-10 (AISC 2010a) that make SPSWs uneconomical compared to other systems that are particularly proposed for regions with low seismicity such as ordinary concentrically braced frames and ordinary moment frames.

The Canadian provisions CSA S16-09 (CAN/CSA 2009) provide a limited-ductility SPSW option (Type LD) with relaxed ductility requirements compared to high-ductile SPSW option (Type D) that is equivalent to special SPSWs given in AISC 341-10 (AISC 2010a). Type LD SPSWs are required to have fully-connected web plates similar to Type D and special SPSWs. As opposed to Type D and special SPSWs that have moment-resisting beam-column connections, use of simple beam-column connections instead of moment-resisting beam-column connections is permitted for Type LD SPSWs (CAN/CSA 2009).

There is an alternative SPSW configuration in literature called SPSWs with beam-connected web plates and simple beam-column connections (B-SPSWs). The web plate behavior and member demands of B-SPSWs (Figure 4) are different than the web plate behavior and member demands of conventional SPSWs (Figure 5) due to the differences in the boundary conditions of web plates and beam-column connection types. The columns of conventional SPSWs resist significant flexural demands due to both TFA and moment frame action (Figure 5(b)). These flexural demands, when combined with the axial demands, might lead to substantial column sections (Berman 2011; Gholipour and Alinia 2016). The columns of B-SPSWs primarily resist axial loads owing to the elimination of inclined web plate tension forces acting on the columns and the lack of moment frame action (Figure 4(a)); as a result, B-SPSW columns are expected to be smaller compared to comparable SPSWs with fully-connected web plates. Similarly, connecting the web plates to beams only results in a reduction in required field welding compared to fully-connected web plates, and adopting simple beam-column connections eliminates the costly detailing requirements for full moment-resisting connections, which may make B-SPSWs more cost-effective in certain applications. On the other hand, the redundancy in B-SPSWs is reduced compared to conventional SPSWs due to the lack of

moment frame action which might limit the use of B-SPSWs in high-seismic regions. Hence, B-SPSWs are proposed as a viable and competitive lateral-force resisting system option for applications in regions with low and moderate seismicity.

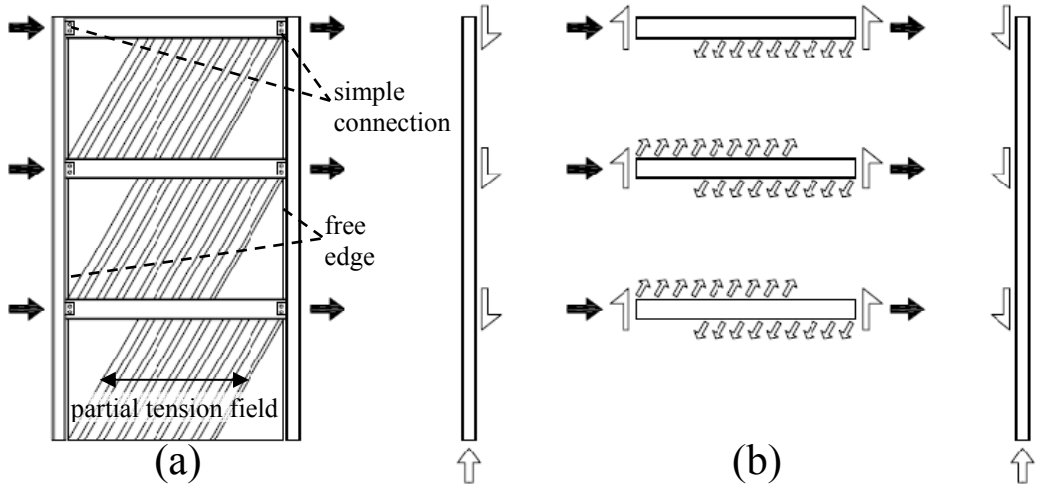

Figure 4. Schematic view of a three-story B-SPSW: (a) formation of partial tension field and (b) free-body diagrams of the beams and columns

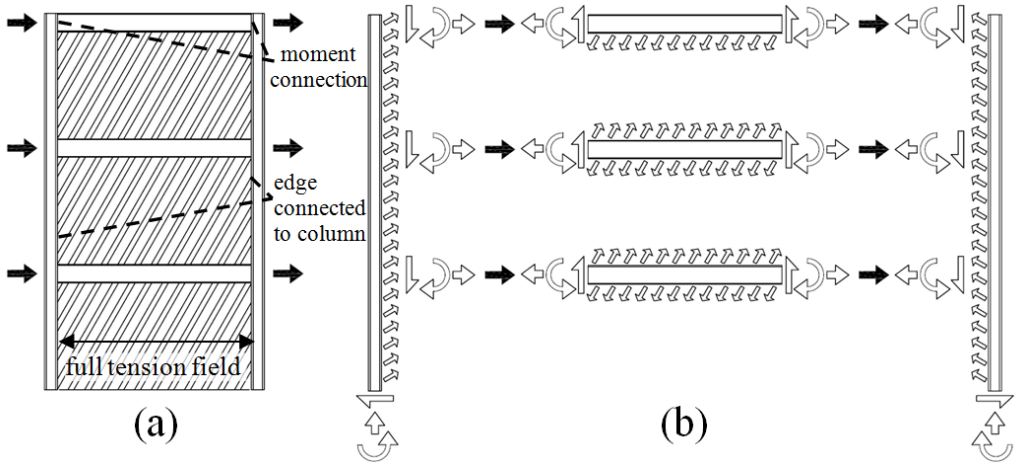

Figure 5. Schematic view of a three-story conventional SPSW: (a) formation of full tension field and (b) free-body diagrams of the beams and columns

1.2 RESEARCH OBJECTIVES

As discussed in Chapter 1.1, the behaviors of fully-connected and beam-connected web plates are different due to the difference in the boundary conditions of the web plates along the web plate-column interface; consequently, the system behaviors of conventional SPSWs and B-SPSWs differ. Previous research has mainly focused on conventional SPSWs, and there has been little work done on B-SPSWs. This research focuses on the seismic behavior and design of B-SPSWs in low-seismic regions. To assess the viability and applicability of B-SPSWs as an efficient lateral-force resisting system in low- and moderate-seismic regions, the main objectives of the proof-of-concept research are determined as follow:

- to characterize beam-connected web plate behavior under lateral loads for a range of web plate aspect ratios and slenderness ratios using validated numerical analyses.
- to develop a simple numerical model for beam-connected web plates that accurately captures the web plate shear strength, stiffness, energy dissipation, and beam and column demands.
- to outline a design procedure for the design of B-SPSWs.
- to evaluate the seismic performance of B-SPSWs using numerical analyses.

1.3 ORGANIZATION OF DISSERTATION

In *Chapter 1*: Introduction, an introduction to the basics of the system and the research objectives have been presented. A literature review of relevant research on B-SPSWs is presented in *Chapter 2*: Literature Review. In *Chapter 3*: Executive Summary and Conclusions, an overview of three journal manuscripts accepted and/or submitted for publication is presented and a summary of the key findings is discussed. In *Appendix A*, the article "Strip model for steel plate shear walls with beam-connected web plates"

investigates the behavior of beam-connected web plates and proposes a simple numerical model for beam-connected web plates. In *Appendix B*, the article "Seismic design and performance of SPSWs with beam-connected web plates" provides equations for the member design of B-SPSWs and evaluates the seismic performance of B-SPSWs designed for a low-seismic site. In *Appendix C*, the article "Behavior of columns of SPSWs with beam-connected web plates" evaluates the stability of B-SPSWs columns under earthquake loads.

Chapter 2: Literature Review

In this chapter, past research on steel plate shear walls with simple beam-connections, steel plate shear walls with beam-connected web plates, modeling of web plates is discussed[1].

2.1 STEEL PLATE SHEAR WALLS WITH SIMPLE BEAM-COLUMN CONNECTIONS

Caccese, Elgaaly, and Chen - 1993

The cyclic tests of one-quarter scale, three-story SPSW specimens investigated the effects of beam-to-column connection and web plate thickness. The six specimens tested include a moment-resisting frame (i.e., bare frame with no web plate), three specimens with moment-resisting beam-column connections (Type 1) and varying web plate thickness, and two specimens with simple beam-column connections and varying web plate thicknesses (Type 2). ASTM A36 steel (nominal yield strength of 248 MPa) was used for beams and columns. The details of the SPSW specimens and the elevation view are given in Table 1 and Figure 6, respectively, where F_y is the yield strength of the web plate material.

Table 1. Details of SPSW specimens

Specimen Name	Plate thickness (mm)	F_y (MPa)	Beam-column connection
F0 (bare frame)	N/A	N/A	Type 1 (moment-resisting)
M22	0.76 (22 Gage)	306	Type 1 (moment-resisting)
M14	1.90 (14 Gage)	291	Type 1 (moment-resisting)
M12	2.66 (12 Gage)	295	Type 1 (moment-resisting)

[1] In Chapter 2, all figures are adapted from cited studies (except for Figure 15)

S22	0.76 (22 Gage)	256	Type 2 (simple)
S14	1.90 (14 Gage)	332	Type 2 (simple)

The cyclic displacement history consisted of displacement peaks that were increased in eight increments (0.25% drift per increment) until reaching a 2% drift. Each cycle was repeated three times; consequently, a total of 24 cycles was considered. After reaching the 2% drift, the specimens were pulled monotonically to the displacement limit of the actuator. The hysteretic response of each specimen is given in Figure 7.

The authors concluded that the influence of the beam-column connection type on the lateral response of SPSWs is minor. This results was attributed to the fact that simple beam-column connections acted as moment-resisting beam-column connections when the web plates were continuously connected to beams and columns due to the restraint to connection rotation provided by the web plate in the immediate vicinity of the connection.

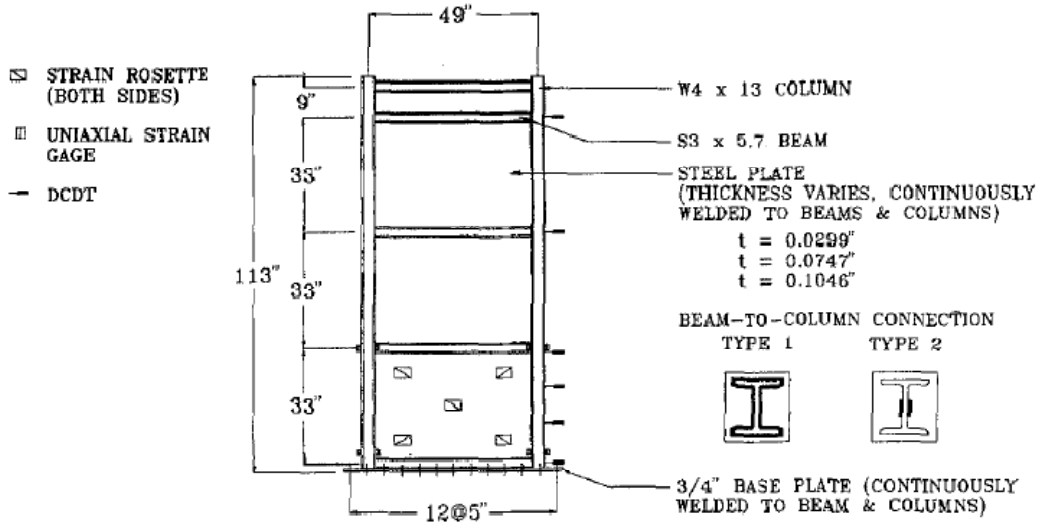

Figure 6. Elevation view of the SPSW specimen

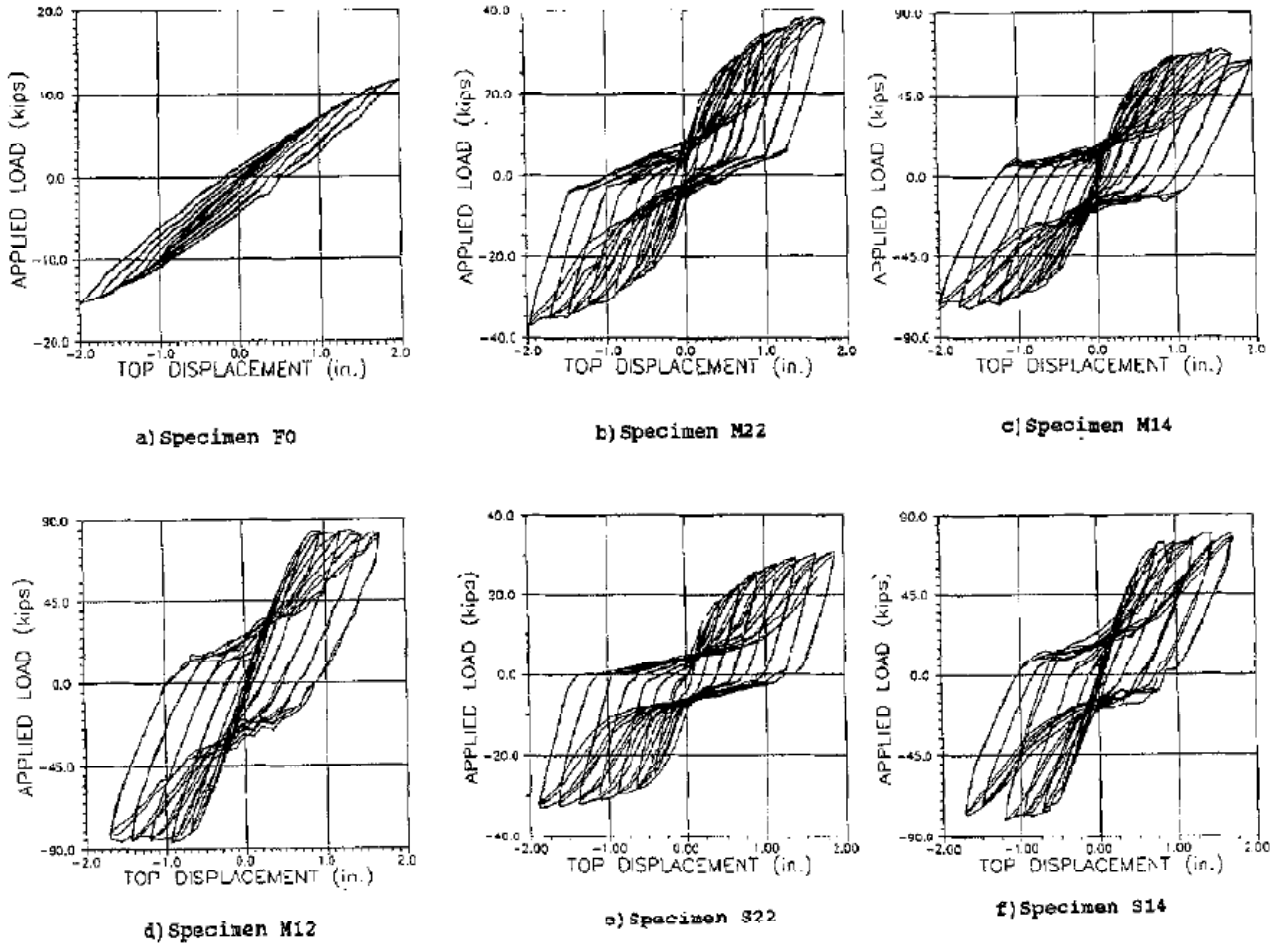

Figure 7. Hysteretic responses of the specimens: (a) F0, (b) M22, (c) M14, (d) M12, (e) S22, and (f) S14

Chen and Jhang - 2011

Under cyclic loading, two one-third scale two-story SPSW specimens with low-yield-point (LYP) steel web plates were tested. The LYP-100 steel was used for web plates while ASTM A572 Gr.50 steel was selected for beams and columns. The stress-strain diagrams of both materials are given in Figure 8. Stiffeners were added to the web plates in both horizontal and vertical directions. To examine the effect of the beam-column connection type on the lateral response of SPSWs, moment-resisting beam-column connections were adopted for one specimen (Specimen No.5) and simple beam-column connections were adopted for the other specimen (Specimen No.6). The details of the SPSW specimens and the elevation view are given in Table 2 and Figure 9, respectively.

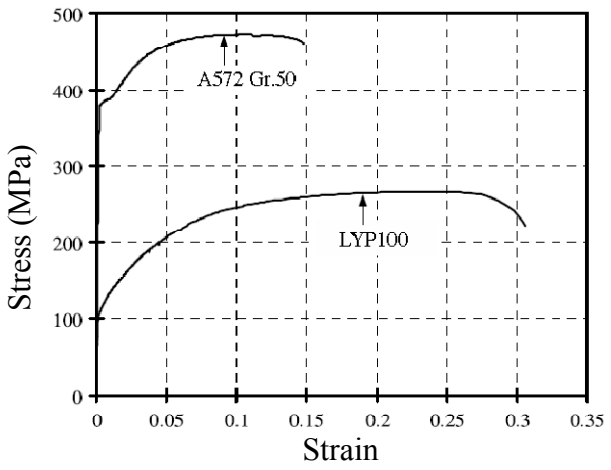

Figure 8. Stress-strain diagrams of LYP-100 and A572 Gr. 50

Table 2. Details of SPSW specimens

Specimen Name	Plate thickness (mm)	Beam	Column	Beam-column connection
No.5	3.5	H250x125x6x9	H250x125x9x14	Moment-resisting
No.6	3.5	H250x125x6x9	H250x125x9x14	Simple

A total of 24 cycles of lateral load was applied to each specimen until reaching a drift ratio of 6.0%. The hysteretic response and the deformed shape at 6% drift of each specimen are given in Figure 10 and Figure 11, respectively. The results of the experimental study suggested SPSWs with LYP steel provided good seismic resistance regardless of the beam-column connection type; however, the specimen with moment-resisting beam-column connections (No.5) had a 28% higher lateral strength and an 18% higher energy dissipation capacity compared to the specimen with simple beam-column connections (No.6) due to moment-frame action.

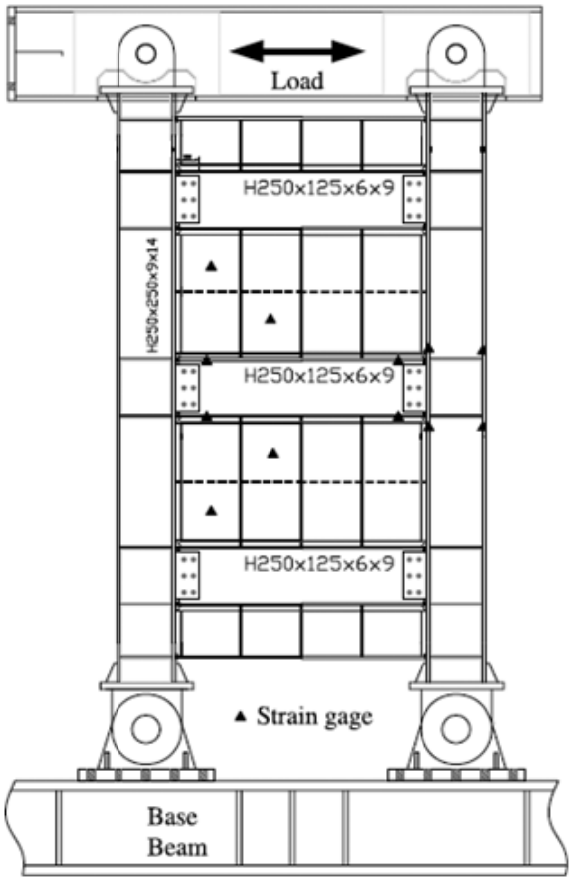

Figure 9. Elevation view of the SPSW specimen

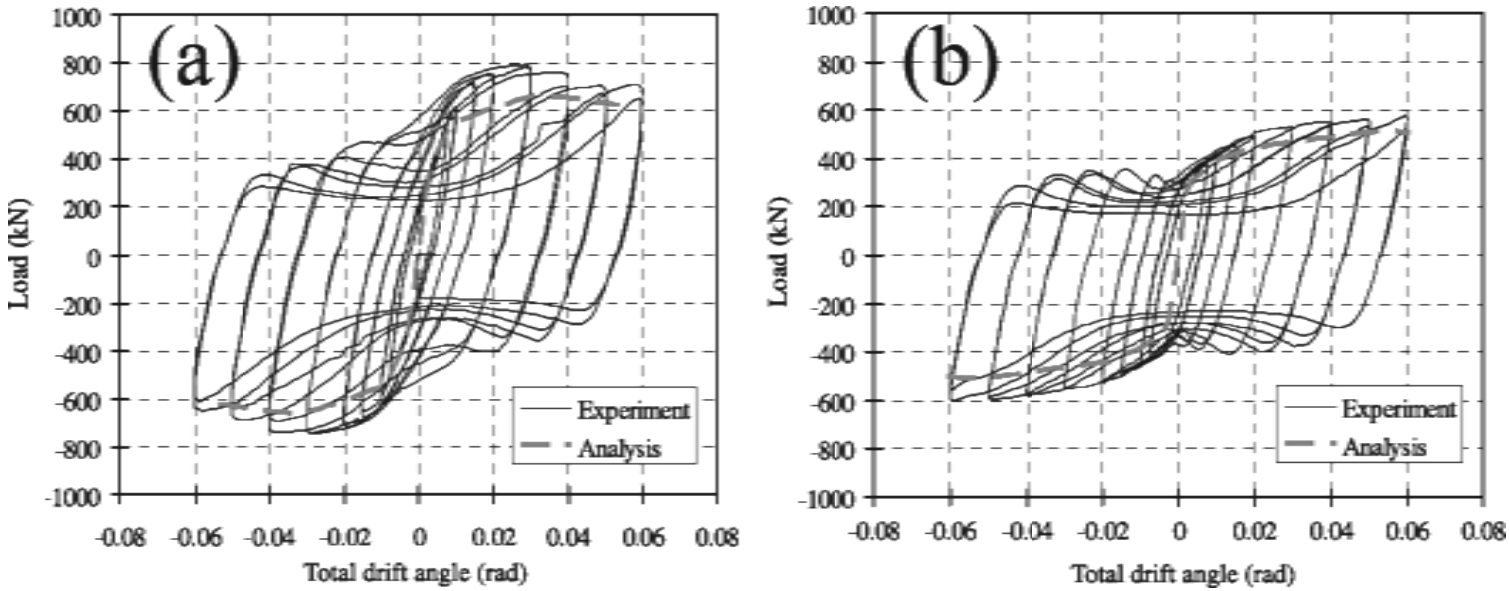

Figure 10. Hysteretic responses of the specimens: (a) No.5 and (b) No.6

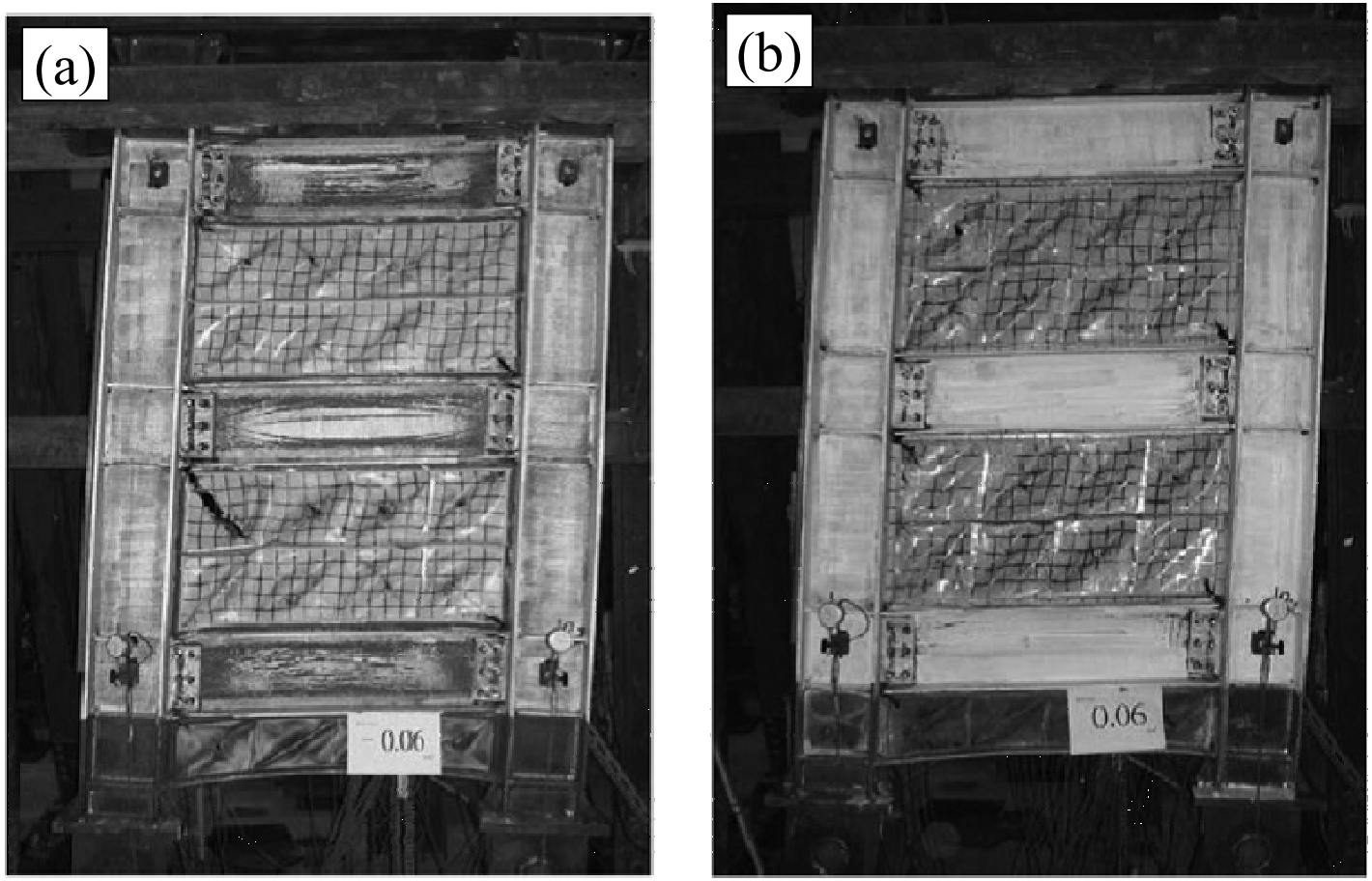

Figure 11. Deformation of specimens at 6% drift: (a) No.5 and (b) No.6

Moghimi and Driver - 2013

A half-scale two-story modular SPSW designed for low-seismic regions was tested under gravity and cyclic loads. In the modular SPSW system, the web plates of each story were divided in the two segments. The upper segment of the web plate was welded to the beam of the story above and the lower segment of the web plate was welded to the beam of the story below in the shop. The upper and lower half of the web plates were connected in the field at the mid-story height using bolts. Similarly, bolts were used for the web plate-column connections. Double-angle simple beam-column connections were used. The short legs of the angles were shop welded to the beam and the long legs were bolted to the columns. The elevation view of the specimen is given in Figure 12.

The loading history given by the Applied Technology Council (1992) was adopted. The specimen underwent a total of 25 cycles until reaching a roof drift ratio of 3.65%. The hysteretic responses of the modular specimen and the specimen tested earlier by Driver et al. (1997) that had moment-resisting beam-column connections are given in Figure 13.

The results suggested that although the modular test specimen had a lower elastic stiffness and lower yield strength compared to the Driver et al. (1997) specimen due to the effects of simple beam-column connections and geometrical differences, the modular test specimen demonstrated remarkably similar behavior in terms of overall ductility and robustness. The conventional double-angle shear connections (Figure 14) showed a good performance with no significant damage. The column demands were reduced due to the rotational freedom at the beam-column joints. The rotations at the beam-column joints improved the distribution of yielding in the web plates.

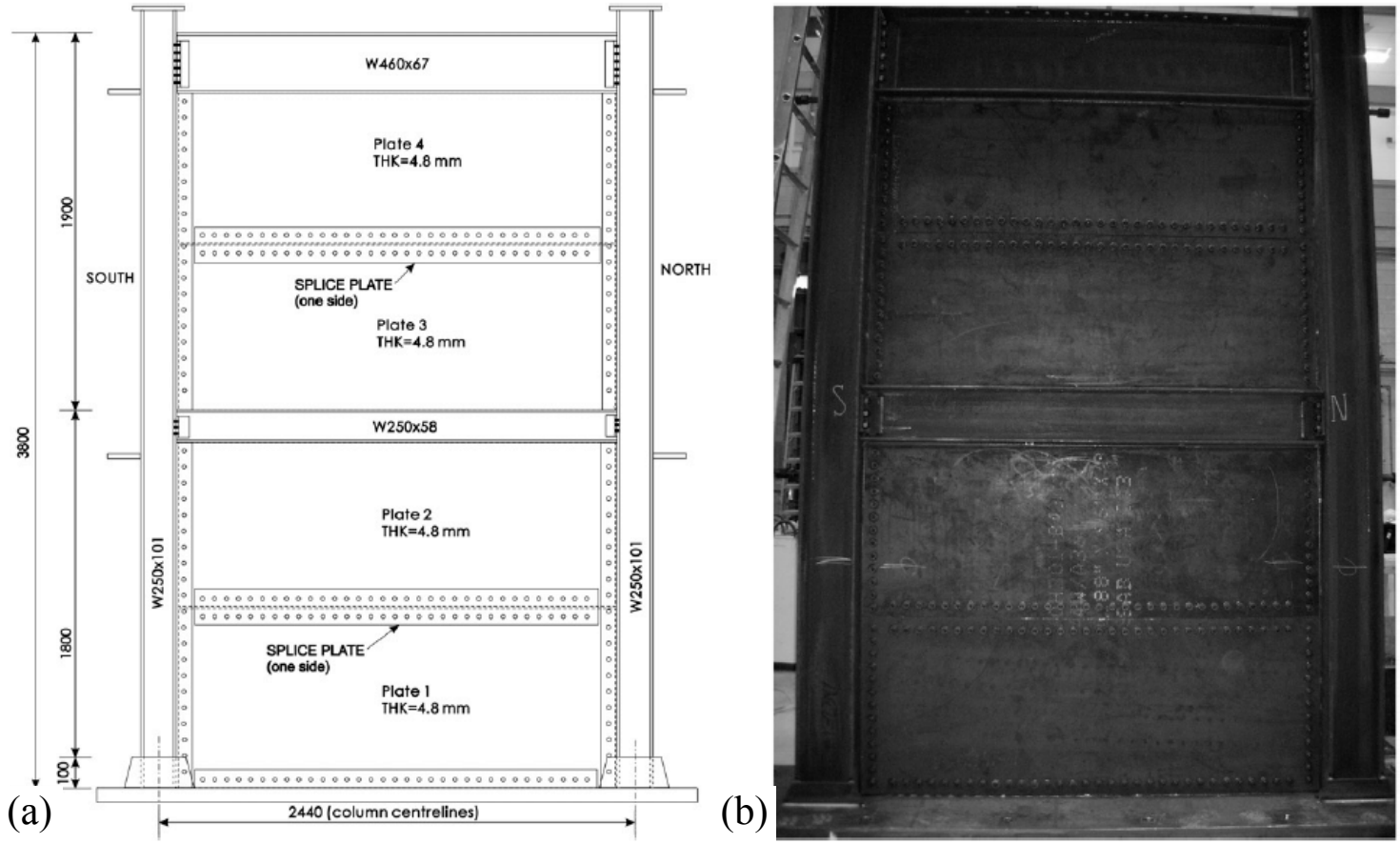

Figure 12. Test specimen: (a) schematic view and (b) elevation view

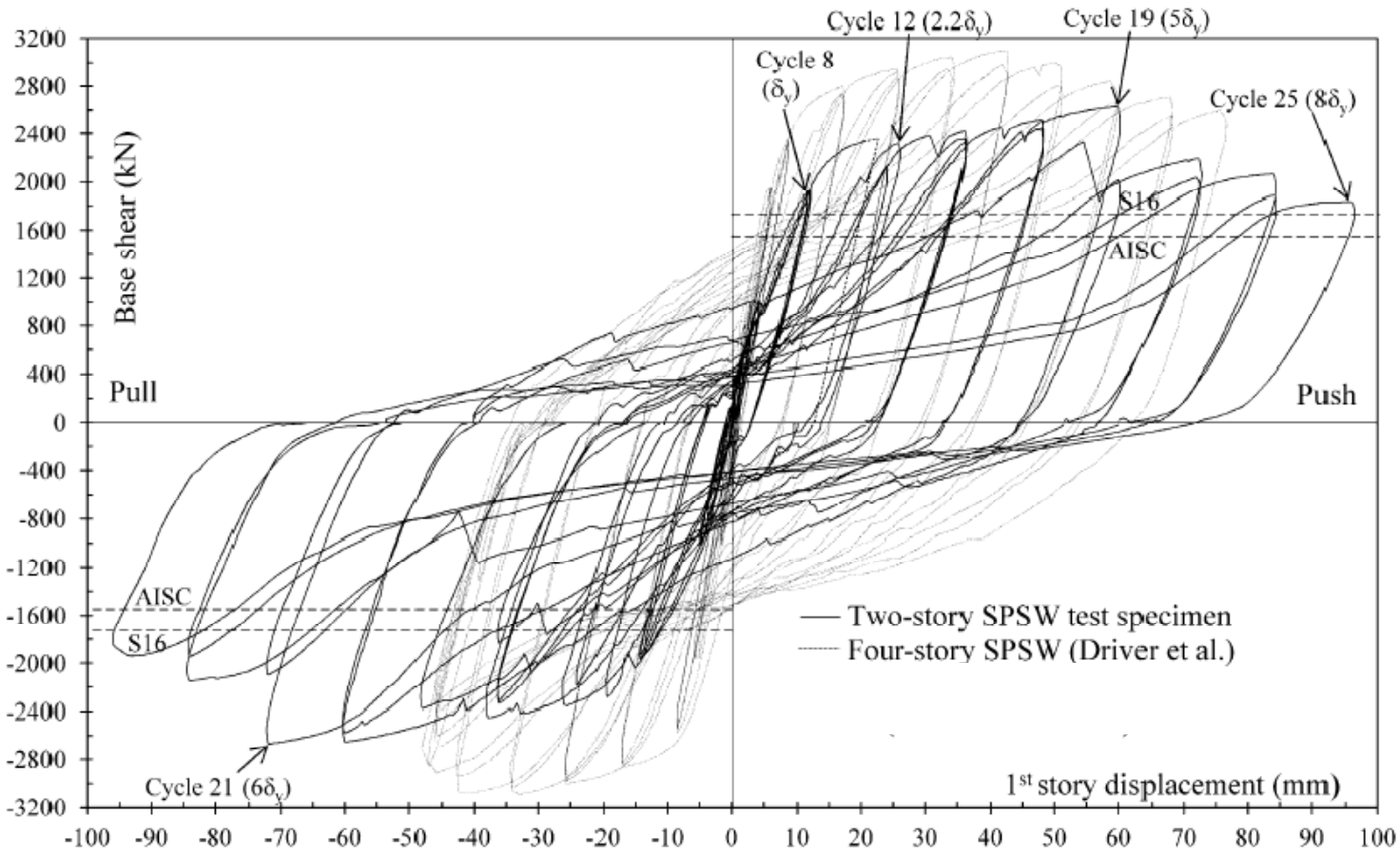

Figure 13. Hysteretic response of the specimen

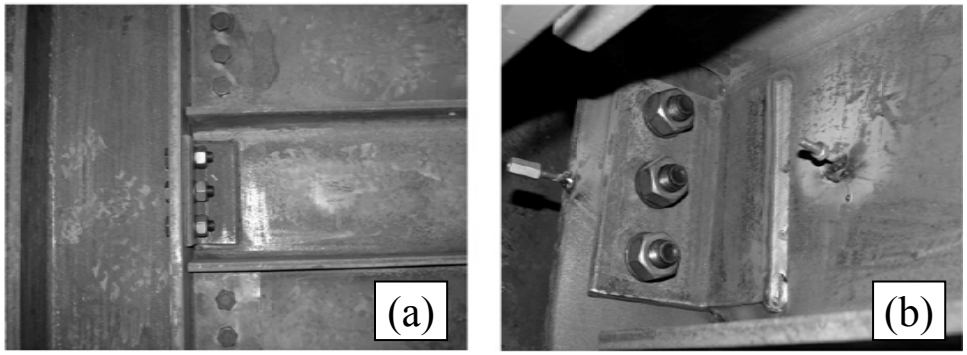

Figure 14. Double-angle beam-column connections: (a) before test and (b) after test

2.2 STEEL PLATE SHEAR WALLS WITH BEAM-CONNECTED WEB PLATES

Thorburn, Kulak, and Montgomery - 1983

An analytical study was conducted to understand the behavior of SPSWs with fully-connected thin web plates and the study was extended to SPSWs with infinitely flexible columns. As explained in Chapter 1.1, a partial tension field forms in web plates between adjacent floor beams when web plates are not anchored by the columns of SPSWs. Note that infinitely flexible columns do not provide restraint to the web plates and cannot anchor the web plate stresses resulting from tension field action. Hence, the idealized system investigated by Thorburn et al. (1983) showed a similar behavior to B-SPSWs.

Thorburn et al. (1983) proposed a simple web plate model where the web plate was represented by a series of evenly-spaced tension-only inclined strips that were connected to the beams over the length of the partial tension field. The model was dependent on one variable, which is the inclination angle of the partial tension field, θ (Figure 15). Assuming the partial tension field orients itself to resist the maximum lateral load and using virtual work methods, Eq. 1 was proposed for θ, where L and H are the length and height of the web plate, respectively:

$$\theta = 0.5 \tan^{-1}(L/H) \quad \text{(Eq. 1)}$$

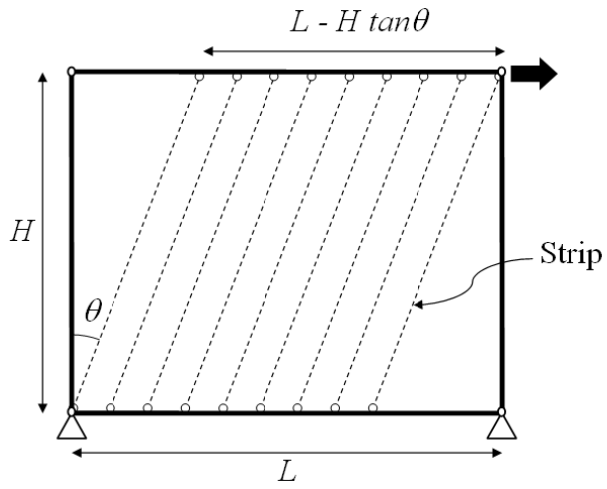

Figure 15. Strip model of SPSWs with infinitely flexible columns

Xue - 1995

A numerical study was undertaken to study the effects of web plate-boundary frame connection types (beam-connected or fully-connected web plates) and beam-column connection types (partial or full moment-resisting connections) on the behavior of SPSWs. A twelve-story SPSW with partial moment-resisting connections and beam (girder)-connected web plates (P-G) was designed for the specified gravity and lateral loads. The same member sizes were adopted for the other three SPSWs, namely, (1) the SPSW with partial moment-resisting beam-column connections and fully-connected (connected to girders and columns) web plates (P-GC), (2) the SPSW with full moment-resisting beam-column connections and fully (girder and column)-connected web plates (F-GC), and (3) the SPSW with full moment-resisting beam-column connections and beam (girder)-connected web plates (F-G). The elevation view of the SPSW and the member sizes are given in Figure 16.

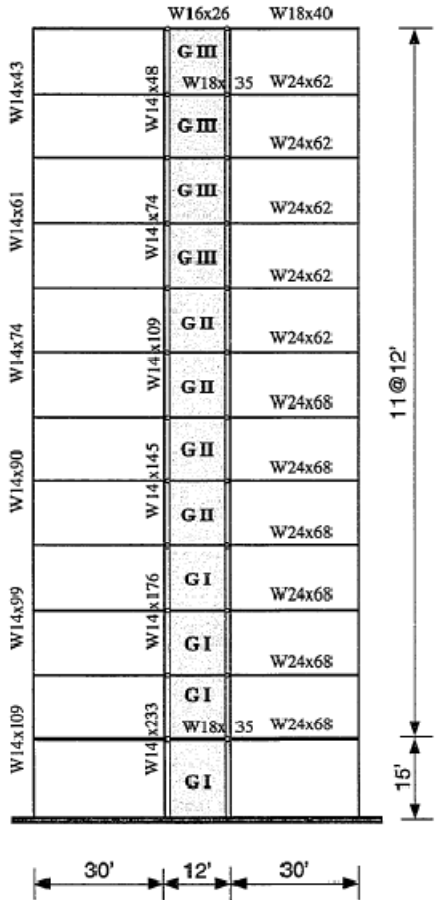

Figure 16. The elevation view of the SPSW

The analyses were conducted using a software called ADINA where web plates were modeled using shell elements and columns and beams were modeled using elastic frame elements. The responses of the SPSWs under monotonic loading suggested the following conclusions: (1) The web plates of the P-G system contributed to the lateral resistance earlier than other SPSWs with full moment-resisting connections and fully-connected web plates, which made the P-G system more desirable due to more effective utilization of the web plates and more favorable yielding sequence in the system. (2) The forces distribution in the P-G system was simpler, which made the P-G system more desirable in terms of design. (3) The F-G and P-G systems had a reduced initial lateral

stiffness compared to the F-GC and P-GC system; however, the difference was deemed acceptable.

In addition to the analysis of the twelve-story SPSWs, a parametric study was conducted to characterize the behavior of web plates in the P-G system. The following conclusions were drawn from the results of single-story P-G systems loaded monotonically: (1) The width-to-thickness ratio (L/t_w) of the web plate does not affect the post-buckling stiffness of the web plate. (2) The width-to-height ratio (L/H) of the web plate prominently affected the yield strength of the web plate. Similarly, it had an influence on the post-buckling stiffness. (3) The yield strength of unstiffened, beam-connected web plates, Q_{sy}, could be calculated using the following empirical equation, Eq. 2, where τ_y is the shear yield stress of the web plate:

$$Q_{sy} = 0.755\, L\, t_w \tau_y \left[1 - 0.3(L/H)^{-1.7L/H}\right] \quad \text{(Eq. 2)}$$

Guo et al. - 2011

Two one-third scale one-story SPSWs with beam-connected web plates and true-pin beam-column connections (S1 and S2) were tested under cyclic loading. To limit the out-of-plane deformations of the free edges of the web plates, the web plate of specimen S2 was reinforced with stiffeners along the free edges of the web plate. The details of the SPSWs and the elevation view of the test setup are given in Table 3 and Figure 17, respectively.

Table 3. Details of SPSW specimens

Specimen Name	**t_w (mm)**	**L (mm)**	**H (mm)**	**F_y (MPa)**	**Edge Stiffener**
S1	2.75	1100	1100	295	Without
S2	2.75	1100	1100	295	With

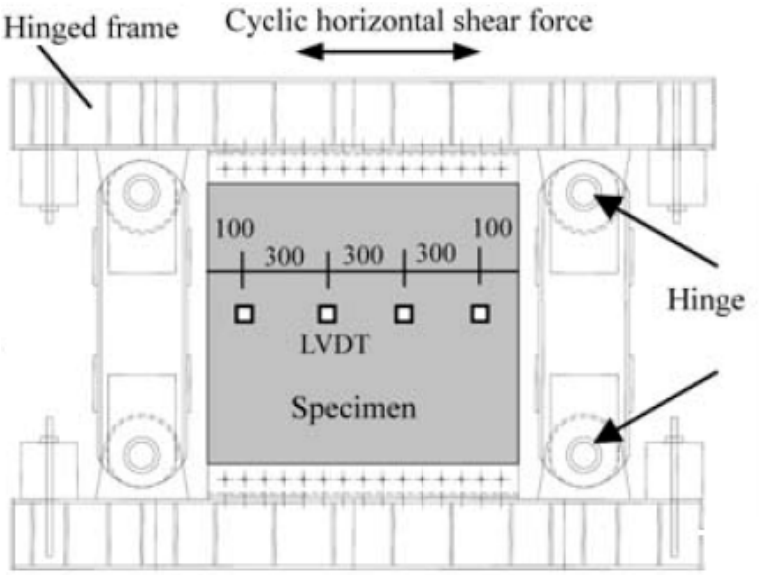

Figure 17. Experimental setup

The loading history given by the Chinese Code JGJ 100-96 (1996) was used for the test. The hysteretic behavior of the specimens and the analytical models are given in Figure 18.

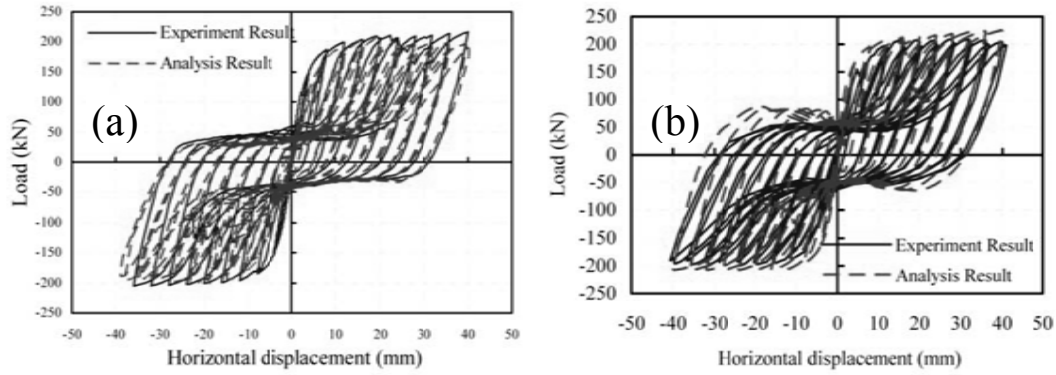

Figure 18. Hysteretic responses of the specimens: (a) S1 and (b) S2

The results suggested that both specimens (S1 and S2) showed a ductile and stable hysteretic behavior with a significant energy dissipation capacity; however, S2 had

a higher energy dissipation capacity due to the stiffeners provided along the free edges of the web plate.

In addition to the experimental study, a parametric study was conducted to investigate the effects of width-to-thickness ratio and width-to-height ratio on the cyclic behavior of beam-connected web plates. Based on the results of the parametric study, an empirical equation (Eq. 3) was proposed to estimate the ultimate lateral load carrying capacity of the beam-connected web plates, V_u.

$$V_u = L\, t_w \tau_y \left[0.23\, ln\left(\frac{L}{H}\right) - \, 0.13\, ln\left(\frac{H}{t_w}\right) + 1.22\right] \quad \text{(Eq. 3)}$$

Vatansever and Yardimci - 2011

Two one-third scale SPSWs with partial moment-resisting beam-column connections were tested under cyclic loads. One of the specimens (SW-A-H) had a fully-connected web plate where the other specimen (SW-B-H) had a beam-connected web plate. The details of the SPSWs and the elevation views of the specimens are given in Table 4 and Figure 19, respectively.

Table 4. Details of SPSW specimens

Specimen Name	**t_w (mm)**	**L (mm)**	**H (mm)**	**F_y (MPa)**	**Web Plate**
SW-A-H	0.50	1800	1200	198	Fully-connected
SW-B-H	0.50	1800	1200	179	Beam-connected

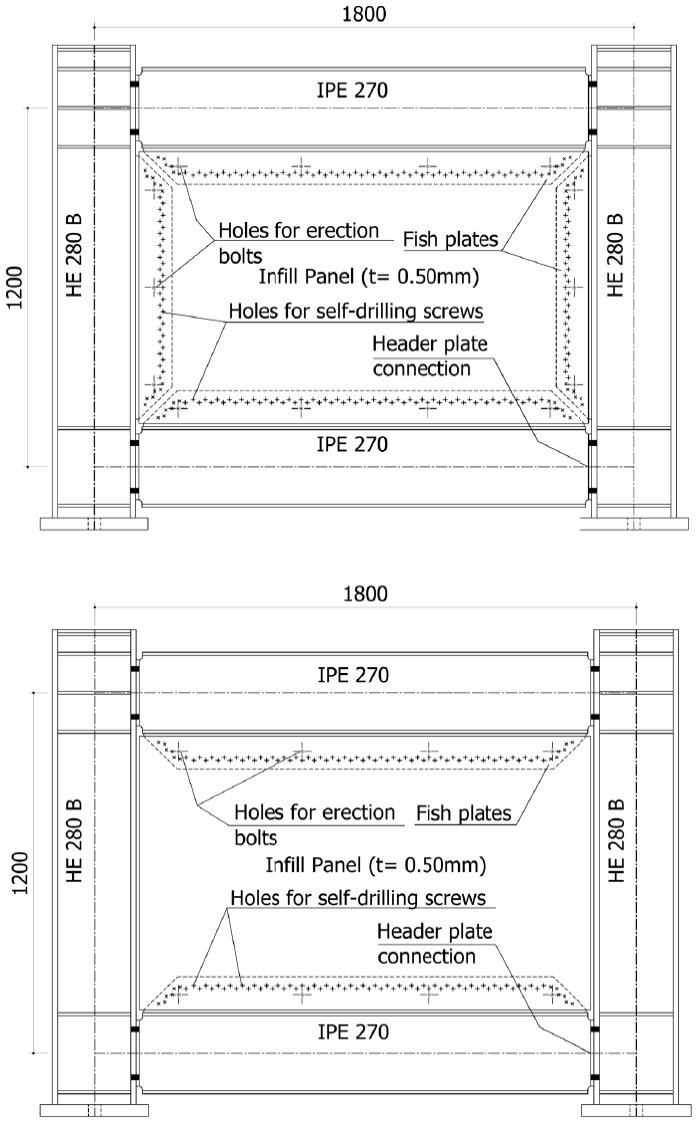

Figure 19. Test specimens: (a) SW-A-H and (b) SW-B-H

The loading history given by the Applied Technology Council (1992) was adopted. The SW-A-H was pushed laterally until 4% drift while the testing of the SW-B-H was terminated at 3% drift since fractures were observed in the corners of the web plate and further loading might have caused damage in the test equipment in case of a sudden failure. The cyclic responses of the specimens are given in Figure 20.

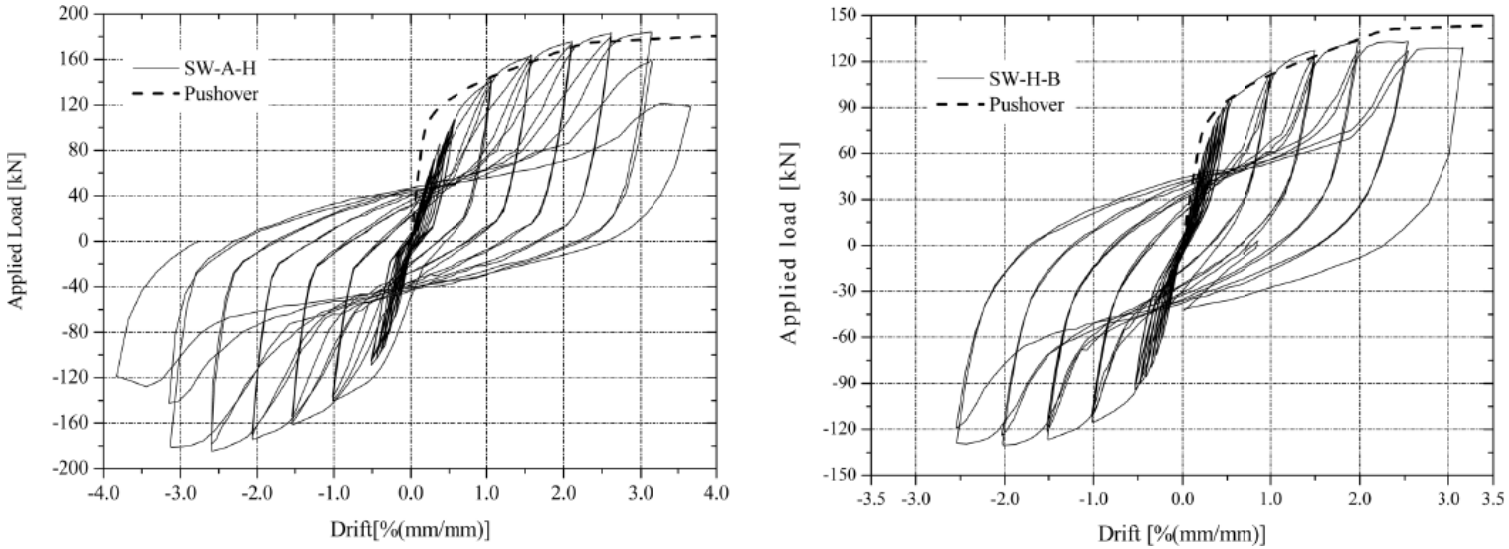

Figure 20. Hysteretic responses of the specimens: (a) SW-A-H and (b) SW-B-H

Based on the cyclic tests, it was concluded that the specimen SW-B-H had a lower energy dissipation capacity compared to the specimen SW-A-H; consequently, the authors suggested that use of beam-connected web plates would be a viable option for retrofitting of steel frames with inadequate lateral stiffness and strength.

Clayton - 2013

An experimental and numerical study was undertaken to assess the seismic performance of SPSWs with post-tensioned rocking beam-column connections. Under cyclic loads, fifteen half-scale, two-story specimens were tested, one of which had a beam-connected web plate. The details of the specimen with beam-connected web plates are given in Table 5.

Table 5. Details of SPSW with beam-connected specimen

Specimen Name	**L (mm)**	**H (mm)**	**t_w (mm)**	**F_y (MPa)**
W14-8s100k-16GaHBE	3235	1724	1.52 (1^{st} story)	235 (1^{st} story)
			1.52 (2^{nd} story)	181 (2^{nd} story)

The displacement history applied to the SPSW with beam-connected web plate (Figure 3) comprised two cycles at target peak drifts of 0.08%, 0.1%, 0.25%, 0.5%, 1%, 1.5%, 2%, 2.5%, 3%, 4%, 4.5% and 5%. The cyclic response of the specimen is given in Figure 21.

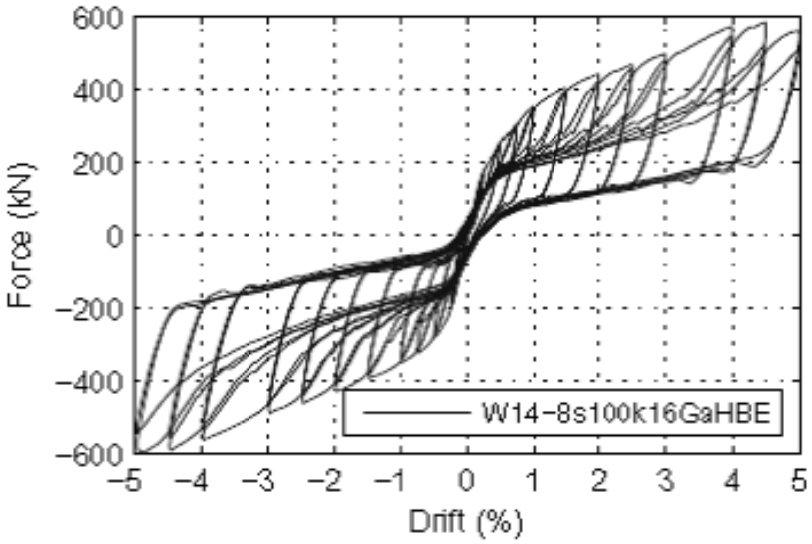

Figure 21. Hysteretic response of the specimen

The main purpose of adopting beam-connected web plates was to reduce strain demands at the corners of the web plates and to mitigate the web plate tearing resulting from the expansion associated with the opening and closing of the rocking beam-column connections; however, the results of SPSWs tests with fully-connected and beam-connected web plates revealed that beam-connected web plate led to a reduction in the overall steel weights in spite of the fact that thicker web plates were required for SPSWs with beam-connected web plates compared to SPSWs with fully-connected web plates since the partial tension field led to reduced web plate lateral strengths compared to full tension field. This reduction mainly stemmed from the significant reduction in column axial and flexural demands. For the analytical part of the study, several three- and nine-story SPSWs were designed adopting beam-connected web plates that had the same lateral strengths as the SPSWs with fully-connected web plates. A comparison of column demands for the three-story SPSWs with fully-connected web plates and beam-connected web plates designed for the same lateral load demand is given in Figure 22. As can be

seen from Figure 22, column demands were significantly lower for SPSWs with beam-connected web plates.

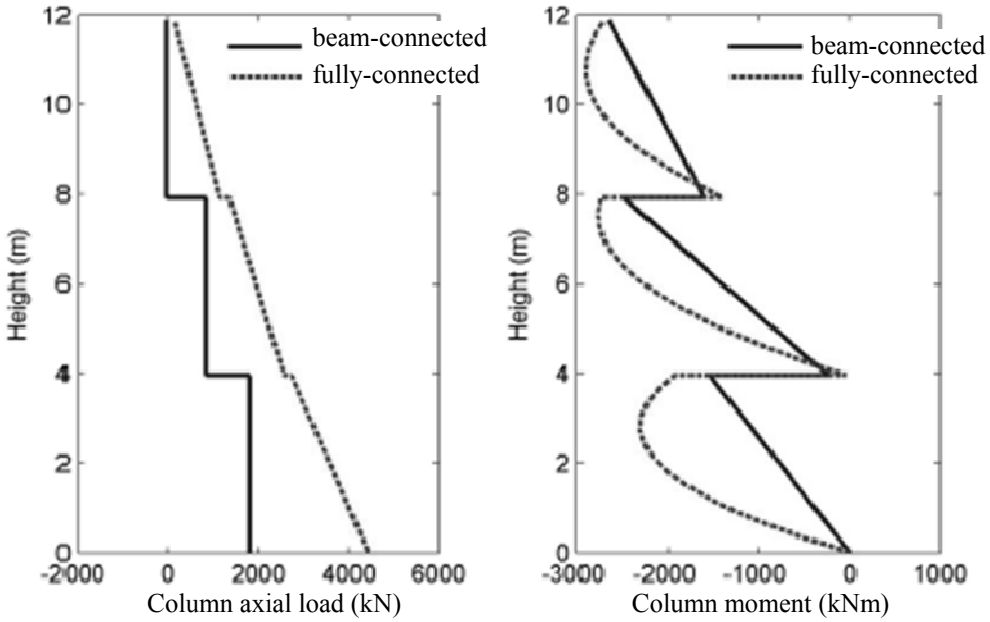

Figure 22. Comparison of column demands for beam-connected and fully-connected web plates

2.3 MODELING OF WEB PLATES

There are two typical modeling techniques to simulate the web plate behavior: the continuum model and the strip model. In the continuum models, web plates are modeled using shell elements and the initial imperfections in the web plates are specified explicitly to simulate the shear buckling of web plates. Either implicit or explicit finite element analysis can be implemented for the continuum models. Due to the complex shear buckling behavior of web plates resulting in reorientation of out-of-plane deformations in the web plate during cyclic loading and unloading, the implicit algorithm generally has difficulty finding a converged solution (Behbahanifard et al. 2004; Webster 2013; Xue

1995). The explicit algorithm has been implemented successfully by several researchers for quasi-static analysis of web plates with proper control of kinetic energy; however, the small time increment required to control the kinetic energy and achieve numerical stability results in computationally expensive models (Behbahanifard et al. 2004; Webster 2013).

The strip model is a simplified web plate model where the web plate is represented by a series of tension-only inclined truss elements. This technique is included by several design codes for the analysis of SPSWs (AISC 2010a; CAN/CSA 2009), and it has been implemented and modified by several researchers to represent web plate behavior (Clayton et al. 2015; Driver et al. 1998; Guo et al. 2012; Shishkin et al. 2009; Vatansever and Yardimci 2011).

Behbahanifard, Grondin, and Elwi - 2004

The authors tested a half-scale three-story SPSW under the loading history given by the Applied Technology Council (1992). The material properties of the SPSW components and the elevation view of the specimen are given in Table 6 and Figure 23, respectively.

Table 6. Material properties of the SPSW components

	Yield Stress (MPa)	Ultimate Stress (MPa)	Strain Hard.
W310x118	313	482	1.41%
W310x60	332	478	1.76%
W530x82	349	493	1.85%
Web plate (Story 1)	341	456	2.62%
Web plate (Story 2)	257	344	2.44%
Web plate (Story 3)	262	375	1.53%

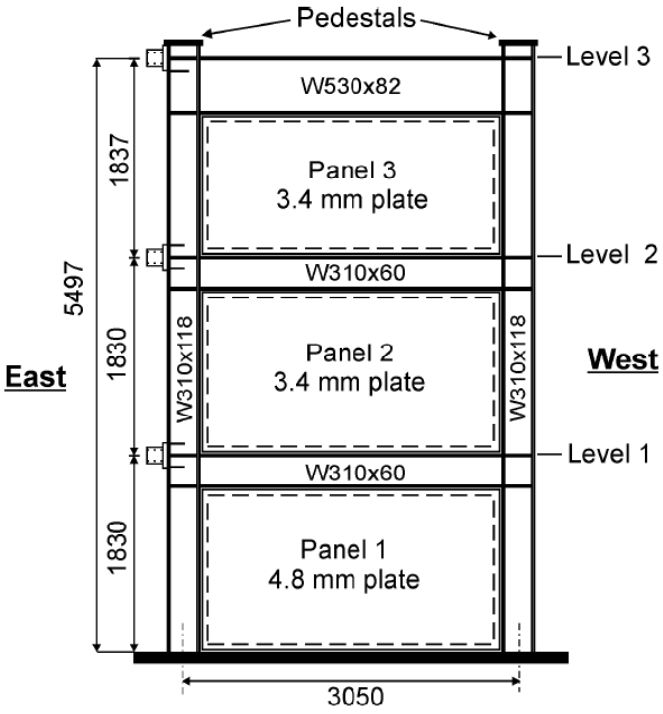

Figure 23. The elevation view of the SPSW

The specimen was modeled in ABAQUS/Explicit (ABAQUS 2010) and the results of the analysis and the test were compared. All members of the specimen (i.e., columns, beams, and web plates) were modeled using the four-node shell element S4R in the ABAQUS element library. Measured out-of-plane deformations in the first-story web plate of the specimen were mapped on the finite element mesh with an amplitude of 39 mm. Using the same initial imperfection pattern, initial imperfections with an amplitude of 10 mm were specified for the second and third-story web plates. To conduct the quasi-static analysis, a very small time increment was selected to control the kinetic energy.

The comparisons of the hysteretic responses and energy dissipations of the test and the finite element analysis (labeled as FEA) are given in Figure 24 and Figure 25, respectively. The comparisons suggested that the results of finite element analysis

showed an excellent agreement with the test results in terms of the hysteresis loop, the stiffness, and the energy dissipation. The pinching behavior was also captured successfully. Hence, the finite element model of unstiffened SPSWs based on explicit dynamic formulation was deemed valid and effective.

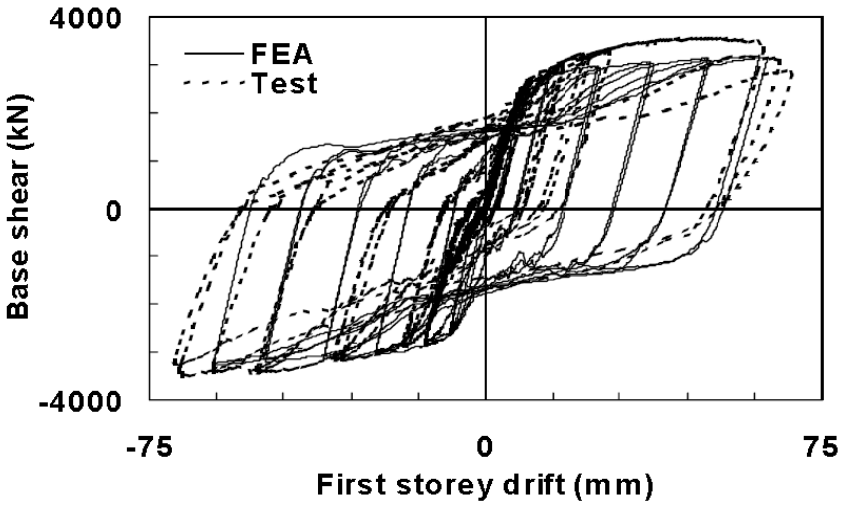

Figure 24. Comparison of hysteretic responses

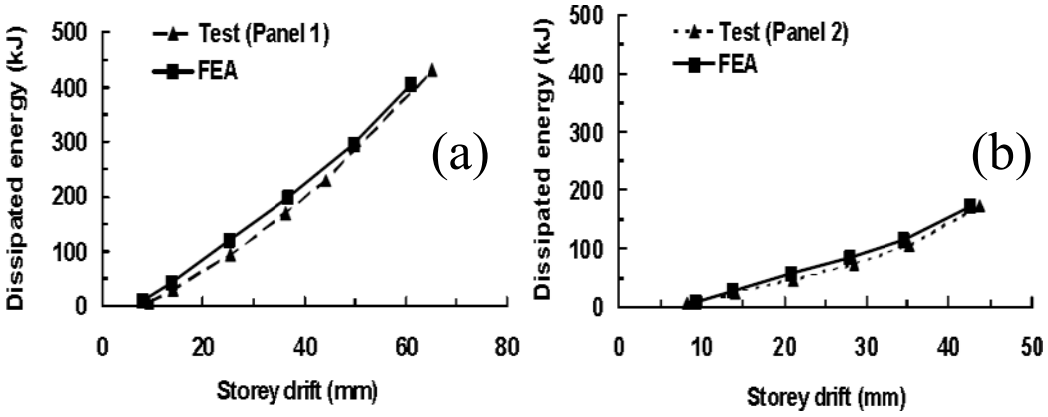

Figure 25. Comparison of energy dissipation: (a) first-story web plate and (b) second-story web plate

Webster, Berman, and Lowes - 2014

The authors tested two one-sixth scale one-story SPSW specimens (Test #2-22 and Test #3-22) to investigate the development and change in the web plate tension field orientation. A purely pin-connected frame (that was designed to remain elastic) was used to anchor the web plates. Cold-rolled 22 Ga A1008 SS Grade 40 sheet was selected as the web plates. The details of the SPSW specimens and the stress-strain diagram of the web plate material are given in Table 7 and Figure 26.

Table 7. Details of SPSW specimens

Name	**L (mm)**	**H (mm)**	**t_w (mm)**
Specimen of Test #2-22	711.2	711.2	0.710
Specimen of Test #3-22	711.2	711.2	0.710

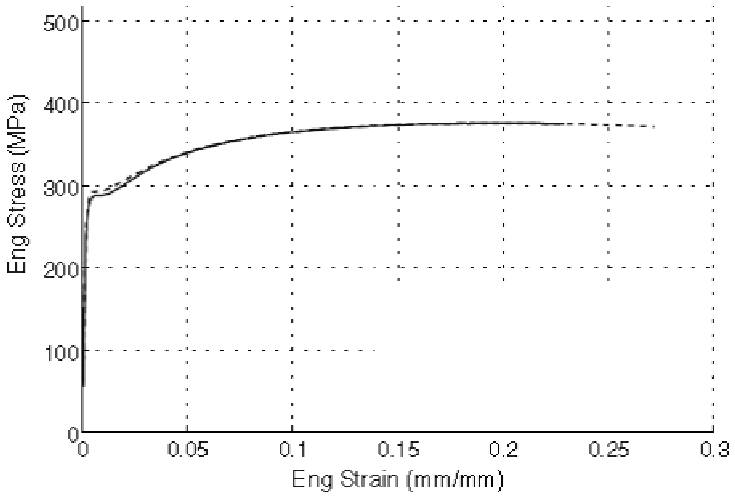

Figure 26. Stress-strain diagram of ASTM A1008 steel

Test #2-22 consisted of an initial elastic cycle to 0.3% drift followed by three complete cycles in excess of 6% drift. The target drift history of Test #3-22 consisted of three cycles each at 0.25, 0.5, 0.75, 1.0, 1.5, 2.0, 3.0, and 4.0% drift. The test specimens

were modeled in ABAQUS/Explicit (ABAQUS 2010) to verify the experiment results. The four-node shell element S4R in the ABAQUS element library was used to model the web plates. Initial imperfections were specified for the web plates considering the first two shear buckling modes with a total amplitude of 2 mm, which was approximately equal to the measured maximum imperfection from the test specimens. An isotropic strain hardening rule was implemented for the web plate material. A mass scale factor of 50 was used to increase the stable time increment of the explicit dynamic analysis. The comparisons of the hysteretic responses of the test results and finite element analysis results are given in Figure 27 for Test #2-22 and Test #3-22. The results suggested that the finite element model matched the hysteretic behavior of the experiments well.

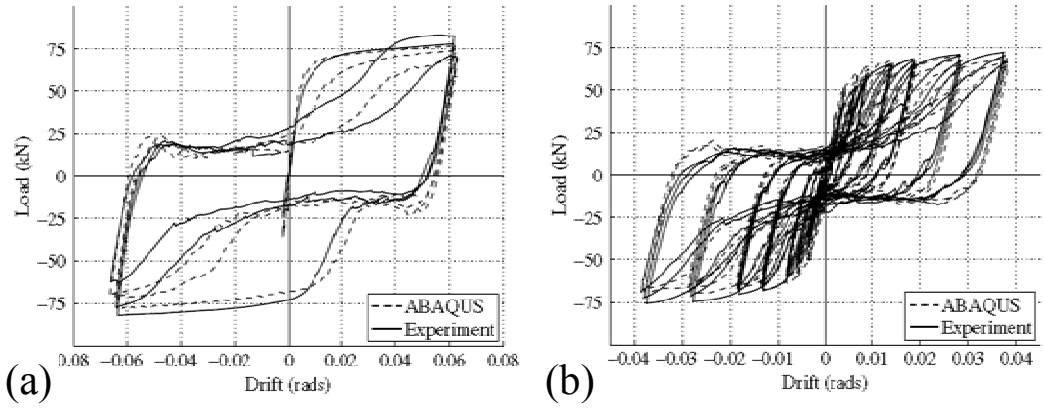

Figure 27. Comparison of hysteretic responses: (a) Test #2-22 and (b) Test #3-22

Vatansever and Berman - 2015

The specimens previously tested by Vatansever and Yardimci (2011) (Figure 19 and Figure 20) were modeled in OpenSEES (Mazzoni et al. 2006) adopting the strip model approach. While the web plates were represented by a series of inclined tension-only truss elements (Figure 28), nonlinear beam-column elements were used for beams and columns. Zero-length elements were used to simulate the semi-rigid beam-column

connection behavior. The inclination angle of the strips for the SPSW with fully-connected web plates (SW-A-H) was calculated using the equation F5-2 given in AISC 341-10 (AISC 2010a). The inclination angle of the strips for the SPSW with beam-connected web plates (SW-B-H) was calculated using Eq. 1 proposed by Thorburn et al. (1983). The authors adopted a unique web plate-boundary frame connection type since the infill plate thickness of 0.50 mm prohibited the use of welds or bolts. Self-drilling screws with a nominal diameter of 5.50 mm were used to connect the web plates to the boundary frame. A detailed finite element model was developed to investigate the behavior self-drilling screws. The load vs. displacement behavior of self-drilling screws was idealized by a trilinear curve and was used in the OpenSEES models. The OpenSEES models of Specimen SW-A-H and Specimen SW-B-H are given in Figure 29 and Figure 30, respectively.

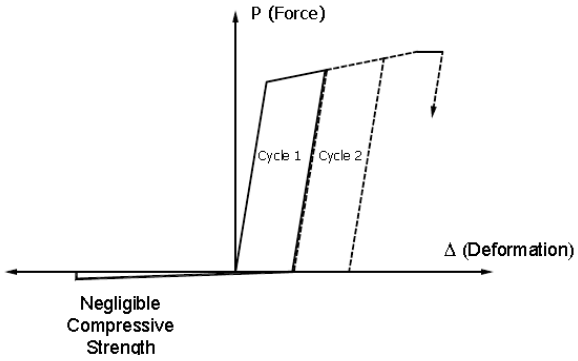

Figure 28. Cyclic axial load behavior of a strip

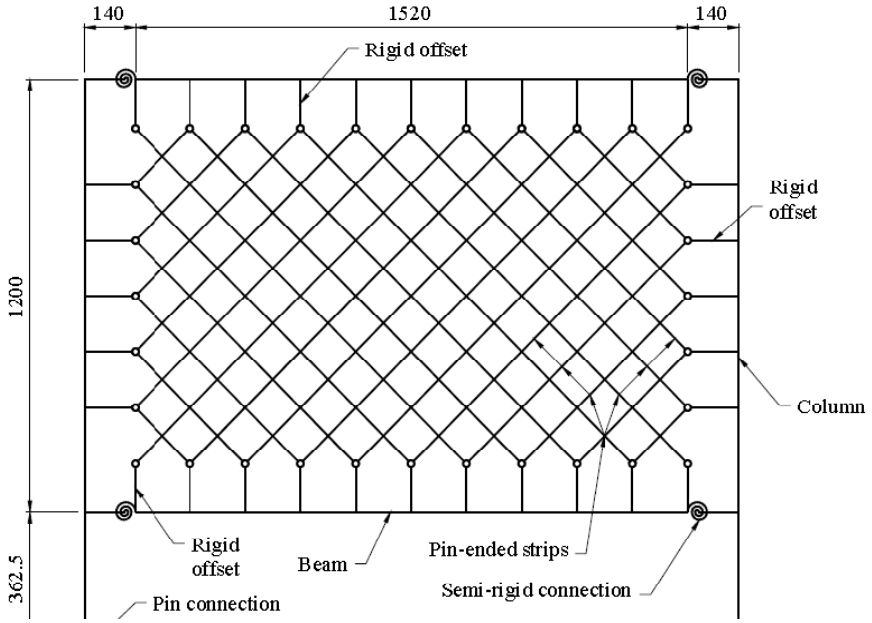

Figure 29. Strip model of Specimen SW-A-H

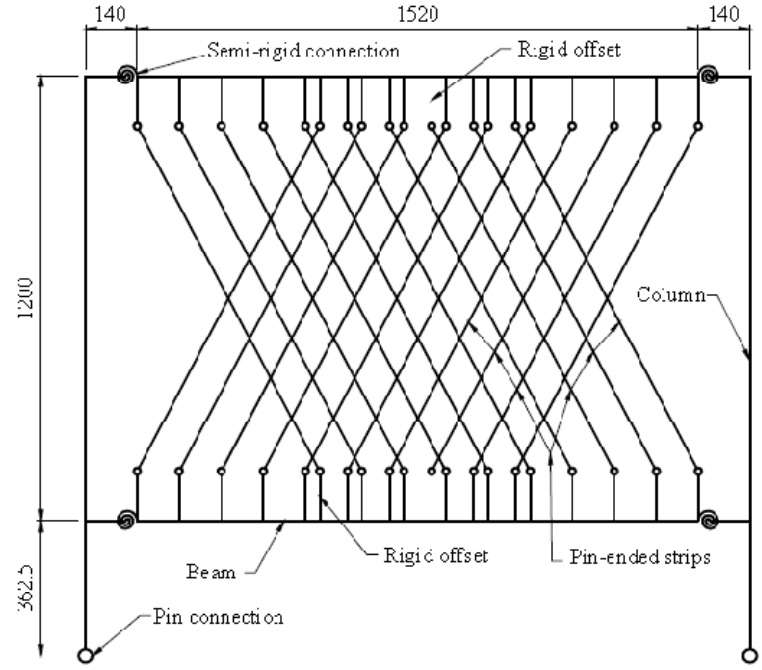

Figure 30. Strip model of SW-B-H

The hysteresis loops of Specimen SW-A-H and Specimen SW-B-H are given in Figure 31 and Figure 32, respectively. The results suggested that the strip model predicted the test results reasonably well in terms of the initial stiffness, post-yield stiffness, and unloading stiffness of the specimens. The authors also noted that the yield load of Specimen SW-B-H was underestimated by the strip model with the screw connection model. This was attributed to the fact that Eq. 1 given for SPSWs with fully-connected web plates and infinitely flexible columns might not represent the orientation of the partial tension field of beam-connected web plates.

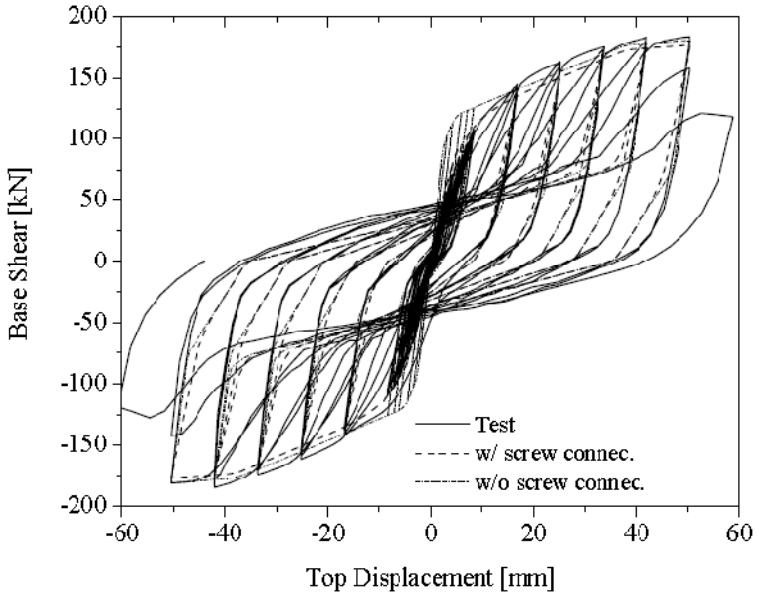

Figure 31. Comparison of analytical and experimental hysteresis curves for SW-A-H specimen

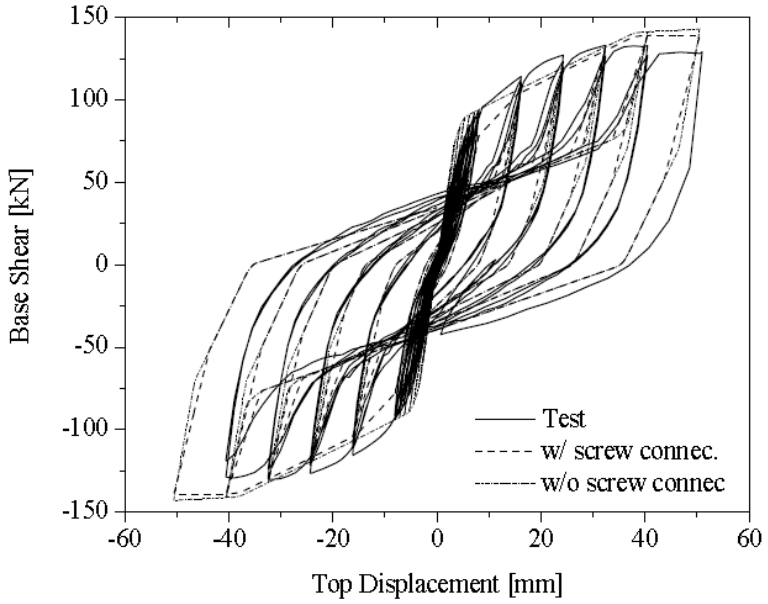

Figure 32. Comparison of analytical and experimental hysteresis curves for SW-B-H specimen

Chapter 3: Executive Summary and Conclusions

3.1 PROBLEM STATEMENT

As opposed to many lateral-load resisting systems such as braced frames and moment-resisting frames that have ordinary, intermediate, and special options in the *AISC Seismic Provisions* (AISC 341-10) (AISC 2010b) offering varying levels of ductility and response modification factors (R), only special SPSWs are covered in AISC 341-10 (AISC 2010b), which are mostly applicable in high-seismic regions where high ductile systems are required. AISC 341-10 (AISC 2010b) requires special SPSWs to have fully-connected web plates with moment-resisting beam-column connections. With R=7 (or R=8 when SPSWs are used as part of a dual system with special moment-resisting frame that resists at least 25% of the seismic lateral demand), the beams and columns of SPSWs are designed following capacity design principles and the beam-column connections are required to satisfy stringent detailing requirements prescribed by AISC 341-10 (AISC 2010b). These requirements enforced by AISC 341-10 (AISC 2010b) lead to overly conservative and uneconomical SPSW designs for low- and moderate-seismic regions where more relaxed ductility requirements might be sufficient (Berman and Bruneau 2008).

As discussed in Chapter 2: Literature Review, in spite of the reduction in the lateral load capacity, energy dissipation, and ductility compared to fully-connected web plates due to the development of partial tension field action, beam-connected web plates exhibit a promising seismic response and lead to significant reduction in column demands, which is a common design challenge for special SPSWs (Berman and Bruneau 2008; Gholipour and Alinia 2016). Similarly, compared to moment-resisting beam-column connections, the use of simple-beam column connections further reduce the column flexural demands, improve the distribution of yielding in the web plates due to

rotational freedom at the beam-column joints, and do not affect the overall seismic response of SPSWs drastically, despite reduced system redundancy and lateral load capacity due to the lack of frame action. SPSWs with beam-connected web plates and simple beam-column connections (B-SPSWs) combine the aforementioned benefits. In addition, B-SPSWs have the following benefits: (1) potential decrease in the total steel weight of the components, (2) cost reduction due to elimination of expensive moment-resisting beam-column connections, and (3) reduction in field welding required for web plate-to-boundary frame connections.

B-SPSWs offer several advantages over conventional special SPSWs although B-SPSWs are expected to have less ductility and reduced redundancy, which might make B-SPSWs a viable option for low- and moderate-seismic regions. In this dissertation, B-SPSWs were analytically investigated in three phases to evaluate their potential use in low- and moderate-seismic regions as an economical and adequately ductile SPSW option. The details of each phase are discussed in the subsequent sections (Figure 33).

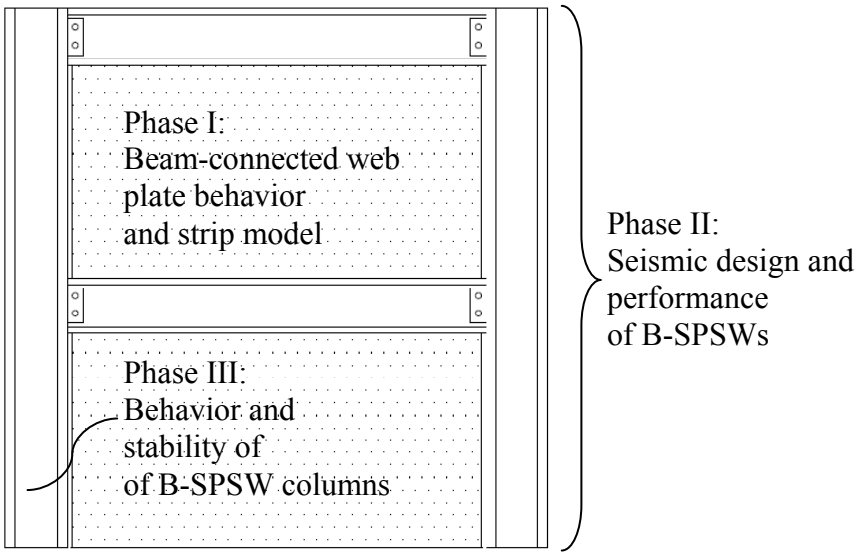

Figure 33. Phases of the study

3.2 STRIP MODEL FOR BEAM-CONNECTED WEB PLATES

In this study (detailed in Appendix A), the cyclic behavior of beam-connected web plates was characterized using validated finite element models. Based on the findings a simplified web plate model was proposed to facilitate the analysis of B-SPSWs. Beam-connected web plates with different geometric characteristics and steel yield strengths were analyzed under cyclic loads adopting the continuum model approach using the general-purpose finite element software ABAQUS/Explicit (ABAQUS 2010). An example of a buckled beam-connected web plate analyzed in ABAQUS/Explicit (ABAQUS 2010) is given in Figure 34. Based on the analysis results, a strip model that accurately estimates the shear strength, energy dissipation capacity, unloading strength of the web plate, and beam and column demands was proposed. The proposed strip model was based on the strip model previously proposed by Thorburn et al. (1983) for SPSWs with infinitely flexible columns and described in Chapter 2.2.

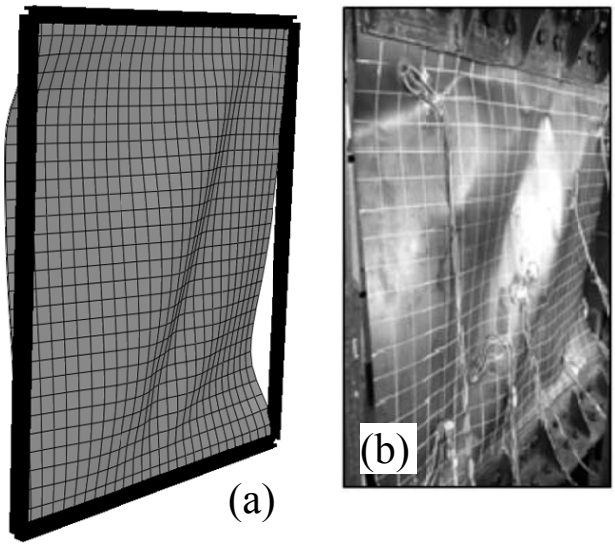

Figure 34. Buckled shape of Specimen S1 at 1.8% drift: (a) ABAQUS model, (b) test photo (Guo et al. 2011)

The key parameter of the strip model proposed by Thorburn et al. (1983) was the inclination angle of the strips. Thorburn et al. (1983) proposed an equation (Eq. 1) for the inclination angle assuming the tension field orients itself to resist the maximum lateral force. Some simplifying assumptions were made for the derivation of Eq. 1 that might not hold true for beam-connected web plates, including the assumption that web plates are restrained against out-of-plane deformation along the column edges and the assumption that the PTF inclination angle remains constant at increasing drift demands. Similarly, in the Thorburn et al. model (1983), the compressive strength of the web plate was assumed to be negligible; consequently, the strips were assumed to be tension-only strips. Previous research showed that the compressive strength of web plates can conservatively be ignored when proportioning web plates in the design of SPSWs; however, including the compressive strength of the strips in the model is crucial for nonlinear response-history analysis, since the energy dissipation capacity of the web plate is significantly underestimated when tension-only strips are adopted (Clayton et al. 2015; Webster et al. 2014). Note that the compressive strength of the strips of beam-connected web plates may be larger compared to fully-connected web plates since the partial tension field requires thicker web plates compared to the full tension field to resist the same lateral load demand (Clayton et al. 2015).

In the first part of this study, analytical and numerical models of one-story B-SPSWs with thin, beam-connected plates were used to develop an expression for partial tension field inclination angle that can be used in the proposed strip model for beam-connected web plates. The expression developed for the PTF inclination angle is a modification of Eq. 1 proposed by Thorburn et al. (1983) for fully-connected web plates with infinitely flexible columns. Due to the simple beam-column connections, B-SPSWs are a determinate system; consequently, the equations of beam and column demands can

be derived using free-body diagrams for very thin plates (i.e., the web plates have negligible compressive strength) as a function of the inclination angle. Equating the closed-form equations of the beam and column demands to the beam and column demands obtained from the finite element analyses, the corresponding inclination angle was calculated. Then, a new equation for the inclination angle of the strips was proposed.

In the second part, one-story beam-connected web plates with various aspect ratios (*L/H*) and thicknesses were analyzed to determine how aspect ratio and thickness affects compressive strength and hysteretic behavior of beam-connected web plates. Assuming that the inclination angle of the strips is independent of the web plate thickness, the loading and unloading strengths of the web plate hysteretic responses were idealized to determine a parameter called β, which represents the compressive strength of the strips as a proportion of the web plate yield strength (Figure 35).

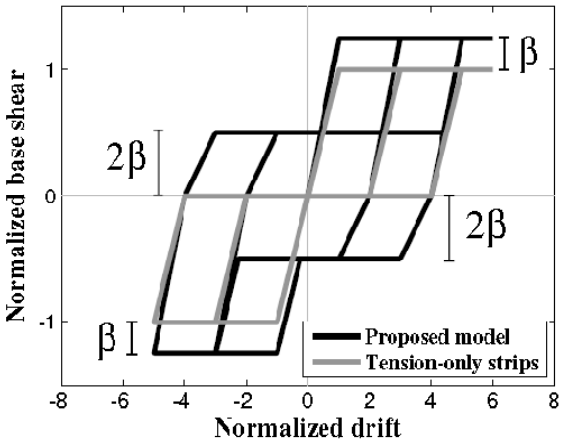

Figure 35. The hysteretic responses of the proposed strip model and the tension-only strip model (i.e., the Thorburn et al. model (1983))

Adopting these two parameters (the inclination angle, θ, and the compressive strength, β), a beam-connected web plate strip model was proposed as a modification of

the Thorburn et al. (1983) model shown in Figure 15. The comparison of the Thorburn et al. (1983) model and the proposed model revealed that the proposed model showed a better agreement with the test result of Guo et al. (2011) and the continuum models, and estimated the beam and column demands, web plate shear strength, energy dissipation capacity of B-SPSWs accurately. Note that although the proposed model captures the web plate behavior better compared to the Thorburn et al. (1983) model, the proposed model has limitations such as not simulating web plate tearing and overestimating the initial lateral stiffness of beam-connected web plates compared to the B-SPSW test available in the literature (note the Thorburn et al. (1983) model also has the same limitations). Similarly, the proposed model was not compared with the results of experiments that were performed under unsymmetrical drift histories since such experiments are not available in the literature; consequently, the proposed model needs to be validated against further experimental results when these results become available.

3.3 SEISMIC DESIGN AND PERFORMANCE OF STEEL PLATE SHEAR WALLS WITH BEAM-CONNECTED PLATES

In this proof-of-concept study (detailed in Appendix B), eighteen B-SPSWs with various geometric characteristics were designed for a low-seismic site (Boston, MA) and analyzed under ground motions to evaluate the seismic behavior of B-SPSWs which were designed adopting two design approaches: (1) without specific seismic detailing considerations and (2) using capacity design principles used in seismically detailed systems.

Figure 4(a) shows the formation of the partial tension field in the web plates of a three-story B-SPSW when the system resists earthquake forces. The equation F5-1 given in AISC 341-10 (AISC 2010b) for the shear strength of fully-connected web plates was modified considering the differences between the partial and full tension field and can be

used to proportion beam-connected web plates for a given design lateral load. Figure 4(b) shows the free-body diagrams of the beams and columns of the B-SPSW under the lateral loading. Using these free-body diagrams, the beam axial, shear, and moment demands were provided as closed-form equations that are a function of average web plate stress in the partial tension field, the inclination angle of the partial tension field, and web plate geometry. As depicted in Figure 4(b), the columns of the B-SPSWs resist axial loads due to the beam end shears and moments resulting from the beam shears acting offset from the column centerline. However, as will be discussed in Chapter 3.4, the columns of B-SPSWs resist significant moment demands associated with differential interstory drifts. Three-, six-, and nine-story buildings with aspects ratios (bay width/story height) of 1.15, 1.54, and 1.84 were designed considering two different design approaches. For the non-seismically detailed design approach (ND), a response modification factor (R) of 3 was adopted for non-seismically detailed steel systems (ASCE 2010). In this design approach, the average web plate stress under the design story shear demands was used to determine beam and column demands, i.e., the overstrength in the web plates was not considered for the beam and column designs. For the seismically-detailed design approach (SD), an R of 3.25 was adopted and the web plate stress used to determine the member demands was taken as the expected yield strength of the web plate material, i.e., the beams and columns were capacity-designed. Note that B-SPSWs are not codified and there are very limited experimental studies on B-SPSWs in literature; consequently, the R of ordinary concentrically braced frames given in AISC 341-10 (AISC 2010a) was conservatively adopted for the SD B-SPSW design in this proof-of-concept study. Further details of the basis of this assumption are provided in Appendix B.

Two-dimensional models of the B-SPSWs were constructed in OpenSEES (Mazzoni et al. 2006). The beams and columns were modeled using nonlinear beam-

column elements, and the web plates were modeled using the strip model described in Chapter 3.2. Each B-SPSW was subjected to two suites of ground motions representing two different seismic hazard levels for the Boston, MA site. The first set comprised of twenty ground motions scaled to a seismic hazard level of 10% exceedence in 50 years (10/50), while the second set comprised of twenty ground motions scaled to a seismic hazard level of 2% exceedence in 50 years (2/50) (Somerville et al. 1997). The ground motions were scaled such that, on average, their spectral values match with a least square error fit to the United States Geological Survey's mapped values at 0.3, 1.0, and 2.0 seconds, and an additional predicted value at 4.0 seconds. The performance of the B-SPSWs was evaluated considering the following response parameters: (1) maximum peak interstory drift (ISD), (2) maximum beam demand-to-capacity ratio for axial load and moment interaction (PM_B), (3) maximum beam demand-to-capacity ratio for shear (V_B), (4) maximum column demand-to-capacity ratio for axial load and moment interaction (PM_C), and (5) maximum beam-column joint rotation (C_R). Since the models were two-dimensional, the beams and columns were modeled using line elements, and some parameters such as residual stresses and initial imperfections in columns were not included in the models. The axial, shear, and moment capacities of the members were calculated per the *AISC Specifications* (AISC 360-10) (AISC 2010b) considering both in-plane and out-of-plane unbraced lengths and assuming resistance factors of 1.0. The demands were obtained considering all sections along the length of all beams or columns throughout the entire response-history analysis. The highlights of the analysis results can be listed as follow:

- The 84th percentile of the peak ISDs of all buildings were below 2% at the 10/50 hazard level and the mean ISDs at the 2/50 hazard level were between 1.2% and

2.4%, which are smaller than the ISDs observed in special SPSWs at the 2/50 hazard level (Berman 2011; Purba and Bruneau 2015).

- The design approach (ND vs. SD) did not have a significant influence on the ISDs. This was attributed to the fact that the lateral stiffness of the B-SPSW stems from the web plates only and the web plate thicknesses were similar for both design approaches since similar response modification factors were used.
- The 84th percentile PM_B values were less than 1.0 for all buildings at both hazard levels, which suggested that the beams remained essentially elastic.
- The 84th percentile V_B values were less than 1.0 for most of the buildings at both hazard levels; however, for the B-SPSWs with narrower web plates (smaller aspect ratios) designed per the ND approach, the V_B values were larger than 1.0 at the 2/50 hazard level. The V_B values larger than 1.0 signify that localized shear yielding may occur at the ends of B-SPSW beams designed using the ND approach.
- For both design approaches, PM_C values larger than 1.0 were obtained for some B-SPSWs although the axial load demands in the columns were less that the design axial load. This result was attributed to the fact that significant moment demands were observed in the columns even though the columns were considered as leaner columns and moment demands due to interstory drift were not considered in the design stage. It was concluded that the differential interstory drifts led to column rotations at floor levels that resulted in unanticipated flexural demands in the columns. This behavior is explained and studied in detail in Chapter 3.4.
- The 84th percentile C_R values were less than 0.031 rad and 0.047 rad at the 10/50 and 2/50 hazard levels, respectively, which were less the rotation capacities of

single plate shear tabs and double-angle simple connections reported by Astaneh-Asl (2005a, 2005b). Hence, it was concluded that simple beam-column connections could accommodate expected cyclic rotation demands in low-seismic regions and were appropriate to adopt as the beam-column connections of B-SPSWs provided that these simple connections satisfy strength limit states.

These results suggested that B-SPSWs designed per both design approaches (ND and SD) showed acceptable seismic performance. Note that the SD exhibit better performance compared to the ND and the ND is more prone to local failure modes such as connection failures and panel zone failures (that are not considered in this study) since the capacity design principles are not adopted. The results indicate that B-SPSWs would be a viable SPSW option in low-seismic regions.

3.4 BEHAVIOR COLUMNS OF STEEL PLATE SHEAR WALLS WITH BEAM-CONNECTED WEB PLATES

In this study (detailed in Appendix C), the columns of the eighteen B-SPSWs discussed in Chapter 3.3 were investigated in detail to assess their stability under earthquake loads.

As discussed in Chapter 3.3, nonlinear response-history analyses were conducted to assess the overall seismic behavior of B-SPSWs, and it was observed that the demand-to-capacity ratios of the columns of the B-SPSWs calculated per AISC 360-10 (AISC 2010b) were larger than 1.0 for some cases because of the significant flexural demands in the columns associated with differential interstory drifts that were not considered in design. Note that the columns of B-SPSWs were designed primarily for axial loads resulting from beam end shears, adopting the Equivalent Lateral Force method. The demand-to-capacity ratios larger than 1.0 signified potential column failure due to column yielding or buckling; however, it did not necessarily mean that column instability

occurred. Further research was needed to better identify expected column failure modes and understand their effects.

The models considered in the previous study had some limitations to simulate column buckling due to the following reasons: (1) While the P-Δ effects were included in the analysis, the P-δ effects were not included in the columns since no initial imperfections were specified in the columns; consequently, the stability of individual columns was not simulated even though the global stability of B-SPSWs was considered in the models. (2) The residual stresses in the columns were not included. (3) The models were two-dimensional; consequently, the out-of-plane deformations were not captured by the models. Note that the columns of B-SPSWs are generally oriented for strong-axis bending in the plane of B-SPSWs; consequently, the out-of-plane stability of columns that was not considered in the two-dimensional models is more critical compared to the in-plane stability of columns. In this study, to assess the stability of the columns of the B-SPSWs, three-dimensional finite element models of isolated columns were constructed in ABAQUS/Standard (ABAQUS 2010) adopting brick elements and considering initial imperfections and residual stresses to explicitly simulate column buckling. Since isolated columns were used in the finite element models, appropriate boundary conditions at floor levels were implemented to simulate the effects of web plates, beams, and slabs. It was assumed that slabs provided adequate torsional bracing at floor levels to avoid twist and torsional buckling of columns. (The detailing requirements for this assumption require further study.) The discretized interstory drift demands and beam end shears at each floor level recorded throughout each response-history analysis of the previous study at the 2/50 hazard level were applied to the isolated column models as translations and loads to simulate the system demands on the columns. The results revealed that although differential interstory drifts might cause yielding at floor levels, it might not lead to

stability problems; consequently, it was concluded that the demand-to-capacity ratios of columns calculated per the demands of two-dimensional analysis and the capacities given in AISC 360-10 (AISC 2010b) were not directly related to column stability. Another observation was that except for the three-story ND SPSWs under a couple of ground motions, none of B-SPSWs experienced stability problems although column yielding occurred at floor levels for most of the cases. Note that in the previous study, the six- and nine-story B-SPSWs had larger demand-to-capacity ratios compared to the three-story B-SPSWs, which suggested that the six- and nine-story B-SPSWs were more prone to stability problems; however, an opposite trend was observed in this detailed study.

Note that the flexural demands in the columns associated with differential drifts cannot be captured when traditional seismic design methods (the Equivalent Lateral Force method and Modal Response Spectrum analysis) are implemented (AISC 2010a). Hence, column stability might be a problem when these traditional design methods are applied, as observed in the first part of this study. A parametric study was undertaken to propose a simple column design approach that considers the axial load demands from the Equivalent Lateral Force method and considers the effect of the flexural demands associated with differential drifts implicitly. Adopting a similar three-dimensional finite element modeling approach as used the first part, five W14 sections were investigated considering various patterns of interstory drift distributions along the column height at different target drifts to assess the reduction in the column buckling strength due to the flexural demands not considered in design. The results revealed that column yielding occurred at floor levels when the differential interstory drift was larger than 1% and the reduction in the column buckling capacity appeared to be independent of peak interstory drift demands for target drifts larger than 2%. Based on these results, an empirical equation only considering the column geometric properties was proposed as an upper-

bound estimate of the column buckling strength reduction that can be easily implemented in traditional design methods.

3.5 CONCLUSIONS

A three-phase study was undertaken to evaluate the seismic behavior of B-SPSWs for applications in low-seismic regions. In the first phase, beam-connected web plate behavior was characterized and a simplified beam-connected web plate model was proposed. In the second phase, eighteen B-SPSWs were designed per the proposed design equations and were analyzed under ground motions scaled to two different seismic hazard levels. In the third phase, the stability of the columns of the B-SPSWs was studied in detail and an equation was proposed as a column buckling strength reduction factor to ensure column stability when traditional design methods are implemented.

The results of this proof-of-concept study suggested that B-SPSWs might be a viable and cost-effective lateral-force resisting system option for low-seismic regions. Future research should focus on the following topics:

- verifying the findings of this study through subassembly and full-scale testing.
- conducting seismic collapse risk analyses adopting FEMA P-695 (FEMA 2009) to verify the R factors using numerical models based on strength degrading behaviors observed in the tests.
- investigating beam shear limit states for narrow B-SPSWs and potential details to mitigate these effects.
- comparing B-SPSWs with other low-seismic lateral-force resisting systems.

Appendix A

Paper 1. Strip model for steel plate shear walls with beam-connected web plates

Yigit Ozcelik, Patricia M. Clayton

Published in *Engineering Structures* 136: 369-379

ABSTRACT

Steel plate shear walls comprise web plates connected to beams and columns, also referred to as vertical and horizontal boundary elements, respectively. When loaded laterally, web plates induce high flexural and axial demands in the columns due to the development of an inclined tension field. An alternative lateral force-resisting system is proposed in which the steel plate shear wall web plates are attached only to the beams to avoid high flexural demands in the columns resulting from the inclined tension. In this study, beam-connected web plate behavior is characterized using validated finite element models, a simplified strip model is proposed to simulate hysteretic web plate behavior, and equations for the inclination angle of the partial tension field and compressive strength of strips are presented. A comparison between the finite element model, the current strip model from the literature, and the new proposed strip model is provided. Results indicate that the proposed model successfully estimates beam and column demands, base shear capacity, and energy dissipation capacity of the beam-connected web plate for a wide range of web plate aspect ratios and height-to-thickness ratios.

KEYWORDS

Steel plate shear wall, Beam-connected web plate, Strip model, Partial tension field, Inclination angle, Compressive strength

INTRODUCTION

Steel plate shear walls (SPSW) have proven to be a reliable earthquake force-resisting system due to their high energy dissipation capacity, stable hysteresis characteristics, and high lateral stiffness [1–6]. A conventional SPSW comprises web plates, the primary lateral load-resisting element, connected to the beams and columns of a surrounding boundary frame. Although earlier SPSW designs used thick or stiffened web plates to preclude out-of-plane buckling [7], later studies [2–5] revealed that slender web plates show substantial post-buckling strength and ductility under lateral load. This post-buckling strength results from a mechanism called tension field action (TFA) [8] that requires very stiff beams and columns to anchor the web plate to develop diagonal tension to resist lateral loads. This diagonal tension causes significant axial and flexural demands in columns. For multistory SPSWs, design of columns becomes more challenging due to high axial load and moment demands and stiffness requirements [9]. SPSWs with beam-connected web plates (B-SPSW) (Fig. 1(a)) are proposed as an alternative to conventional SPSWs to mitigate high flexural demands in the columns due to TFA and to facilitate field installation of web plates. The focus of this paper is on the behavior and modeling of beam-connected web plates that are employed in the B-SPSW system. Details of B-SPSW system design and seismic performance are the topics of ongoing research and are outside the scope of this paper.

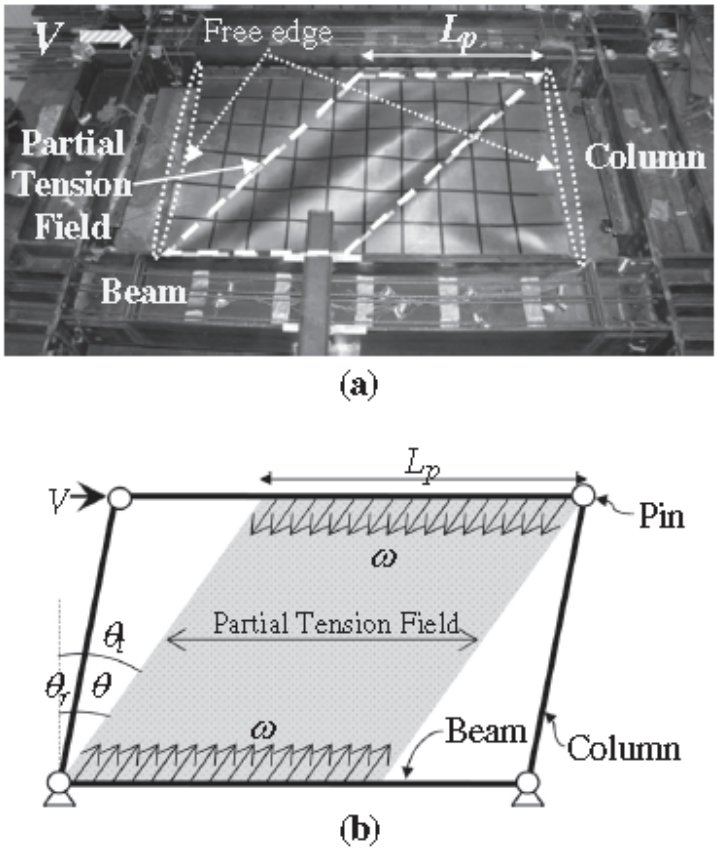

Figure 1. Partial tension field: (a) test photo (adapted from Clayton et al. [21]) and (b) schematic view.

There are two generally accepted modeling techniques to simulate SPSW web plate behavior, namely, the continuum model and the strip model. In the continuum model, the web plate is represented by shell elements that explicitly buckle under lateral load to develop TFA. A simpler analytical model known as strip model was proposed by Thorburn et al. [1] where a series of inclined tension-only truss elements connected to beams and columns are used to represent the diagonal tension field of the web plate. The strip model has been employed and modified by several researchers [10–12] to simulate the cyclic response of fully-connected web plates (i.e., connected to beams and columns)

in SPSWs; however, little work has been done on developing a strip model to simulate the cyclic response of beam-connected web plates in B-SPSWs.

The extent and angle of inclination of the tension field and the hysteretic behavior of individual strips are important considerations in accurately simulating the cyclic behavior of web plates and the boundary element demands using the strip method. Several design codes [13,14] provide an equation for the inclination angle of TFA for fully-connected SPSW web plates derived from elastic analysis, and recent research has proposed a 45 degree inclination angle be assumed for SPSW web plates after yielding [15]; however, these recommendations assume beams and columns have sufficient stiffness to anchor the web plate to develop full TFA. Beam-connected web plates, alternatively, are not anchored along the vertical column edges, and thus the extent and inclination angle of the tension field will be different. Regarding strip hysteretic behavior, recent research has shown that the commonly assumed tension-only strip behavior [1] does not adequately capture the non-negligible compressive resistance of fully-connected web plates upon unloading and reloading [16,17]. This compressive capacity contribution of the strips depends on web plate edge support conditions and thickness and should be investigated for beam-connected web plates.

A mechanics-based analytical model and a detailed finite element model of a beam-connected web plate in a pinned boundary frame are used to characterize web plate behavior and to provide a rational basis for strip model recommendations. First, a parametric study of thin web plates with various aspect ratios are analyzed to determine the extent and inclination angle of TFA. Second, cyclic analyses are performed for web plates of varying thicknesses to obtain the relationship between compressive capacity, aspect ratio, and plate thickness. The details of the strip model are explained, and comparisons of the strip model and finite element model results are presented.

MECHANICS OF B-SPSWS WITH THIN WEB PLATES

The behavior of B-SPSWs is similar to the mechanics of a plate girder loaded in shear presented by Basler [8], where the web panel, stiffeners, and flanges of the wide-flange section are analogous to web plate, beams, and columns of a B-SPSW, respectively. The ultimate shear strength of plate girders can be decomposed into two components: shear buckling strength of the web panel and the component of inclined tension field in the applied shear direction [8]. For thin web panels, the shear buckling strength can be neglected since the web panels are expected to buckle almost immediately upon loading [1]. Note that the plate girder analogy assumes that girder flanges have negligible flexural stiffness to anchor the web panel tension field. This assumption, while shown to be inappropriate for SPSWs with fully-connected web plates [18], is applicable to B-SPSWs in which the detached columns do not restrain the web plate. Without restraint from the columns the inclined tension field forms over some portion of the web plate between beams of the B-SPSW, which is called the partial tension field (PTF), similar to the PTF that forms between the stiffeners of a plate girder. The portion of web plate inside the PTF (Fig. 1) resists the applied lateral force, V, whereas the remainder of the web plate is assumed to provide no contribution to the shear strength. Experimental studies on B-SPSWs with various beam-to-column connections [19–21] verified the PTF behavior for beam-connected web plates.

A single-story, single-bay analytical model is used to investigate beam-connected web plate behavior. As shown in Fig. 1(b), pinned connections are assumed at all beam-column joints and at column bases to isolate web plate response without any frame action, resulting in a statically determinate system. A thin web plate is assumed such that the shear buckling strength is negligible and the lateral load is resisted only by the PTF. When the system undergoes a lateral sway, beams resist axial force and bending moment

due to the distributed diagonal loads, ω, acting over the PTF length, L_p, oriented at an angle (measured relative to the vertical axis), θ_t (Fig. 1(b)), and B-SPSW columns resist only axial loads.

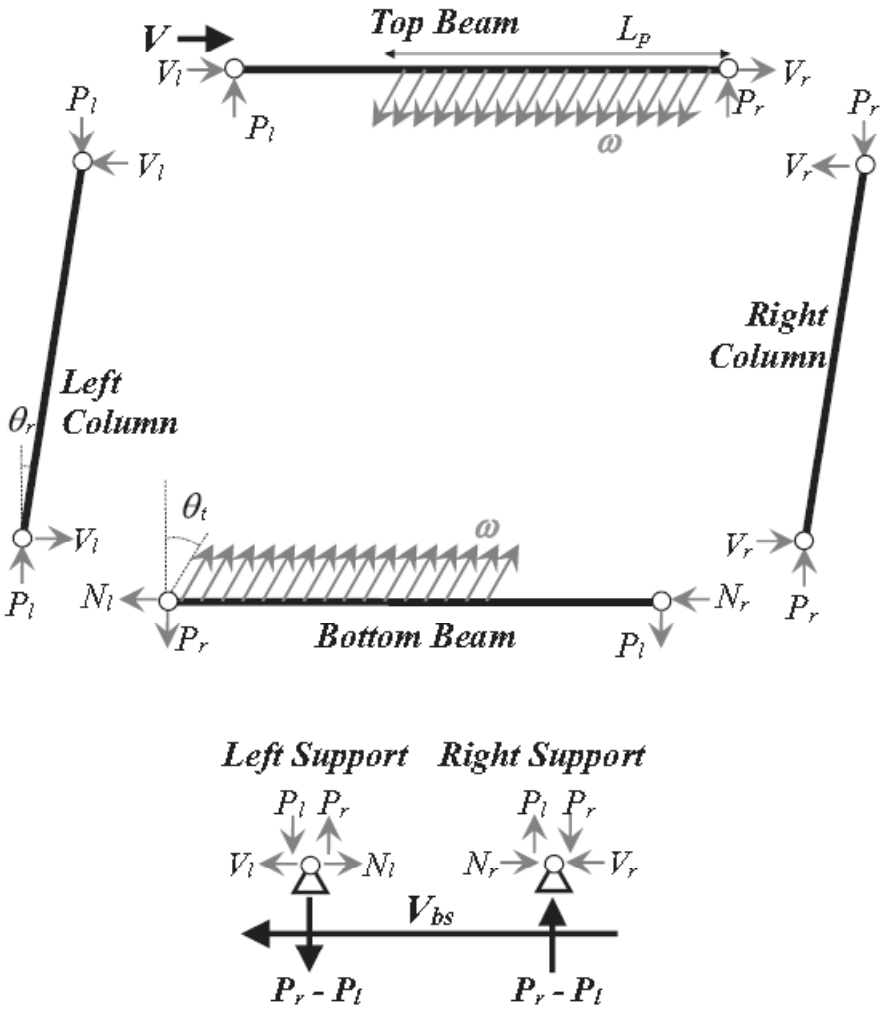

Figure 2. Free-body diagrams of the beams, columns, and supports of B-SPSW.

Fig. 2 shows the free-body diagrams of the beams, columns, and supports of a single-story B-SPSW with a pin-connected boundary frame. In these free-body diagrams,

the following simplifying assumptions are made: (1) columns and beams are very stiff so that the deflections are negligible and the web plate stress in the PTF, σ_w, is uniform, (2) σ_w is equal to the web plate yield strength, F_y, and, (3) L_p is a function of the tension field inclination angle, θ (measured relative to the free edge of the plate as shown in Fig. 1(b)), and is independent of the column drift angle, θ_r. Using the deformed configuration of the single-story B-SPSW given in Fig. 1(b) and the free-body diagram shown in Fig. 2; the beam and column demands, and other design parameters of the B-SPSW are derived as follow:

$$\theta_t = \theta + \theta_r \tag{1}$$

The horizontal and vertical components of ω (ω_x and ω_y, respectively) and the ratio between them are given in Eqs. (2)–(4), respectively. Derivation of ω_x and ω_y, can be found in Sabelli and Bruneau [7].

$$\omega_x = F_y t_w \cos\theta_t \sin\theta_t = 0.5\, F_y t_w \sin(2\theta_t) \tag{2}$$

$$\omega_y = F_y\, t_w \cos\theta_t \cos\theta_t \tag{3}$$

$$\omega_x/\omega_y = \tan\theta_t \tag{4}$$

Assuming θ_r is small compared to θ and using the geometry given in Fig. 1(b), L_p can be estimated by Eq. (5) where L is the beam length and H is the column height:

$$L_p = L - H\,tan\,\theta = L\left(1 - \frac{tan\,\theta}{L/H}\right) \tag{5}$$

Having pin connections at the beam-column joints (i.e., zero moment at the beam ends) and ω_y acting over L_p; the maximum moment in the beam, M_m, the shear at the end of the beam away from the PTF, P_l (i.e., the axial load in the column with the smaller compressive axial load), the shear at the end of the beam nearer the PTF, P_r (i.e., the axial load in the column with larger compressive axial load), and the location of M_m measured from the beam end carrying P_r, x, can be calculated by Eqs. (6)–(9), respectively:

$$M_m = 0.125\, F_y t_w L^2 (\cos\theta_t)^2 \left[2\left(1-\frac{\tan\theta}{L/H}\right)-\left(1-\frac{\tan\theta}{L/H}\right)^2\right]^2 \quad (6)$$

$$P_l = 0.5\, F_y t_w\, L\, (\cos\theta_t)^2 \left(1-\frac{\tan\theta}{L/H}\right)^2 \quad (7)$$

$$P_r = 0.5\, F_y t_w\, L\, (\cos\theta_t)^2 \left[2\left(1-\frac{\tan\theta}{L/H}\right)-\left(1-\frac{\tan\theta}{L/H}\right)^2\right] \quad (8)$$

$$x = 0.5\, L \left[2\left(1-\frac{\tan\theta}{L/H}\right)-\left(1-\frac{\tan\theta}{L/H}\right)^2\right] \quad (9)$$

The columns have pin connections on both ends, i.e. they are leaner columns with no moment at the ends. Therefore, the axial loads in the columns due to the vertical web plate forces, P_l and P_r, create an overturning moment in the leaning columns displaced to a drift of θ_r, which is only resisted by the force couple of the horizontal forces, V_l and V_r, at both column ends that cause a destabilizing effect on the web plate. Summing these horizontal forces resulting from the P-Δ effects in the left and right columns (V_l and V_r as shown in Fig. 2, respectively) and the horizontal reactions of the bottom beam on the left and right ends (N_l and N_l as shown in Fig. 2, respectively), the base shear, V_{bs}, can be calculated by Eq. (10):

$$V_{bs} = (N_l + N_r) - (V_l + V_r) = \omega_x L_p - (V_l + V_r)$$

$$= 0.5\, F_y t_w\, L \left(1 - \frac{\tan\theta}{L/H}\right) \sin(2\theta_t) \left(1 - \frac{\tan\theta_r}{\tan\theta_t}\right) \quad (10)$$

A simplified strip model for beam-connected web plates must accurately simulate web plate strength and the boundary frame demands described in the above equations. It is noted that the PTF inclination angle, θ, is a key parameter in the expressions for strength and boundary frame demand and must be accurately quantified.

SIMPLIFIED STRIP MODEL FOR BEAM-CONNECTED WEB PLATES

In this study, a strip model to represent beam-connected web plates (Fig. 3) is proposed based on Thorburn et al.'s [1] strip model for SPSWs with infinitely flexible columns. In Thorburn et al.'s [1] model a series of evenly-spaced tension-only inclined strips are connected to the beams over L_p (Eq. (5)), which is defined based on web plate geometry and an assumed θ. The total cross sectional area of all the strips in each direction, A, is given by Eq. (11); where A_s is the area of a strip, and n_s is the number of strips in each direction.

$$A = n_s A_s \qquad \text{where} \quad A_s = t_w\, L_p \cos\theta\, / n_s = t_w\, L \left(1 - \frac{\tan\theta}{L/H}\right) \cos\theta\, / n_s \quad (11)$$

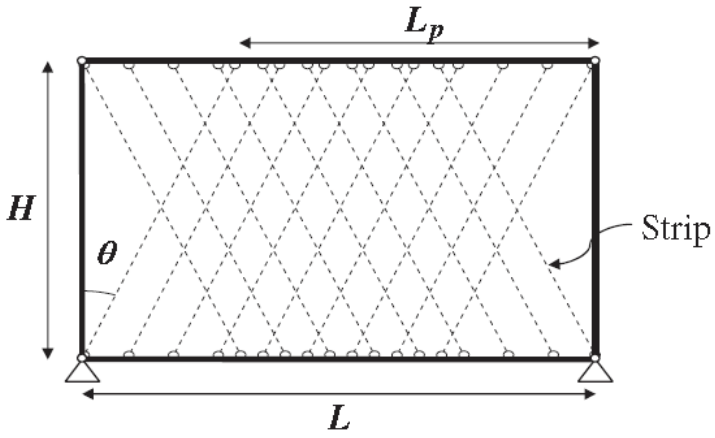

Figure 3. Strip model of B-SPSW.

To define strip layout and cross-section properties an accurate estimation of θ is needed. Additionally, the strip hysteretic behavior must account for the potentially significant compressive strength that has been found in thicker web plates that can be roughly defined as the web plates with height-to-thickness ratios (H/t_w) less than 500. To investigate these two critical parameters, continuum finite element models are used in a series of two numerical parametric studies. Details of the finite element model are given below, followed by discussion of the current literature and parametric studies on these two parameters.

FINITE ELEMENT MODEL OF BEAM-CONNECTED WEB PLATES

The finite element model is of the single-story B-SPSW with pin-connected boundary frame described previously (Fig. 1). A continuum web plate model is employed to explicitly capture web plate buckling and development of tension field action. This continuum modeling approach has been shown to accurately capture cyclic behavior of a wide range of SPSW systems with various web plate boundary conditions and beam-column connection types, including those with beam-connected web plates [15,19,22–25].

For continuum finite element models, an implicit or explicit finite element analysis can be implemented. SPSW web plates exhibit complex ‘‘snap through” buckling behavior under cyclic load as the plates are unloaded and a reoriented tension field forms upon loading in the opposite direction. Due to this complex behavior, implicit finite element analysis approaches can have difficulty finding a converged solution during cyclic analysis [22,26,27]. To overcome this convergence problem, an explicit dynamic method can be adopted for quasi-static analysis of SPSWs with proper control of the kinetic energy [22,27]; however, this method is generally computationally expensive due to small time increments required to control the kinetic energy and to maintain numerical stability.

The finite element analysis is done using the ABAQUS/Explicit software [28]. The web plate is modeled using four-noded shell elements (S4R), whereas columns and beams are modeled as very stiff line elements (B31). The mesh size used for web plates is 102x102 mm (4x4"). An initial imperfection with a maximum amplitude of approximately $H/1000$ is assigned as a combination of first four elastic buckling modes under vertical loads. The web plate material is assumed to behave as an elasto-plastic material with a modulus of elasticity, E, of 200 GPa (29,000 ksi), Poisson’s ratio of 0.3, F_y of 248 MPa (36 ksi), and a small post-yield stiffness to improve numerical stability. It is worthwhile noting that the negligible strain hardening is assumed (1) to be consistent with the current SPSW design assumptions where the boundary frame is designed to resist a uniform web plate stress with no strain hardening [7], and (2) to have a fair comparison between σ_w in the finite element model and σ_w of F_y assumed for Eqs. (2)–(10). The built-in tie constraint is used to model the welded connections between web plate and beams. For this numerical study focused on web plate mechanics, pin connections are used at beam-column joints and at column bases, and the discrete depths

of the boundary frame elements are ignored as depicted in Fig. 1(b). A typical model is shown in Fig. 4.

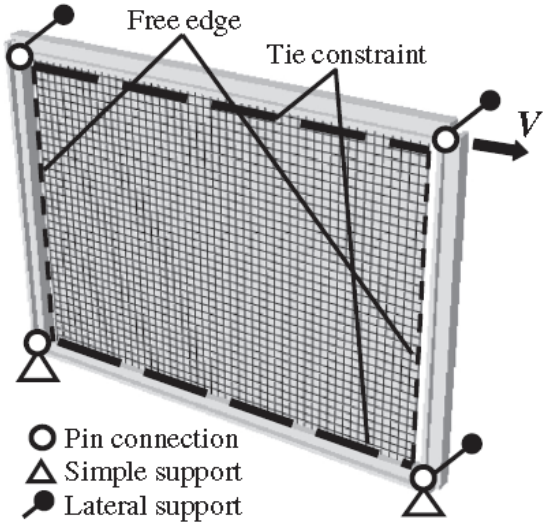

Figure 4. Typical ABAQUS model.

The quasi-static analysis of the 1/3 scale one-story one-bay BSPSW (designated as S1) tested by Guo et al. [19] is conducted using the continuum model approach described herein. The lateral loading protocol given in the Chinese Code JGJ 100-96 [29] was adopted for the experiment [19]. The base shear vs. lateral displacement responses of the test and the computational model are given in Fig. 5. The comparison of the results reveals that the finite element analysis successfully predicts the base shears during loading and unloading. However, the finite element model produces higher lateral loading and unloading stiffnesses than the experiment. This difference can be attributed, in part, to the fact that the finite element model assumes no slip along the beam-web plate interface, whereas the web plate and the beam of the test specimen are fastened using bolts that might induce slip at the beam-web plate connection and result in a lower lateral

stiffness. Similarly, the difference in the lateral stiffness might be related to the difference between the initial imperfections in the test specimen and in the continuum model. As discussed by Qu et al. [30] and other researchers [31–33], the influence of the initial imperfection on the base shear and the lateral stiffness is more prominent for lower drifts whereas the influence tends to diminish with increasing drifts. As seen in Fig. 5, the lateral stiffness shows a relatively better agreement with the experiment results for higher drifts compared to the trend observed for lower drifts.

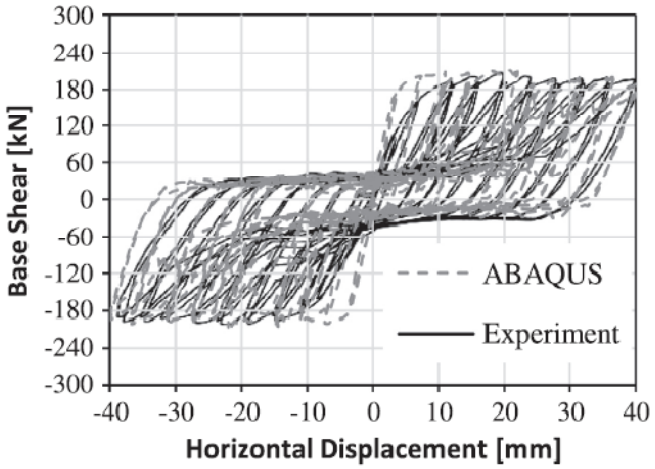

Figure 5. Base shear vs. displacement of the experiment (adapted from Guo et al.[19]) and the ABAQUS model.

STUDY OF PARTIAL TENSION FIELD INCLINATION ANGLE

For SPSWs with infinitely flexible columns Thorburn et al. [1] derived an equation (Eq. (12)) to calculate the strip orientation angle, θ, where the non-dimensional inclination angle parameter, γ, was given as 0.5 assuming that the PTF orients itself to resist the maximum shear force.

$$\theta = \gamma \tan^{-1}(L/H) \tag{12}$$

This equation can be extended to calculate θ of the strip model for beam-connected web plates; however, γ must be verified and/or calibrated since the γ of 0.5 was based on the following assumptions that may not hold true for B-SPSW strip models: (1) in Thorburn et al.'s model [1], the web plate was assumed to be restrained against out-of-plane deformations along the column edges; however, the vertical edges of beam-connected web plates are free to deform out-of-plane, which might affect θ. (2) Thorburn et al. [1] did not account for the change in θ_t with θ_r, which could be notable at large drift demands. (3) When strips are defined based on an assumed θ, L_p remains constant; whereas in a real web plate or in a continuum model the extent of the PTF change as the orientation of PTF changes with increasing drifts. A proposed strip model should account for this fact to ensure that the proposed θ, and thus the assumed L_p, is representative of web plate behavior at larger drifts. Choi and Park [34] also provided an approximate expression for γ given by $\gamma = [0.65 - 0.04(L/H)]$ based on the principle of least work applied to B-SPSWs with stiffeners along the free edges. Similar to Thorburn et al.'s model [1], Choi and Park [34] did not consider the difference between θ_t and θ observed for a strip model and also assumed no out-of-plane deformation along the stiffened free edge of the web plate.

A numerical parametric study is undertaken using the previously described continuum finite element model to estimate θ for the beam-connected web plate strip model, considering the fact that θ_t changes with θ_r and L_p remains constant for a strip model. In this study web plate aspect ratios ranging between 0.8 and 2.5 are investigated, corresponding to the limits given in SPSW design [13]. H is selected as 4.06 m (160") for all analyses, and L is altered as aspect ratio changes.

Because the proposed strip model assumes lateral load is resisted only by the PTF, a thin plate with a tw of 2.75 mm (0.108") is used in this study to eliminate the possible

effects of shear buckling strength on θ. The contribution of shear buckling strength in thicker web plates will be considered in the following parametric study for defining the non-negligible compressive resistance of web plate strips. Note that the tw of 2.75 mm (0.108") is chosen here to represent thin plates used in real steel construction applications. Results from the analyses with 2.75 mm (0.108") thick plates are similar to those of thinner plates with even lower, near zero, shear buckling capacities (results from the thinner plates are not presented here for brevity), suggesting that the 2.75 mm (0.108") plate is suitable for this study of PTF inclination angle. Each model is pushed monotonically up to a θ_r of 2.5%.

For each analysis, ω_x, ω_y, and moment (M) diagrams are plotted for both top and bottom beams at θ_r of 0.5, 1.0, 1.5, 2.0, and 2.5%. To facilitate estimation of θ, the distributed load and moment diagrams are normalized by the terms that are constant with respect to θ to produce non-dimensional parameters. Typical plots for the top beam of a B-SPSW with an aspect ratio of 1.4 at a θ_r of 1.5% are given in Fig. 6. From the ω_y distribution plots (Fig. 6(b)) L_p is taken as the extent over which the normalized ω_y is larger than 0.5. Over the estimated L_p, average values for the normalized ω_x and ω_y are determined as shown in Fig. 6(a) and Fig. 6(b), respectively. M_m, x, P_l, and P_r are determined from analysis results. The values of L_p, M_m, P_l, P_r, x, ω_x, ω_y determined from analysis for both the top and bottom beams, along with the associated web plate material properties, web plate geometry, and θ_r, are plugged into Eqs. (4)–(9) to produce twelve estimates of θ for a given L/H and θ_r. γ values are obtained for each h estimate using Eq. (12).

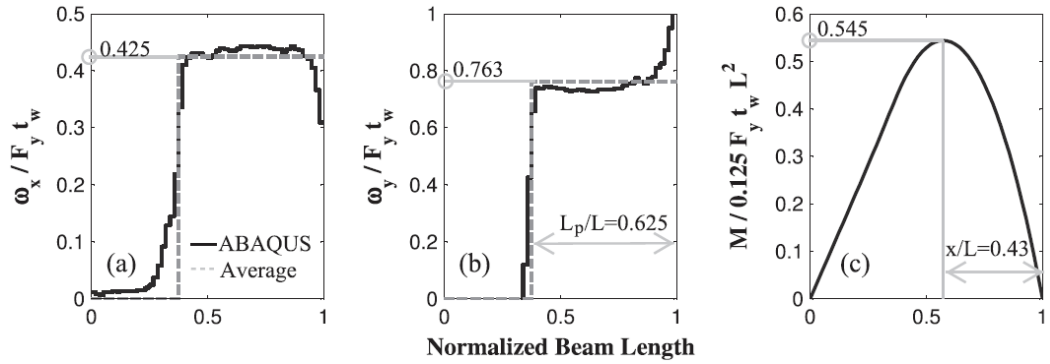

Figure 6. Force diagram of top beam at a drift of 1.5% (L/H=1.4)

Fig. 7 shows the average of twelve γ values given for various aspect ratios and θ_r values. The γ values provided by Thorburn et al. [1] and Choi and Park [34] are also shown in Fig. 7 for comparison purposes. As can be seen in Fig. 7, the γ values determined at 0.5% drift are higher than those at larger drift demands. This difference can be attributed to the fact that Eqs. (6)–(8) assume a uniform stress distribution of F_y along the entire PTF; however, at early drifts, although much of the PTF in the web plate is yielded, some portions of the PTF have not reached F_y. Another observation in Fig. 7 is that as the drifts increase the γ values decrease at a smaller rate, converging to a γ value slightly larger than the 0.5 assumed by Thorburn et al. [1], particularly for aspect ratios greater than 1.2. Based on Fig. 7, an equation for c (Eq. (13)) is proposed using regression analysis excluding the data for θ_r of 0.5%.

$$\gamma = 0.55 - 0.03\,(L/H) \geq 0.51 \tag{13}$$

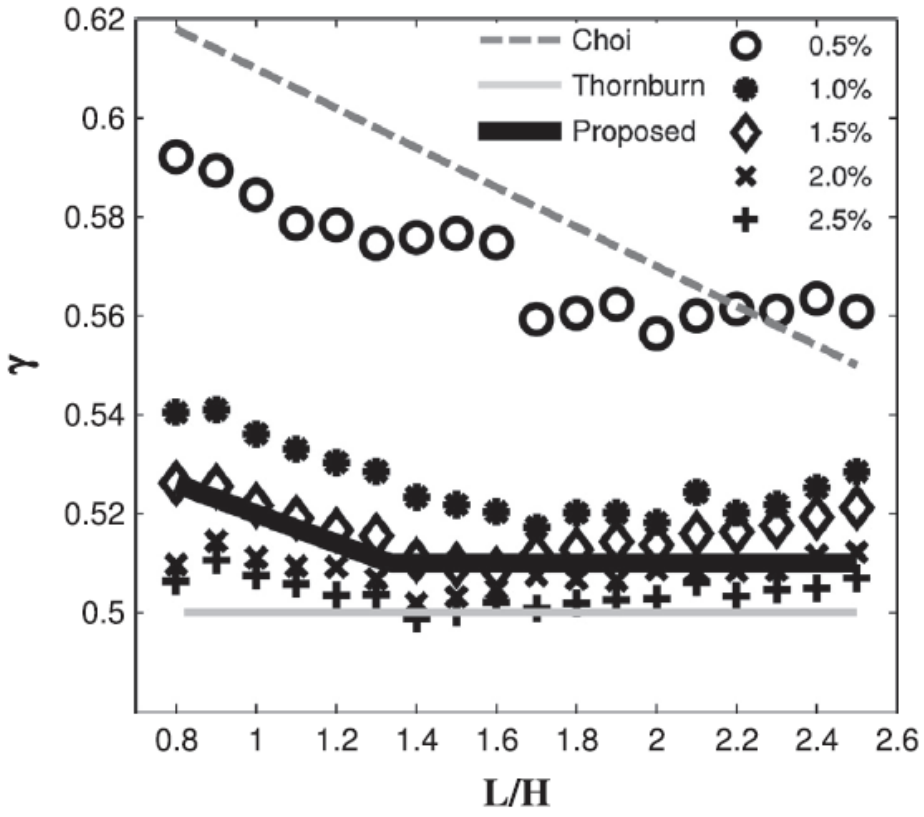

Figure 7. Average γ values for various drifts

The ratios of beam and column demands and base shear obtained from Eqs. (6)–(8) and (10) to those obtain from ABAQUS [28] are tabulated in Table 1. Results indicate that θ calculated using Eqs. (12) and (13) predicts M_m, P_l, P_r, and V_{bs} successfully. Results for those equations at θ_r of 0.5% are slightly higher than finite element analysis results due to the assumption in the equations that the entire PTF has yielded, which was inconsistent with finite element results as described previously. At drifts over 1%, all equation to finite element ratios are very close to unity, indicating that the proposed γ equation (Eq. (13)) for determining θ is applicable for predicting web plate strength and boundary frame demands at drifts expected under seismic loading.

Table 1. Beam Moment, Column Axial Load, and Base Shear Ratios at Various Drifts (Equation to ABAQUS Ratios)

			M_m (bottom beam)			M_m (top beam)			P_l			P_r			V_{bs}		
	Eq.13	Eq.12	Drift			Drift			Drift			Drift			Drift		
L/H	γ	θ(°)	0.5%	1.5%	2.5%	0.5%	1.5%	2.5%	0.5%	1.5%	2.5%	0.5%	1.5%	2.5%	0.5%	1.5%	2.5%
0.8	0.526	20.3	1.26	1.02	0.98	1.27	1.02	0.98	1.44	1.08	1.02	1.06	0.95	0.93	0.92	0.90	0.90
1.1	0.517	24.7	1.25	1.03	0.99	1.25	1.03	0.99	1.39	1.06	1.01	1.08	0.97	0.94	0.94	0.92	0.92
1.4	0.510	27.8	1.25	1.04	1.01	1.25	1.04	1.01	1.36	1.07	1.02	1.10	0.98	0.96	0.95	0.93	0.93
1.7	0.510	30.4	1.25	1.05	1.02	1.25	1.05	1.02	1.35	1.08	1.03	1.11	0.99	0.97	0.96	0.94	0.93
2.0	0.510	32.4	1.27	1.06	1.02	1.27	1.06	1.02	1.36	1.08	1.03	1.13	1.00	0.97	0.96	0.94	0.94
2.3	0.510	33.9	1.30	1.07	1.02	1.30	1.07	1.02	1.38	1.09	1.02	1.16	1.01	0.98	0.97	0.95	0.94
2.5	0.510	34.8	1.33	1.08	1.02	1.33	1.08	1.03	1.41	1.09	1.03	1.18	1.02	0.98	0.98	0.95	0.94
		Average	1.27	1.05	1.01	1.27	1.05	1.01	1.38	1.07	1.02	1.12	0.99	0.96	0.96	0.93	0.93
		Std. Dev.	0.02	0.02	0.02	0.02	0.02	0.02	0.03	0.01	0.01	0.03	0.02	0.02	0.02	0.01	0.01

Note that Eqs. (12) and (13) are functions of only L/H and independent of F_y and t_w. The form of these equations is adopted from the previous research [1,34] and found to be consistent with the parametric analysis results. The equation of the inclination angle of TFA for conventional SPSWs given in the AISC Seismic Provisions [13] is also independent of F_y, and is a function of the ratios of t_w to the cross-sectional properties of the boundary elements (area of the beam, area of the column, and inertia of the beam) rather than a direct function of t_w. These ratios converge to zero for stiff boundary elements and the equation of the inclination angle becomes independent of t_w. Similarly, Webster et al. [15] stated that the inclination angle after yielding is 45 degrees regardless of the geometry and material properties for conventional SPSWs. It is also worthwhile noting that θ proposed by Thorburn et al. [1], which is similar to θ proposed herein, showed a good agreement with the experiments of beam-only connected as reported by Vatansever and Yardimci [20] and Clayton et al. [21]. Consequently, Eq. (12) and (13) can estimate θ accurately considering only L/H and serve practical uses better since these equations need no iterations with the change in the web plate design.

STUDY OF STRIP COMPRESSIVE STRENGTH

Compressive strength of SPSW web plates is commonly neglected since normally proportioned web plates typically have limited shear buckling strength. However, recent research [25,27] has shown that the compressive resistance of SPSW web plates can be significantly larger than the shear buckling strength. This compressive resistance becomes more significant for thicker web plates, which may be more prominent in B-SPSWs. Compared to SPSWs, B-SPSWs require thicker web plates to resist the same lateral load due to the fact that (1) the entire web plate in a SPSW is engaged in full TFA, whereas only a portion of the beam-connected web plate of B-SPSWs is engaged in the

PTF, and due to (2) the difference between inclination angles of B-SPSW and SPSW tension fields. As seen from Table 1, θ values for B-SPSWs are between 20 and 35 degrees for typical aspect ratios, resulting in lower horizontal components of the PTF compared to the approximately 45 degree inclination angle for SPSW TFA [13–15]. For web plate design, the web plate lateral load capacity, V_y, can be calculated using Eq. (14), which conservatively neglects the potential compressive resistance of the web plate and the changes in tension field inclination at increasing drifts. Based on this design equation, the ratio of B-SPSW to SPSW web plate thicknesses required for the same lateral demand is given in Fig. 8 [21]. For SPSWs, L_p is replaced by L in Eq. (14) due to full TFA and θ is assumed as 45 degrees.

$$V_y = 0.5\, F_y t_w L_p \sin 2\theta \tag{14}$$

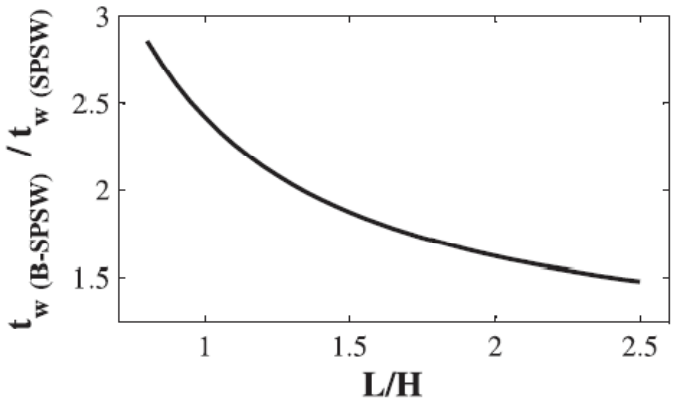

Figure 8. Ratio of B-SPSW to SPSW web plate thickness

As seen in Fig. 8, B-SPSWs require web plates from 1.5 to three times as thick as SPSWs to resist the same load for the same aspect ratio; therefore, the compressive strength of B-SPSW web plates might become more significant. Although it is a

conservative assumption to ignore the compressive strength of web plate in design, accounting for the additional capacity provided by the web plate in compression might lead to material savings. Further, the compressive demands affect unloading and reloading hysteretic behavior of the web plate, which are important to account for in nonlinear response history analyses. Hence there is a need for investigating the compressive strength of strips.

To simulate the compressive behavior of the web plate, an additional material with compression resistance can be added in parallel to the tension-only material generally assumed for thin web plate strip models. Fig. 9 shows normalized stress (σ/F_y) vs. normalized strain ($\varepsilon/\varepsilon_y$) for various materials that are employed in the proposed strip model. As shown in Fig. 9(a), tension-only web plate behavior is generally modeled using a pinched material [7] for which tensile stresses do not develop until reaching the maximum plastic strain from previous cycles. An elasto-plastic material can be used to model the compressive strength of strips as shown in Fig. 9(b), since the compressive web plate resistance contribute to its strength during loading and unloading. Both of these material behaviors can be easily implemented in a wide range of commercially-available analysis software. These two material models can be used in parallel (Fig. 9(c)) to model a strip with compressive strength, β, where β is defined as the ratio of compressive strength of the strip to the yield strength, F_y, of the web plate material.

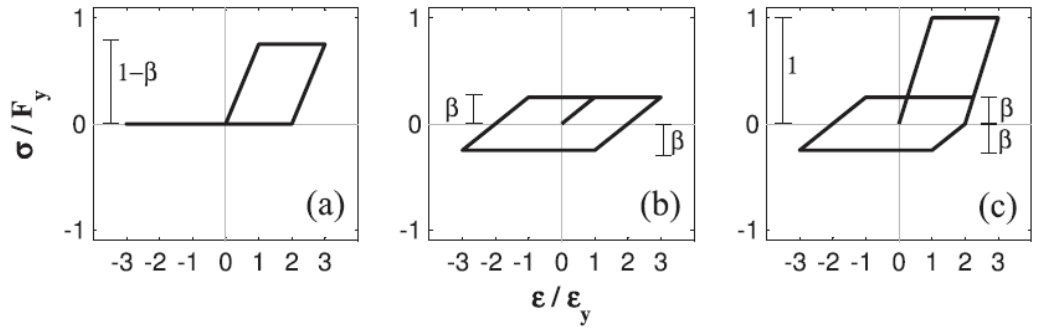

Figure 9. Material models for strips: (a) pinched tension-only material, (b) elasto-plastic tension-compression material, and (c) resulting strip response when (a) and (b) are used in parallel.

Fig. 10 shows the normalized base shear (V/V_y, where V_y is calculated per Eq. (14)) vs. normalized drift (Δ/Δ_y, where Δ_y is the drift at yield) for a typical B-SPSW strip model in which strips are oriented in both PTF directions (as shown in Fig. 3) with strips employing the parallel material given in Fig. 9(c). As seen in Fig. 10 for a beam-connected web plate strip model, the normalized maximum base shear during loading and unloading are $1 + \beta$ and 2β, respectively. During lateral sway as shown in Fig. 3, the set of strips in tension reaches F_y; whereas the strips oriented in the other direction can resist stresses up to βF_y in compression. Because the strips oriented in both PTF directions have the same total cross-sectional area, the maximum normalized base shear during loading is $1 + \beta$ (as opposed to the case of 1 that is observed for tension-only strips), indicating that web plate compressive resistance does contribute to larger lateral load capacity as will be verified in finite element analyses presented later. During unloading, previously yielded strips in tension develop compressive stresses and previously compression-resisting strips develop tensile stresses up to βF_y prior to development of the PTF in the opposite loading direction resulting in a normalized maximum base shear of 2β during unloading.

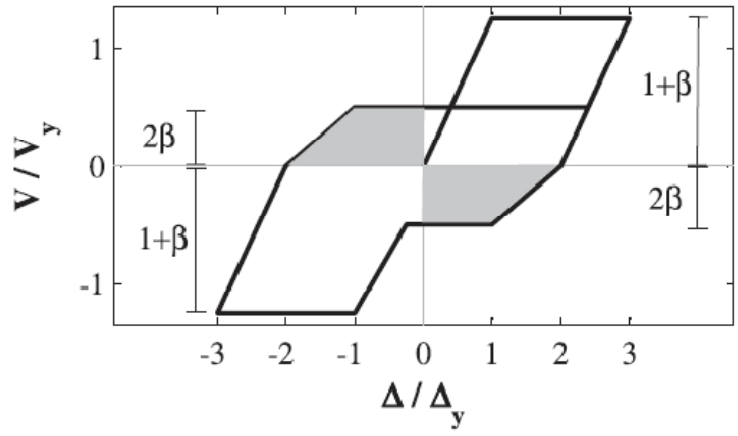

Figure 10. Normalized base shear vs. normalized drift for a typical B-SPSW.

A parametric numerical study is undertaken to determine β from beam-connected web plates of varying thicknesses and aspect ratios. Cyclic pushover analyses are performed in ABAQUS [28] using the cyclic drift history given in Fig. 11. The model details used to determine γ are also used for the determination of β; however, several web plate thicknesses (1.27 mm, 2.54 mm, 6.35 mm, 12.7 mm, 19.1 mm, and 25.4 mm) are selected instead of a thin plate assumed in the previous analyses. As a result, B-SPSWs with aspect ratios between 0.8 and 2.5 and with height-to-thickness ratios between 160 and 3200 are analyzed, which covers a wide range of applications. The maximum base shear during loading, V_t, and the base shear during unloading, V_r, are determined from finite element analysis results. Using the ratio of V_r to V_t obtained from finite element analysis and the normalized maximum base shear for both loading and unloading expected for idealized strip model (Fig. 10), β can be calculated by using Eq. (15).

$$\frac{2\beta}{1+\beta} = \frac{V_r}{V_t} \tag{15}$$

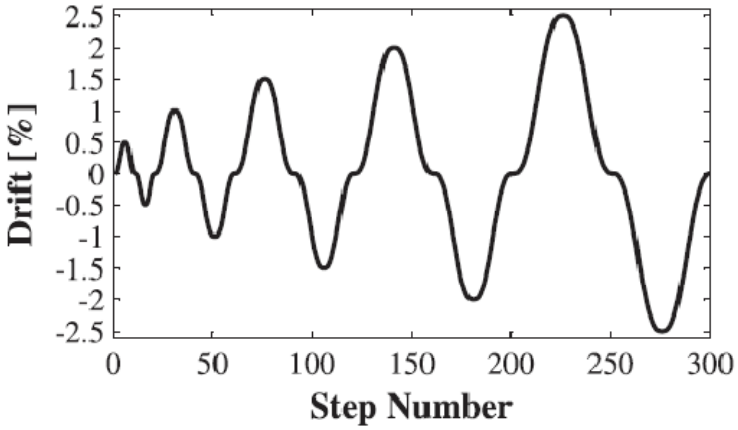

Figure 11. Cyclic drift amplitudes.

V_t is taken as the peak base shear during the 1.5% drift cycle loading to avoid local peaks in base shear that occur in the first cycles due to shear buckling strength of web plate that vanishes in the following cycles where only residual buckling strength is observed. V_r is taken as the average base shear during unloading from all cycles by integrating the area under base shear vs. drift in the unloading region and dividing by the corresponding drift range over which the integration was done. The unloading region used for the integration is defined as the region on the base shear vs. drift where the base shear and the drift are opposite in sign. The shaded regions in Fig. 10 show the unloading region for one cycle.

Fig. 12 shows data points for β calculated for various H/t_w values. As seen from Fig. 12, lower H/t_w values yield higher β values as expected. For thick plates β can be as high as 25%, which if accounted for in design would result in almost 20% reduction in plate thickness compared to the designs that assume tension-only plate behavior. Similarly, considering β (especially for thick plates) in a strip model can contribute significantly to energy dissipation capacity during cyclic or response history analyses that is not accounted for in the tension-only strip model. Eq. (16) gives an approximate

expression for β, determined using regression analysis of the data from the finite element analyses, that is also plotted for various H/t_w values in Fig. 12.

$$\beta = -0.04 + 0.02\,(L/H) + \frac{2.75}{\sqrt{H/t_w}} \geq 0 \tag{16}$$

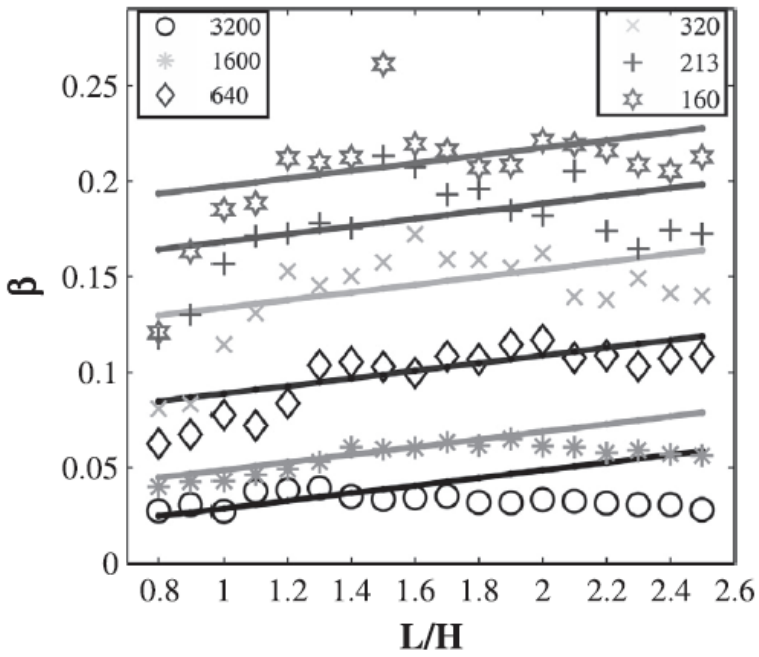

Figure 12. β for various height-to-thickness ratios.

Although the approximate β values do not fit all data points precisely, the error in β estimation does not lead to significant error in response. For example, Fig. 13 shows a comparison of normalized base shear vs. drift response of strip models plotted for β obtained by using finite element analysis results (β = 0.261) and for β estimated by using Eq. (16) (β = 0.207) for L/H of 1.5 and H/t_w of 160. Note that from Fig. 12, this model (L/H = 1.5 and H/t_w = 160) represents the ‘‘worst case” where the deviation in the actual (from finite element) and predicted (from Eq. (16)) β values is largest, and as seen in Fig.

13, the estimated β still provides a reasonable approximation of web plate response. A second set of parametric analyses is conducted to test the validity of Eq. (16) using a web plate yield strength and height different than those assumed in the calibration models. Using a lower F_y (165 MPa) and taller H (8.13 m), the parametric analyses reveal that Eq. (16) predicts β within ± 0.034 of those determined from analysis. This magnitude of deviation between predicted and actual β is less than the deviation of β shown in Fig. 13, indicating that the predicted β is able to capture web plate behavior with acceptable accuracy for model parameters different than those considered in the calibration.

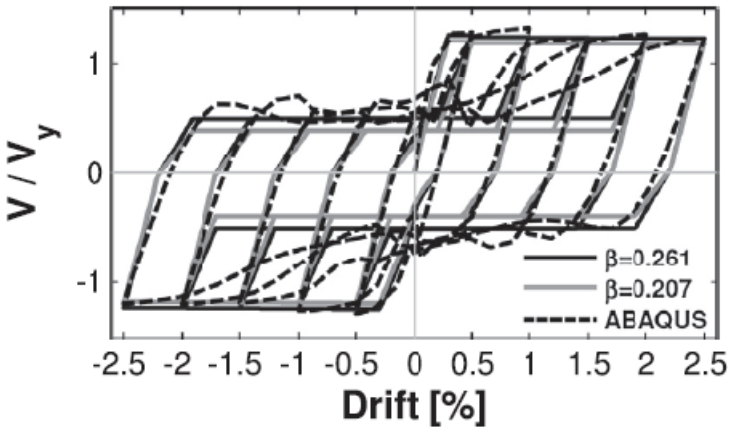

Figure 13. Effect of the difference between calculated and estimated β on base shear.

STUDY OF SENSITIVITY TO THE NUMBER OF STRIPS

The base shear capacity, lateral stiffness, and member demands of SPSWs are sensitive to n_s used in the strip models. For conventional SPSWs, some strips are connected to the columns on one end and to the beams on the other end whereas other strips are connected to the beams on both ends; therefore, adequate n_s should be used in the models to distribute the web plate forces between the beams and the columns accurately. B-SPSWs are less sensitive to n_s because all of the inclined strips of B-SPSWs are only connected to the beams. The equal length strips of B-SPSWs lead to the

same lateral stiffness regardless of n_s assuming the beams have enough flexural stiffness to develop a uniform σ_w. Similarly, the base shear capacity and the column axial load demands remain the same regardless of n_s since the beams of B-SPSWs are statically determinate and the load center of σ_w does not change with n_s. The only parameter of B-SPSWs that is sensitive to n_s is the maximum moment in the beams.

The influence of n_s on M_{max} is observed in the parametric study to assess the sensitivity to n_s. For the parametric study, five aspect ratios (0.8, 1.2, 1.6, 2.0, and 2.4) and seven n_s (5, 7, 9, 15, 25, 50, and 100) in each direction are considered. The B-SPSWs are monotonically pushed to a roof drift of 1.5%. F_y, H, and t_w are selected as 248 MPa, 4.06 m, and 1 mm, respectively. The maximum beam moments (M_{max}) normalized with respect to M_{max} of the corresponding model with 100 strips and the run times of the analyses are given in Fig. 14(a) and Fig. 14(b), respectively. The results appear to indicate that nine strips provide accurate estimates for M_{max}, within 4–6% of the models with 100 strips, with no significant computational expense. Note that as aspect ratio increases, the accuracy of M_{max} estimate decreases. This situation can be attributed to the fact that the ratio of L_p to L increases with increasing aspect ratio, which means that each strip represents loading over a larger proportion of L_p /L. Hence, it is deemed appropriate to increase n_s for larger aspect ratios to obtain more accurate results. Note that a minimum of 10 strips in each direction is required for conventional SPSWs by the AISC Seismic Provisions [13] and CSA-S16-09 [14]. Accordingly, the code limit of a minimum of 10 strips is sufficient to represent the web plates of BSPSWs while the use of more strips is recommended for the wider web plates to improve the accuracy.

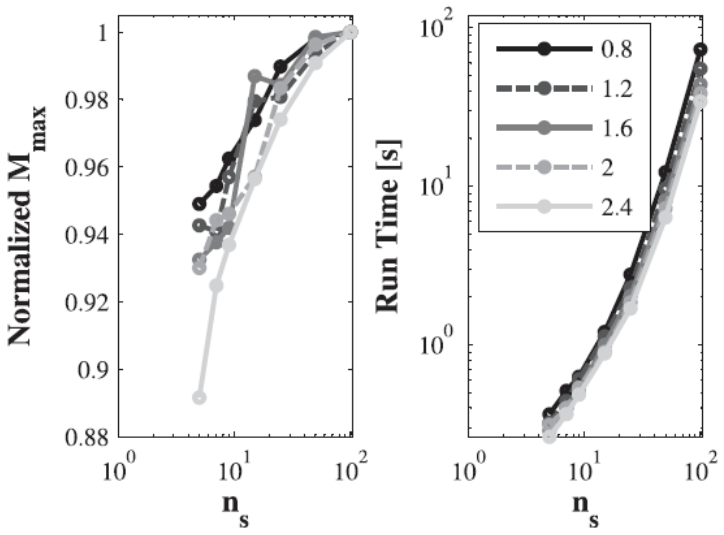

Figure 14. Influence of the number of strips on (a) maximum beam moment and (b) run time.

COMPARISON OF B-SPSWS MODELS

B-SPSWs with various aspect ratios and height-to-thickness ratios analyzed earlier in ABAQUS [28] for the compressive strength parametric study are modeled using the proposed tension-compression (TC) strip model and the tension-only (TO) strip model proposed by Thorburn et al. [1]. The strip models are analyzed in OpenSEES [35] under cyclic drift amplitudes given in Fig. 11. For TC models, γ and β are calculated using Eqs. (13) and (16), respectively; whereas in the TO models, γ is taken as 0.5 and compressive strength of strips is assumed to be negligible, i.e., β is zero, per Thorburn et al.'s proposed model [1]. The proposed strip material for the TC models is implemented in OpenSEES [35] using the built-in Hysteretic material for the pinched tension-only response (Fig. 9(a)) and Steel01 for the elastoplastic material (Fig. 9(b)) combined in parallel (Fig. 9(c)). For the TO models, only the tension-only Hysteretic material (Fig. 9(a)) is adopted. For both TC and TO models, elastic beam-column elements with a very stiff material are used for the boundary elements, and corotational truss elements are used

for the web plate strip model. L_p and A of the TC and TO models are determined by using Eqs. (5) and (11), respectively, for the corresponding θ calculated by using Eq. (12). A typical model is shown in Fig. 3 and a flowchart is provided in Fig. 15 to illustrate the modeling procedure for the TC model.

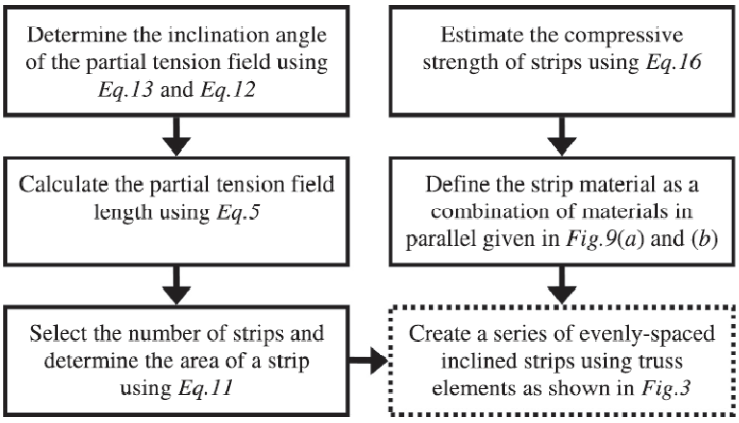

Figure 15. Modeling flowchart for the proposed (TC) model.

Results from the strip models (TC and TO) and the finite element models (FEM) are compared in terms of column and beam demands, base shear capacity, and energy dissipation capacity of B-SPSWs. Comparison of normalized base shears from the three models with an aspect ratio of 1.5 and various height-to-thickness ratios is given in Fig. 16. For thinner web plates (higher H/t_w), both TO and TC closely match FEM results owing to the fact that compressive strength of strips is almost negligible for thin plates. All three models yield a normalized base shear capacity close to 1 and a normalized unloading base shear close to 0 as expected. For thicker plates, TO does not match FEM whereas TC still shows a very similar response as the FEM results. As thicker plates are used, TC is able to predict peak capacities relatively accurately; however, it does tend to underestimate web plate strength during unloading and reloading. This unloading and

reloading response only affects the energy dissipation capacity but does not affect peak column and beam demands as will be discussed later.

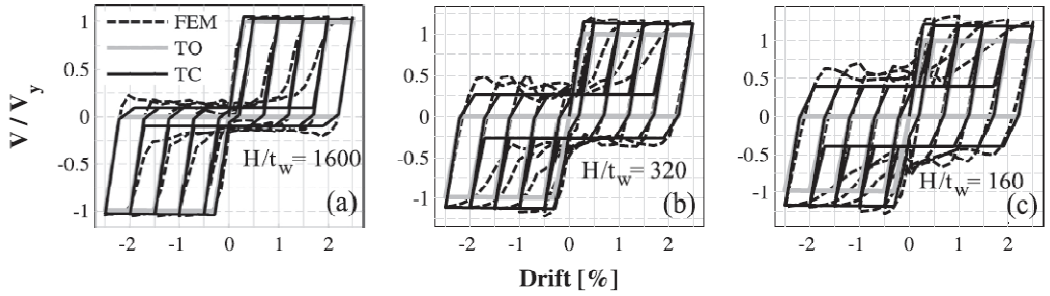

Figure 16. Comparison of normalized base shear vs. drift ratio for a L/H of 1.5.

Energy dissipation (E) is determined by integrating the base shear vs. displacement response for each of the models. These values are normalized with respect to total energy dissipated in FEM (E_{max}) and are compared in Fig. 17 for a L/H of 1.5 and H/t_w of 160. For reasons explained above, the TC model underpredicts energy dissipation by approximately 20% for thicker plates compared with FEM results; however, the TO model underestimates energy dissipation by 75% for the same plate thickness compared to FEM results. Tables 2 and 3 tabulate the ratio of E to E_{max} for various aspect and height-to-thickness ratios for TC and TO models, respectively. As seen in Table 3 TO models can dissipate 52% of E_{max} (on average) for thinner plates (H/t_w of 1600) and 25% of E_{max} (on average) for thicker plates (H/t_w of 160); whereas TC models can dissipate 84% of E_{max} (on average). Hence it can be concluded that although TC models do not dissipate as much energy as the FEM, the TC model shows a great improvement in simulating beam-connected web plate behavior compared to the existing TO model in terms of energy dissipation capacity. Furthermore, the underprediction of energy

dissipation can be considered conservative when used in nonlinear response history analyses.

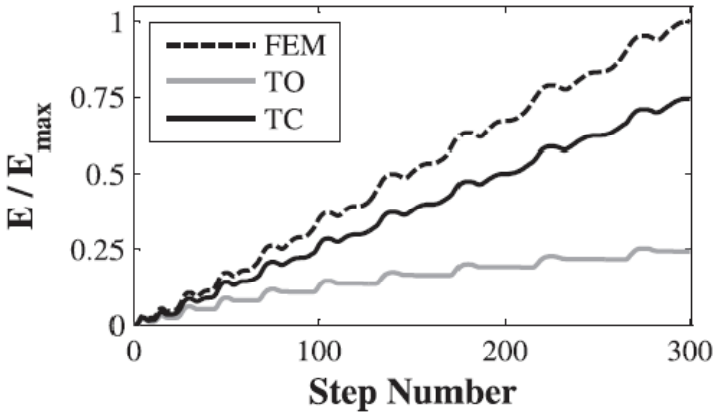

Figure 17. Comparison of normalized strain energy for L/H of 1.5 and H/t_w of 160.

Table 2. Beam Moment, Column Axial Load, Base Shear, and Energy Ratios (TC Model to ABAQUS Ratios)

			M_{max} (bottom beam)			M_{max} (top beam)			P_{max}			V_t			E		
	Eq.13	Eq.12	H/t_w			H/t_w			H/t_w			H/t_w			H/t_w		
L/H	γ	θ(°)	160	320	1600	160	320	1600	160	320	1600	160	320	1600	160	320	1600
0.8	0.526	20.3	0.92	0.97	1.04	0.91	0.97	1.03	0.89	0.94	1.03	0.76	0.88	0.95	0.71	0.88	0.82
1.1	0.517	24.7	1.16	1.06	1.06	1.05	1.05	1.06	0.96	0.98	1.04	0.89	0.92	0.96	0.75	0.76	0.81
1.4	0.510	27.8	1.03	1.16	1.04	1.03	1.16	1.04	0.94	1.05	1.03	0.92	0.98	0.99	0.78	0.79	0.84
1.7	0.510	30.4	1.17	1.14	1.04	1.19	1.11	1.04	1.08	1.03	1.04	0.96	0.98	0.99	0.80	0.80	0.81
2.0	0.510	32.4	1.12	1.12	1.03	1.17	1.15	1.03	1.06	1.07	1.03	0.99	1.01	1.00	0.83	0.83	0.84
2.3	0.510	33.9	1.07	1.16	1.05	1.14	1.15	1.05	1.05	1.06	1.03	1.01	1.02	0.99	0.95	0.92	0.90
2.5	0.510	34.8	1.09	1.17	1.05	1.17	1.18	1.04	1.05	1.07	1.02	1.01	1.01	1.01	0.94	0.94	0.90
		Average	1.09	1.09	1.04	1.10	1.09	1.04	1.01	1.03	1.04	0.94	0.98	0.98	0.82	0.84	0.85
		Std. Dev.	0.07	0.06	0.02	0.08	0.06	0.02	0.06	0.04	0.01	0.07	0.04	0.02	0.08	0.06	0.04

Table 3. Beam Moment, Column Axial Load, Base Shear, and Energy Ratios (TO Model to ABAQUS Ratios)

			M_{max} (bottom beam)			M_{max} (top beam)			P_{max}			V_t			E		
		Eq. 12	H/t_w			H/t_w			H/t_w			H/t_w			H/t_w		
L/H	γ	θ (°)	160	320	1600	160	320	1600	160	320	1600	160	320	1600	160	320	1600
0.8	0.500	19.3	1.13	1.16	1.15	1.13	1.16	1.15	1.02	1.06	1.12	0.60	0.78	0.92	0.26	0.41	0.57
1.1	0.500	23.9	1.45	1.24	1.15	1.31	1.23	1.14	1.09	1.08	1.10	0.64	0.80	0.94	0.24	0.30	0.54
1.4	0.500	27.2	1.31	1.37	1.13	1.31	1.38	1.13	1.07	1.15	1.09	0.76	0.82	0.94	0.23	0.30	0.51
1.7	0.500	29.8	1.48	1.37	1.14	1.51	1.34	1.14	1.23	1.15	1.10	0.77	0.87	0.95	0.27	0.33	0.51
2.0	0.500	31.7	1.44	1.35	1.14	1.51	1.38	1.14	1.21	1.19	1.09	0.79	0.88	0.95	0.27	0.33	0.50
2.3	0.500	33.3	1.36	1.36	1.12	1.45	1.36	1.12	1.21	1.17	1.09	0.82	0.88	0.96	0.28	0.35	0.53
2.5	0.500	34.1	1.53	1.41	1.15	1.53	1.42	1.15	1.24	1.21	1.09	0.84	0.89	0.96	0.29	0.35	0.48
		Average	1.39	1.31	1.14	1.41	1.30	1.14	1.15	1.13	1.10	0.75	0.84	0.94	0.25	0.33	0.52
		Std. Dev.	0.10	0.09	0.02	0.12	0.09	0.02	0.08	0.06	0.01	0.08	0.04	0.01	0.02	0.03	0.03

The ratios of maximum moment in beams (M_{max}), maximum axial compressive load in columns (P_{max}), and V_t of strip models to those of FEM are given in Tables 2 and 3 for TC and TO models, respectively. The TO model conservatively overestimates maximum beams and columns demands for all H/t_w values; however, member demands become overly conservative for thicker plates, especially for M_{max}. M_{max} of TO model can be up to 54% higher than M_{max} of FEM while P_{max} of TO model can be up to 25% higher than P_{max} of FEM. V_t of TO model shows a good agreement with V_t of FEM for thinner plates; however, V_t of TO model can be as low as 60% of V_t of FEM for thicker plates. These differences in member demands and base shear capacity can be mainly attributed to the negligible compressive strength assumption for the TO model. While resisting the lateral load, the strips in tension apply vertical distributed loads along the PTF length on one end of the beam, while the strips in compression apply a vertical distributed load in the opposite direction on the opposite end of the beam. This compression resistance not only increases the lateral load capacity of the system, but it also reduces member demands, which cannot be observed for the TO model. Thus, the TC model is able to predict member demands and base shear capacity accurately for various plate thicknesses. When the TC model predictions do deviate from the actual (FEM) results, the member demands tend to be conservatively overestimated and base shear prediction tends to be conservatively underestimated using the TC model. In brief, TC can be used to model B-SPSWs with a wide range of aspect ratios and height-to-thickness ratios, while to the TO model is only appropriate for B-SPSWs with very thin plates.

Finally, the 1/3 scale one-story one-bay B-SPSW tested by Guo et al. [19] is simulated using both the TO and TC models. The base shear vs. lateral displacement plot is given in Fig. 18(a). As seen in Fig. 18(a), the TC model successfully captures the base shears during loading and unloading whereas the TO model underestimates them. β given

in Eq. (16) significantly improves the capabilities of the TC model to predict the base shear capacities during loading and unloading. Note that H (1100 mm) and F_y (295 MPa) of the test specimen are different than those for which β is calibrated. Both the TC and TO models overestimate the lateral stiffness of the BSPSW. This difference can be attributed to the slip induced in the beam-web plate connection during testing and the initial imperfections in the web plate as discussed earlier for the continuum model.

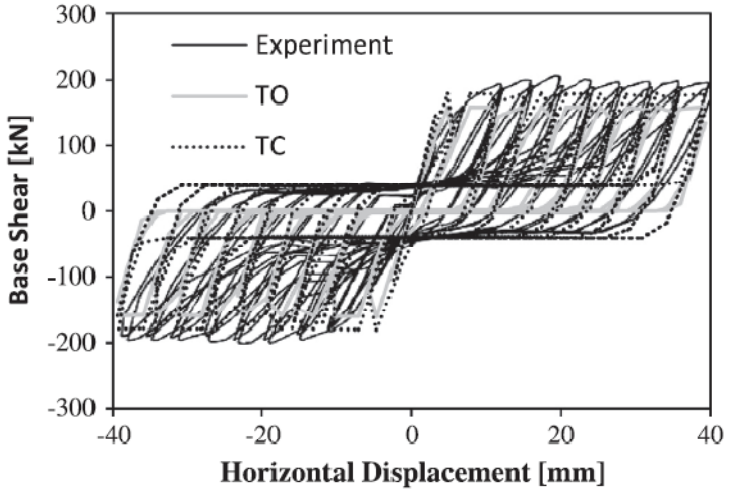

Figure 18. Base shear vs. displacement of the experiment (adapted from Guo et al. [19]) and the strip models.

CONCLUSION

In this study, a two-phase numerical study is undertaken to propose a strip model for B-SPSWs. The new strip model is based on the strip model proposed by Thorburn et al. [1]; however, two important parameters, namely inclination angle of the PTF and compressive strength of strips, are revisited. In the first phase of the study, B-SPSWs with various aspect ratios and thin web plates are analyzed in ABAQUS [28] under monotonic loading to develop an equation to predict the PTF inclination angle for B-SPSWs. In the second phase of the study, B-SPSWs with various aspect ratios and

various height-to-thickness ratios are analyzed in ABAQUS [28] under cyclic loading. Using the ratio of unloading base shear to maximum base shear obtained from finite element analyses, required strip compressive strength is determined as a proportion of the web plate yield strength. An approximate equation is provided for compressive strength of strips. A three-way comparison between the proposed strip model, the tension-only strip model presented by Thorburn et al. [1], and the finite element model is provided. Results appear to indicate that the proposed strip model shows a superior performance compared to Thorburn et al.'s model [1] from existing literature and matches finite element results accurately in terms of column and beam demands, base shear capacity, and energy dissipation capacity of B-SPSWs. Finally, the TC model and the TO model are compared with the experimental results [19]. Similar to the results of the parametric study, the TC model shows a better agreement with the experiment.

Use of the proposed strip model can be extended to investigate the seismic performance of multi-story B-SPSWs accurately without requiring computationally-expensive continuum finite element models. However, it is worthwhile noting that the proposed strip model assumes the beams have enough flexural stiffness to develop a uniform partial tension field. Further research is needed to investigate the stiffness limits of B-SPSWs' boundary elements. Although this study focuses on the web plate behavior of B-SPSWs, one should also note that consideration of web plate compressive strength in design might lead to significant material savings due to its contribution to the lateral shear resistance and the reduction in flexural beam demands and axial column demands. These findings suggest B-SPSWs may be a viable and cost-competitive earthquake-resistant system.

ACKNOWLEDGMENTS

This research was conducted at the University of Texas at Austin, and the first author was supported in part by the Fulbright Foreign Student Program. Any opinions, findings, conclusions, and recommendations presented in this paper are those of the authors and do not necessarily reflect the views of the sponsors.

REFERENCES

[1] Thorburn, L.J. Kulak, G.L. Montgomery CJ. Analysis of steel plate shear walls. Structural Engineering Report No. 107. University of Alberta. Edmonton, AB: 1983.

[2] Roberts TM, Sabouri-Ghomi S. Hysteretic characteristics of unstiffened perforated steel plate shear panels. Thin-Walled Struct 1992;14:139–51. doi:10.1016/0263-8231(92)90047-Z.

[3] Caccese V, Elgaaly M, Chen R. Experimental study of thin steel plate shear walls under cyclic load. J Struct Eng 1993;119:573–87. doi:10.1061/(ASCE)0733-9445(1993)119:2(573).

[4] Elgaaly M. Thin steel plate shear walls behavior and analysis. Thin-Walled Struct 1998;32:151–80. doi:10.1016/S0263-8231(98)00031-7.

[5] Lubell AS, Prion HGL, Ventura CE, Rezai M. Unstiffened steel plate shear wall performance under cyclic loading. J Struct Eng 2000;126:453–60. doi:10.1061/(ASCE)0733-9445(2000)126:4(453).

[6] Qu B, Bruneau M. Design of steel plate shear walls considering boundary frame moment resisting action. J Struct Eng 2009;135:1511–21. doi:10.1061/(ASCE)ST.1943-541X.0000069.

[7] Sabelli R, Bruneau M. Steel design guide: Steel plate shear walls. AISC; 2012.

[8] Basler K. Strength of plate girders in shear. Reprint No. 186 (61-13). Lehigh University Fritz Laboratory. Bethlehem, PA: 1961.

[9] Berman JW, Bruneau M. Capacity design of vertical boundary elements in steel plate shear walls. Eng Journal, AISC 2008;45:55–71.

[10] Driver RG, Kulak GL, Elwi AE, Kennedy DJL. FE and simplified models of steel plate shear wall. J Struct Eng 1998;124:121–30. doi:10.1061/(ASCE)0733-9445(1998)124:2(121).

[11] Shishkin JJ, Driver RG, Grondin GY. Analysis of steel plate shear walls using the modified strip model. J Struct Eng 2009;135:1357–66. doi:10.1061/(ASCE)ST.1943-541X.0000066.

[12] Guo L, Li R, Zhang S, Yan G. Hysteretic analysis of steel plate shear walls (SPSWs) and a modified strip model for SPSWs. Adv Struct Eng 2012;15:1751–64. doi:10.1260/1369-4332.15.10.1751.

[13] ANSI/AISC 341-10 Seismic provisions for structural steel buildings. Chicago, IL: AISC; 2010.

[14] CAN/CSA-S16-09 Design of steel structures. Mississauga, ON: Canadian Standards Association; 2009.

[15] Webster DJ, Berman JW, Lowes LN. Experimental investigation of SPSW web plate stress field development and vertical boundary element demand. J Struct Eng 2014;140:4014011.doi:10.1061/(ASCE)ST.1943-541X.0000989.

[16] Webster DJ, Berman JW, Lowes LN. The elastic and inelastic post-buckling behavior of steel plate shear wall web plates and their interaction with vertical boundary elements. Proc. Annu. Stab. Conf. Struct. Stab.Res. Counc., Grapine, TX: 2012.

[17] Clayton PM, Berman JW, Lowes LN. Subassembly testing and modeling of self-centering steel plate shear walls. Eng Struct 2013;56:1848–57. doi:10.1016/j.engstruct.2013.06.030.

[18] Berman JW, Bruneau M. Steel plate shear walls are not plate girders. Eng Journal, AISC 2004;41:95–106.

[19] Guo L, Rong Q, Ma X, Zhang S. Behavior of steel plate shear wall connected to frame beams only. Int J Steel Struct 2011;11:467–79. doi:10.1007/s13296-011-4006-7.

[20] Vatansever C, Yardimci N. Experimental investigation of thin steel plate shear walls with different infill-to-boundary frame connections. Steel Compos Struct 2011;11:251–71.

[21] Clayton PM, Berman JW, Lowes LN. Seismic performance of self-centering steel plate shear walls with beam-only-connected web plates. J Constr Steel Res 2015;106:198–208. doi:10.1016/j.jcsr.2014.12.017.

[22] Behbahanifard MR, Grondin GY, Elwi AE. Analysis of steel plate shear walls using explicit finite element method. 13th World Conf. Earthq. Eng., Vancouver, B.C.: 2004.

[23] Vian D, Bruneau M, Purba R. Special perforated steel plate shear walls with reduced beam section anchor beams II: Analysis and design recommendations. J Struct Eng 2009;135:221–8. doi:10.1061/(ASCE)0733-9445(2009)135:3(221).

[24] Moghimi H, Driver RG. Beam design force demands in steel plate shear walls with simple boundary frame connections. J Struct Eng 2014;140:4014046. doi:10.1061/(ASCE)ST.1943-541X.0000993.

[25] Clayton PM, Tsai C-Y, Berman JW, Lowes LN. Comparison of web plate numerical models for selfcentering steel plate shear walls. Earthq Eng Struct Dyn 2015;44:2093–110. doi:10.1002/eqe.2578.

[26] Xue M. Behavior of steel shear wall panels and frame-wall systems. Lehigh University, 1995.

[27] Webster DJ. The inelastic seismic response of steel plate shear wall web plates and their interaction with the vertical boundary members. University of Washington, 2013.

[28] ABAQUS. ABAQUS version 6.10 documentation. Simulia; 2010.

[29] JGJ 101-96 Specification of testing methods for earthquake resistant building (in Chinese). Beijing, China: Ministry of Construction of the people's Republic of China; 1996.

[30] Qu B, Sanchez-Zamora F, Pollino M. Mitigation of inter-story drift concentration in multi-story steel concentrically braced frames through implementation of rocking cores. Eng Struct 2014;70:208–17. doi:10.1016/j.engstruct.2014.03.032.

[31] Uriz P, Filippou FC, Mahin SA. Model for cyclic inelastic buckling of steel braces. J Struct Eng 2008;134:619–28. doi:10.1061/(ASCE)0733-9445(2008)134:4(619).

[32] Yang C-S, Leon RT, DesRoches R. Design and behavior of zipper-braced frames. Eng Struct 2008;30:1092–100. doi:10.1016/j.engstruct.2007.06.010.

[33] Ozcelik Y, Saritas A, Clayton PM. Comparison of chevron and suspended-zipper braced steel frames. J Constr Steel Res 2016;119:169–75.

[34] Choi I-R, Park H-G. Steel plate shear walls with various infill plate designs. J Struct Eng 2009;135:785–96. doi:10.1061/(ASCE)0733-9445(2009)135:7(785).

[35] Mazzoni S, Mckenna F, Scott MH, Fenves GL. OpenSees Command Language Manual 2006.

Appendix B

Paper 2. Seismic design and performance of SPSWs beam-connected web plates

Yigit Ozcelik, Patricia M. Clayton

Submitted to *Journal of Constructional Steel Research*

ABSTRACT

Steel plate shear walls with beam-connected web plates (B-SPSWs) are an alternative steel plate shear wall (SPSW) configuration in which the web plate edges are detached from the columns to avoid high flexural demands in the columns resulting from tension field action. Releasing the columns from the web plates results in development of a partial tension field instead of the full tension field observed in conventional SPSWs, which changes system behavior and member demands significantly. A numerical study is undertaken to assess the seismic performance of B-SPSWs designed for low-seismic regions. Equations for the web plate lateral strength and the beam axial force, shear force, and moment demands are provided. Following two design approaches, eighteen B-SPSWs possessing different geometric characteristics are designed based on the provided equations. Each B-SPSW is subjected to forty ground motions representing two seismic hazard levels. The seismic performance of these B-SPSWs is evaluated based on maximum interstory drifts, member demand-to-capacity ratios, and beam-column connection rotations. The results indicate that B-SPSWs show a promising seismic behavior and may be particularly attractive lateral force-resisting alternatives for regions of low and moderate seismicity.

KEYWORDS

Steel plate shear wall, Beam-connected web plate, Seismic performance, Low-seismic design, Nonlinear time-history analysis

INTRODUCTION

Experimental and numerical studies [1–6] have shown steel plate shear walls (SPSWs) to be a reliable earthquake-resistant system due to their high lateral stiffness, ductile behavior, and stable hysteresis characteristics. Web plates, which are typically connected to boundary elements (i.e., beams and columns) on all four sides, are the primary lateral load-resisting elements of SPSWs, where thin web plates are capable of providing high lateral stiffness and strength after shear buckling due to a mechanism called tension field action (TFA) [7]. To develop TFA and to utilize the post-buckling lateral strength and stiffness of the web plates, the web plates must be anchored to properly designed boundary elements with sufficient strength and stiffness to resist the pull-in forces resulting from TFA.

While the *AISC Seismic Provisions* (AISC 341-10) [8] allow the formation of plastic hinges at the beam ends and column bases for special SPSWs, in-span hinges in the beams and columns must be avoided as they can result in excessive deformations that limit formation of TFA and reduces lateral strength capacity [9,10]. The flexural demands in the intermediate-story beams resulting from TFA are typically not as severe as those in the columns due to the fact that the web plates of the stories above and below pull the beams in opposite directions and reduce the flexural demands. As long as web plates with similar thicknesses are provided at adjacent stories, which is the case for typical designs, the beam flexural demands due to TFA are relatively small. Flexural demands on the columns due to TFA, however, can be significant since the columns are pulled in by the web plates on only one side. As the building height increases, the combined axial and

flexural demands on the columns due to TFA and frame action can result in very large steel sections [11,12].

Over the past decades, several methods have been investigated to reduce the flexural demands in the columns of SPSWs. The methods can be categorized in three main groups: (1) reducing the flexural demands resulting from TFA by use of light gage web plates, low-yield-point web plate materials, and/or regular patterns of perforations in web plates [2,13–22]; (2) reducing the flexural demands resulting from frame action by introducing simple shear or partially-restrained moment connections at beam-column joints instead of fully-restrained moment connections and/or adopting reduced beam sections at the beam ends [3,9,10,23–30]; and (3) introducing an alternative SPSW configuration called SPSWs with beam-connected web plates (B-SPSW) where the web plates are connected to beams only and detached along column edges [1,26,27,31–34]. The focus of this study is on B-SPSWs with simple shear beam-column connections.

Past studies have been conducted to understand the behavior of B-SPSWs. Thorburn et al. [1] investigated the behavior of SPSWs with fully-connected web plates and the study was extended to SPSWs with infinitely flexible columns that show a similar behavior to B-SPSWs. Due to the limited or no restraint along the column edges in the plane of the web plate, the development of TFA was limited to some diagonal portion of the web plate between the top and bottom beams (Fig. 1), resulting in a partial tension field (PTF). Thorburn et al. [1] developed equations to calculate the lateral load capacity of the web plate and the inclination angle of the PTF, θ, and proposed a simplified analytical model, called the strip model, where the web plate is represented by a series of inclined tension-only trusses.

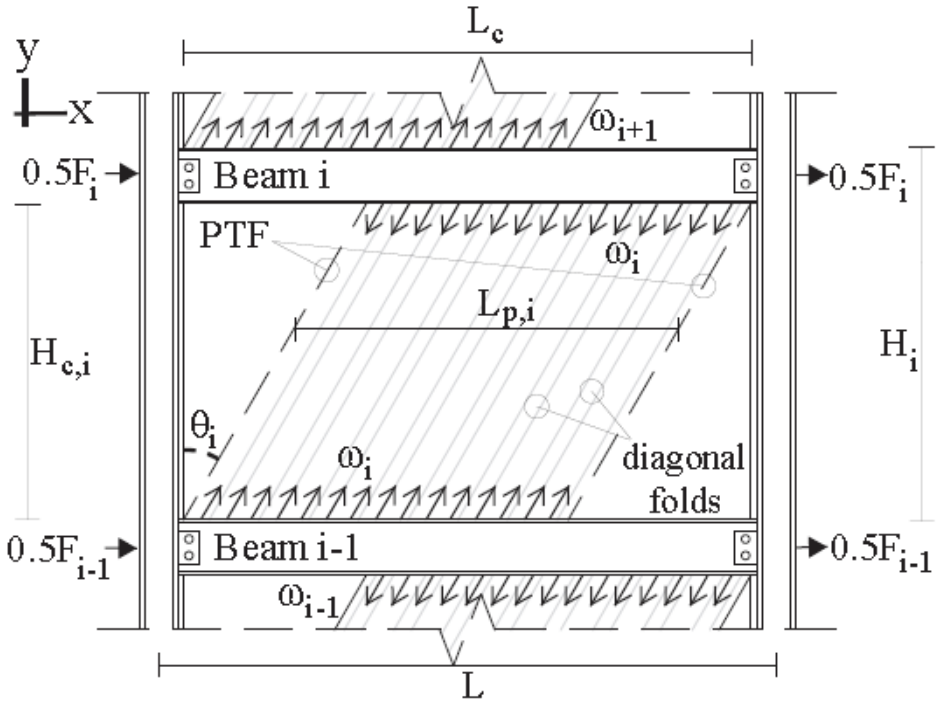

Figure 1. Development of partial tension field.

Xue [27] conducted a numerical study to compare the behavior of SPSWs with different column-web plate connectivity (connected or detached) and different beam-column connections (partial or full moment-resisting). Xue [27] adopted a finite element software ADINA to perform pushover analyses of the different SPSWs in which the web plates were modeled using shell elements and boundary elements were represented by elastic line elements. The results of the monotonic loading suggested that B-SPSWs with partial moment-resisting beam-column connections showed the most desirable overall lateral behavior in terms of the proper utilization and effective participation of the web plates to the lateral strength and stiffness; however, further investigation of the performance under cyclic and dynamic loading was recommended. An empirical equation was proposed to estimate the lateral load capacity of web plates; however, the

boundary element demands and the details of PTF such as the inclination angle and the extend of PTF were not discussed.

Guo et al. [32] tested two one-third scaled, one-story, one-bay B-SPSWs with true-pin beam-column connections. For one of the specimens, the free edges of the web plate were reinforced with stiffeners. The experimental study results suggested that B-SPSWs showed a ductile response with a large energy dissipation capacity. Although the stiffeners improved the energy dissipation capacity, there was no evident influence on the lateral load capacity and ductility. Numerical analyses were performed in a commercially-available finite element software ANSYS [35] in which the web plate, columns, and beams were modeled using shell elements. Based on the numerical study results, Guo et al. [32] proposed an empirical equation to estimate the lateral load capacity of web plates. Similar to Xue [27], Guo et al. [32] did not discuss the boundary frame member demands.

Vatansever and Yardimci [26] tested two one-third scaled SPSWs with partial moment-resisting beam-column connections. The web plate of the one of the specimens was connected to beams and columns while the web plate of the other specimen was free along the column edges, i.e., a beam-connected web plate. A unique connection was employed between the web plates and the boundary elements where the web plates were connected to the fish plates of the boundary elements with self-drilling screws. The results of the cyclic tests revealed that the BSPSW had a lower lateral load capacity and less energy dissipation compared to the SPSW with fully-connected web plates of the same thickness; therefore, the authors suggested that B-SPSWs would be a viable and economical option for retrofitting steel frames with inadequate stiffness and strength.

Clayton et al. [31,36–38] investigated self-centering SPSWs with post-tensioned moment-resisting beam-column connections (SC-SPSWs) and compared the behavior of

SC-SPSWs with beam-connected and fully-connected web plates. The highlights of the experimental and analytical studies can be listed as follow: (1) Detaching the web plates along the column edges resulted in a delayed initiation and propagation of web plate tearing for this particular system. (2) For the same lateral load demand, SC-SPSWs with beam-connected web plates requires web plates from 1.5 to 2.5 times as thick as SC-SPWs with fully-connected web plates for typical aspect ratios. (3) Three- and nine-story SC-SPSWs designed with beam-connected web plates had lower total steel weight of the SPSW elements compared to SC-SPSWs with fully-connected web plates designed for the same lateral loads, and the reduction in steel weight was more prominent for taller SC-SPSWs.

Much of the past work on SPSWs, including the aforementioned work on B-SPSWs, has focused on high seismic applications. Unlike many other seismic force-resisting systems such as moment-resisting frames and concentrically-braced frames that have special, intermediate, and ordinary design options that offer varying levels of ductility and response modification factors used in design, only special (i.e. highly ductile) SPSWs are included in AISC 341-10 [8]. As per AISC 341-10 [8], special SPSWs are required to have fully-connected web plates, full moment-resisting beam-column connections, and boundary elements designed in accordance with the capacity design principles. Berman and Bruneau [39] reported that the capacity design of boundary elements might lead to overly conservative and uneconomical SPSW designs in low- and moderate-seismic regions that makes SPSWs less attractive. In contrast to AISC 341-10 [8], the Canadian provisions CSA S16-09 [40] provide a limited-ductility SPSW option (Type LD), permitting the use of simple beam-column connections instead of moment connections, in addition to high-ductility SPSW option (Type D); however, the web plates of Type LD SPSWs are still required to be attached to the boundary frames on

all four sides of the web plates. Allowing the use of the simple beam-column connections is based on the experimental studies carried out by Timber and Kulak [41] and Tromposch and Kulak [25], which only included fully-connected web plates.

B-SPSWs are proposed here as a feasible SPSW alternative for moderate- and low-seismic regions. As the previous research suggested B-SPSWs with simple shear beam-column connections (hereafter referred to as B-SPSWs, unless otherwise stated) exhibit promising seismic performance despite (i) the reduction in the lateral load capacity, energy dissipation, and ductility due to the development of PTF instead of full TFA, and (ii) the reduced redundancy due to the lack of the moment frame action. In return for the beam-connected web plates and simple beam-column connections, the B-SPSW has the following benefits: (1) significant reduction of column flexural demands, (2) potential decrease in the total steel weight of the components, (3) elimination of costly detailing required for full moment-resisting connections, and (4) ease of construction due to the reduction in field welding required for beam-connected plates compared to fully-connected web plates.

This paper focuses on the seismic design and behavior of B-SPSWs designated for regions with low seismicity. The web plate lateral strength and boundary element demands are discussed and associated closed-form equations are provided. A series of three-, six-, and nine-story BSPSWs adopting different design approaches are designed for a low-seismic site, and their seismic performance is assessed and compared using nonlinear response-history analyses.

DESIGN OF BEAM-CONNECTED WEB PLATES

The lateral resistance of beam-connected web plates has two components: shear buckling strength and the effects of partial tension field action. It is conservative to

ignore the shear buckling strength of web plates in B-SPSW design, because typical designs require thin web plates that have limited shear buckling strength and the buckling strength is expected to be further reduced following web plate yielding, as is expected under design-level earthquakes. Consequently, it is assumed that the web plates of B-SPSWs resist the lateral load by only PTF.

As discussed by Thorburn et al. [1], the beam-connected PTF angle (θ) is different than the fully-connected tension field angle (α) due to the different boundary conditions along the column edges. Only the portion of the beam-connected web plate inside the PTF (Fig. 1) resists the lateral load, leaving the remainder of the web plate to provide little or no contribution to the lateral strength. A partially empirical equation for θ has been proposed based on a numerical parametric study of shell element beam-connected web plate models of different aspect ratios where L_c is the clear length of the web plate between column flanges and H_c is the clear height of the web plate [33]:

$$\theta = max\begin{pmatrix} 0.55-0.03\frac{L_c}{H_c} \\ 0.51 \end{pmatrix} \tan^{-1}\frac{L_c}{H_c} \quad (1)$$

The beam-connected PTF length, L_p, can be determined using the geometry given in Fig. 1:

$$L_p = L_c - H_c \tan\theta \quad (2)$$

The nominal shear strength of a beam-connected web plate, V_n, can be calculated using a modified version of the formula given by AISC 341-10 [8], where α is replaced by θ and L_c is replaced by L_p (where F_y is the nominal yield strength of the web plate material):

$$V_n = 0.42\, F_y t_w L_p \sin(2\theta) \quad (3)$$

Note that the factor of 0.42 in *Eq.3* replaces the theoretical factor of 0.50 (that comes from the integration of the web plate stress (σ) over L_p in the lateral direction) since the theoretical strength is reduced by an overstrength of 1.2 to be consistent with other seismic force-resisting systems [42]. It is also worthwhile noting that B-SPSWs will require thicker web plates than SPSWs for the same lateral load as stated by Clayton et al. [31] since the steeper inclination angle (i.e., θ is smaller than α) and the shorter extent of the PTF (i.e., L_p is shorter than L_c) result in lower load carrying capacity for beam-connected plates of the same thickness as fully-connected web plates.

DESIGN OF BEAMS

The simple beam-column connections of B-SPSWs eliminate the moment frame action; consequently, the beams of B-SPSWs resist demands resulting from the diaphragm collector forces, *F*, and the distributed line load acting on the beam due to the PTF of the web plate (ω) of the story below, $\omega_{(i)}$, and the story above, $\omega_{(i+1)}$ (where *i* is the floor index of the beam under consideration). Similarly, the simple beam-column connections induce negligible moment at the beam ends; as a result, the beams of B-SPSWs are a statically determinate system. The magnitude and location of the maximum beam demands can be calculated precisely assuming a uniform ω distribution oriented at θ along L_p and no distributed line load outside L_p.

Fig. 2(a) shows the free-body diagram of a beam of a B-SPSW when the B-SPSW undergoes a lateral right sway. Fig. 2(b) and Fig. 2(c) show the external forces decomposed in the horizontal and vertical directions, respectively, and their corresponding end reactions. As seen in Fig. 2, there are three distinct zones on the beam:

(1) Zone 1 is the portion on the left end of the beam where only $\omega_{(i+1)}$ acts. (2) Zone 2 is the portion in the middle of the beam where both $\omega_{(i)}$ and $\omega_{(i+1)}$ act. (3) Zone 3 is the portion on the right end of the beam where only $\omega_{(i+1)}$ acts. The horizontal and vertical components of ω (ω_x and ω_y, respectively) can be calculated using the following equations:

$$\omega_x = \sigma\, t_w \sin\theta \cos\theta = 0.5\, \sigma\, t_w \sin 2\theta \tag{4}$$

$$\omega_y = \sigma\, t_w \cos\theta \cos\theta \tag{5}$$

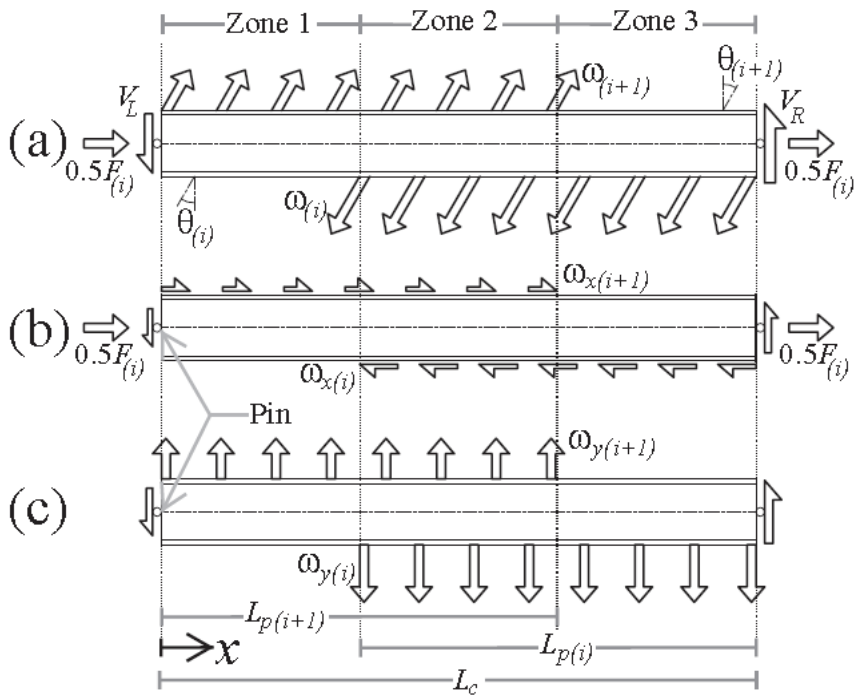

Figure 2. Free-body diagram of an intermediate beam at floor i of a B-SPSW: (a) external forces and end reactions, (b) horizontal components of the external forces and the corresponding end reactions, and (c) vertical components of the external forces and the corresponding end reactions.

Note that for the roof beam, $\omega_{(i+1)}$ is zero; consequently, Zone 3 given in Fig. 2 extends over both Zone 2 and Zone 3 and there is no web plate force acting on Zone 1. It is also worthwhile noting that the minimum L_p/L_c calculated using *Eq.1* and *Eq.2* within the aspect ratio limits of AISC 341-10 [8] is 0.54. Since L_p is always longer than $0.50L_c$ (i.e, $L_{p(i)}$ and $L_{p(i+1)}$ always cross over each other) Zone 2 always exists and the axial load, shear, and moment equations given herein are valid for every aspect ratio within the limits given by AISC 341-10 [8].

Axial load distribution

The beams of B-SPSWs resist axial loads resulting from only ω_x and F. F can be calculated using the following equation considering the equilibrium of the horizontal loads acting on the beam given in Fig. 2(*b*):

$$F_i = \omega_{x(i)} L_{p(i)} - \omega_{x(i+1)} L_{p(i+1)} \tag{6}$$

Assuming the collector forces at the both ends of the beam are equal, the axial load along the beam length, P, is:

$$P(x) = -0.5F_{(i)} + \omega_{x(i)} * max\left(\begin{matrix}0\\ x+L_{p(i)}-L_c\end{matrix}\right) - \omega_{x(i+1)} * min\left(\begin{matrix}x\\ L_{p(i+1)}\end{matrix}\right) \tag{7}$$

Fig. 3 shows typical axial load distributions of intermediate beams in B-SPSWs. Note that the slope of the axial load diagram, *dP/dx*, in Zone 2 in Fig. 3 is either positive or negative depending on the difference between the magnitudes of $\omega_{x(i)}$ and $\omega_{x(i+1)}$. When $\omega_{x(i)} < \omega_{x(i+1)}$, the slope will be negative. The case of $\omega_{x(i)} < \omega_{x(i+1)}$ might occur when $H_{c(i)}<H_{c(i+1)}$ and $t_{w(i)}<t_{w(i+1)}$, which is unlikely for typical designs and is provided herein

for the sake of completeness. The slopes in Zone 1 and in Zone 3 are always negative (or zero for the roof beam) and positive, respectively. Therefore, the maximum compressive axial load occurs at $x=L_c-L_{p(i)}$ when $\omega_{x(i+1)} < \omega_{x(i)}$ or at $x=Lp(i+1)$ when $\omega_{x(i)} < \omega_{x(i+1)}$.

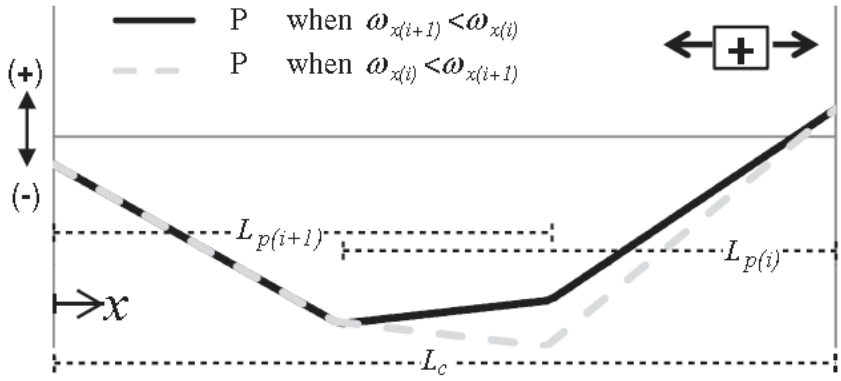

Figure 3. Axial load diagram of the beam of B-SPSWs.

Moment distribution

Fig. 4 shows a typical moment diagram of the beams of B-SPSWs. The total moment distribution in the beam, M, has four components: Moments resulting from $\omega_{y(i)}$ and $\omega_{y(i+1)}$ ($M_{y(i)}$ and $M_{y(i+1)}$, respectively), and moments from resulting from $\omega_{x(i)}$ and $\omega_{x(i+1)}$ acting along the bottom and top flanges of the beam, respectively ($M_{x(i)}$ and $M_{x(i+1)}$, respectively):

$$M_{y(i)}(x) = 0.5\omega_{y(i)}\left[\frac{x}{L_c}{L_{p(i)}}^2 - \left[max\left({}^{0}_{x+L_{p(i)}-L_c}\right)\right]^2\right] \quad (8)$$

$$M_{y(i+1)}(x) = -0.5\omega_{y(i+1)}\left[\left(1-\frac{x}{L_c}\right){L_{p(i+1)}}^2 - \left[max\left({}^{0}_{x+L_{p(i)}-L_c}\right)\right]^2\right] \quad (9)$$

$$M_{x(i)}(x) = -0.5\omega_{x(i)}d_{b(i)} * \left[\left(1-\frac{L_{p(i)}}{L_c}\right) * min\left({}^{L_c-x}_{L_{p(i)}}\right) - \frac{L_{p(i)}}{L_c} * max\left({}^{0}_{L_c-L_{p(i)}-x}\right)\right] \quad (10)$$

$$M_{x(i+1)}(x) = 0.5\omega_{x(i+1)}d_{b(i)} * \left[\left(1 - \frac{L_{p(i+1)}}{L_c}\right) * min\left(\begin{matrix} x \\ L_{p(i)} \end{matrix}\right) - \frac{L_{p(i+1)}}{L_c} * max\left(\begin{matrix} 0 \\ x - L_{p(i+1)} \end{matrix}\right)\right] \quad (11)$$

$$M(x) = M_{y(i)}(x) + M_{y(i+1)}(x) + M_{x(i)}(x) + M_{x(i+1)}(x) \quad (12)$$

where d_b is the beam depth.

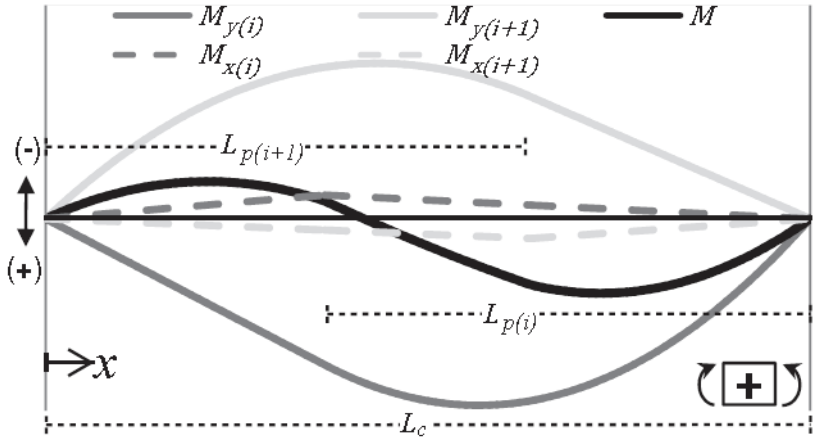

Figure 4. Moment diagram of the beam of B-SPSWs.

The moments resulting from the vertical web plate forces ($M_{y(i)}$ and $M_{y(i+1)}$) account for the vast portion of M. $\omega_{y(i)}$ leads to positive moments with a linear distribution in Zone 1, and a parabolic distribution in Zone 2 and Zone 3; while, $\omega_{y(i+1)}$ causes negative moments with a parabolic distribution in Zone 1 and Zone 2, and a linear distribution in Zone 3. In brief, $\omega_{y(i)}$ and $\omega_{y(i+1)}$ induce mirrored and opposite-sign moment demands that cause double curvature in the beam. Similarly, $M_{x(i)}$ and $M_{x(i+1)}$, that result from the eccentricity of the horizontal web plate forces ($\omega_{x(i)}$ and $\omega_{x(i+1)}$, respectively) also lead to double curvature, although of much smaller magnitude, in the

beam. Note that the beam might undergo a single-curvature moment distribution when $\omega_{y(i+1)} << \omega_{y(i)}$. An example case of $\omega_{y(i+1)} << \omega_{y(i)}$ is the roof beam where $\omega_{y(i+1)}$ is zero.

Shear reactions

The beams of SPSWs have a complex shear distribution; however, the maximum design shear demands occur at the beam ends. The left and right shear end reaction forces (V_L and V_R, respectively, in Fig. 2(a)) are comprised of contributions from the vertical and horizontal web plate stresses (shown in Fig. 2(b) and Fig. 2(c), respectively) and are given as follow:

$$V_{\mathrm{L}} = 0.5\,\omega_{y(i)}\frac{{L_{p(i)}}^2}{L_c} - 0.5\omega_{y(i+1)}\left(2L_{p(i+1)} - \frac{{L_{p(i+1)}}^2}{L_c}\right) - 0.5\,\frac{d_{b(i)}}{L_c}\left(\omega_{x(i)}L_{p(i)} + \omega_{x(i+1)}L_{p(i+1)}\right) \quad (13)$$

$$V_{\mathrm{R}} = 0.5\omega_{y(i)}\left(2L_{p(i)} - \frac{{L_{p(i)}}^2}{L_c}\right) - 0.5\,\omega_{y(i+1)}\frac{{L_{p(i+1)}}^2}{L_c} + 0.5\,\frac{d_{b(i)}}{L_c}\left(\omega_{x(i)}L_{p(i)} + \omega_{x(i+1)}L_{p(i+1)}\right) \quad (14)$$

Note that the shear design might be the critical design limit state for narrow B-SPSWs (BPSWs with aspect ratios less than approximately 1.2) since θ becomes steeper for narrow B-SPSWs and the design beam moments might be small for shorter span lengths.

Combined beam demands

As shown in Fig. 3 and Fig. 4, the maximum axial load and moment in the beam might or might not occur at the same location. Although, the magnitude and location of the maximum compressive axial load, P_u, can be calculated easily; the magnitude and location of the maximum moment, M_u, depends on several parameters such as θ, ω_x, ω_y,

L_p, L_c, and d_b. Hence, the *P-M* interaction needs to be checked for several locations along the beam. Alternatively, it can be conservatively assumed that P_u and M_u act at the same location; however, calculating M_u might still be cumbersome in the preliminary design stage.

To provide a practical design approach for the preliminary design, intermediate-story beams are designed considering a wide range of the main parameters affecting the beam design. A total of 25 web plate thicknesses ranging from 1.06mm to 12.7mm and 10 aspect ratios ranging from 0.8 to 2.5 are examined in the parametric study of an intermediate beam with web plates above and below, resulting in over 26,000 beam designs. Adopting capacity design principles, σ is assumed to be 323MPa (the expected yield strength, R_yF_y, of A36 steel, where R_y is the ratio of the expected yield stress to F_y) to obtain the beam demands using the beam demand equations provided herein. The nominal yield strength of the beam material is assumed as 345MPa. H_c of the web plate below the beam is selected as 3960mm and kept constant for all designs. Accordingly, L_c of the web plates and H_c of the web plate above the beam are calculated for the given aspect ratio of the web plate below the beam. Every combination of aspect ratios and web plate thicknesses is considered, and the *P-M* interaction is checked at 100 locations along the beam length in accordance with the interaction equations given in the *AISC Specifications* (AISC 360-10) [43]. Since this parametric study aims to find a simplified design procedure for the *P-M* interaction, the shear design is omitted. The designs, in which the shear strength ratio of the web plate above the beam to below the beam (μ) is bigger than 1.0, are disregarded, i.e., the web plate below the beam is assumed to always have equal or higher lateral strength than the web plate above the beam, as is typical for lateral force-resisting systems. For each design case the lightest American wide flange section (W shape) satisfying the interaction equations is selected, and the demand-to-

capacity ratio (DCR) of each location is normalized with respect to the maximum DCR along the beam length (DCR_{max}).

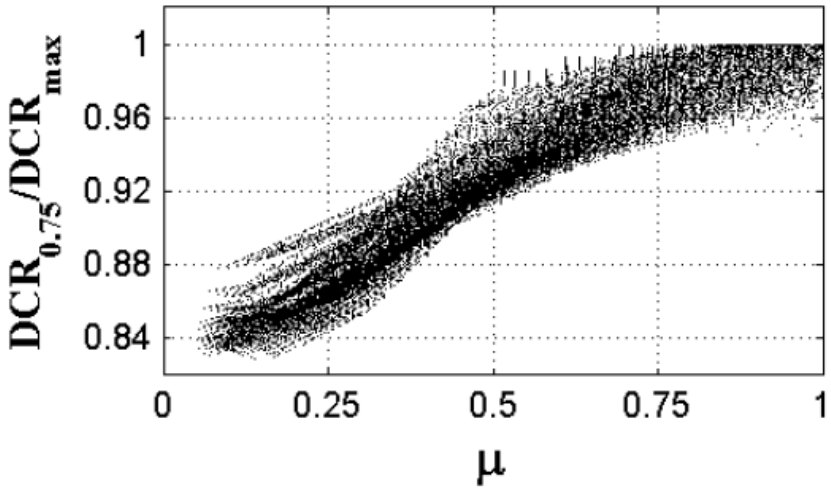

Figure 5. Normalized demand-to-capacity ratio at $0.75L_c$ vs. ratio of web plate strengths

Fig. 5 shows the DCR at $x=0.75L_c$ ($DCR_{0.75}$) normalized with respect to the DCR_{max} vs. μ. As seen in Fig. 5, the $DCR_{0.75}/DCR_{max}$ ratio approaches 1.0 as μ increases, i.e., the design location of $x=0.75L_c$ corresponds to or is close to the critical location along the beam length if the adjacent story web plates have similar web plate shear strengths (i.e., μ is close to 1.0). For values of μ of 0.5 and 1.0 (those limits can be assumed as the minimum and maximum limits for typical designs) the minimum $DCR_{0.75}/DCR_{max}$ ratios are 0.91 and 0.95, respectively, meaning that the $DCR_{0.75}$ may underestimate, if at all, the DCR_{max} by about 5 to 10% for typical designs. Hence, it is recommended to design the beams of B-SPSWs for the demands at $x=0.75L_c$ for the preliminary design stage with an increase in the demands based on μ (about 5 to 10% increase for typical designs). Note that the recommended preliminary design location of $0.75L_c$ for the design of intermediate-story beams is based on the demands resulting from

the earthquake loads only. The critical section will slightly shift towards the midspan of the beam with the application of additional gravity loads; however, the design location of x=0.75L_c still provides good estimates of the beam demands at the preliminary design stage when the earthquake loads are dominant (this conclusion is validated by the design of a wide range of B-SPSWs, the details of which are given in *Building Models*). If the gravity loads are very large relative to the earthquake demands, then the vertical load combinations are expected to govern the design of the beam.

DESIGN OF COLUMNS

The columns of B-SPSWs primarily resist axial loads resulting from gravity loads and the beam end reactions due to the web plate forces, V_L and V_R. Because of the simple beam-column connections used in the B-SPSW and the fact that the web plate is not connected to the columns, the bending moment demands in the columns are expected to be limited as in the case of gravity columns when the deformed geometry is not considered. Therefore, the columns of B-SPSWs can be designed for axial loads and the moments resulting from the beam shears acting offset from the column centerline.

Note that, as will be discussed later in *Section 7*, nonuniform interstory drifts might induce significant bending moment demands in the multistory continuous columns, having maximum demands at floor levels. Estimating differential interstory drifts and associated moment demands adopting common analysis methods, namely, the equivalent lateral force (ELF) method and the modal response spectrum analysis, is problematic [8]. Further work is underway to investigate the moment demands resulting from nonuniform interstory drifts and to propose a simplified column design method accounting for the bending moment demands that cannot be captured by the ELF method or the modal response spectrum analysis.

BUILDING MODELS

To assess the seismic performance of low-seismic B-SPSWs with simple shear connections, eighteen B-SPSWs located in Boston are designed using the member demand equations presented herein and the LRFD principles of AISC 360-10 [43]. The loads and the floor plan of the three-story prototype building used in the SAC steel project [44] are adopted. The story height, H, is selected as 3960mm and kept constant for all stories of all designs. The web plate aspect ratio, L_c/H_c, and the number of stories, N_s, are the key parameters affecting the design of B-SPSWs; accordingly, three different column centerline bay widths, L, (4572, 6092, and 7315mm) and three different building heights (N_s=3, 6, and 9) are considered in this study. The selected bay widths result in aspect ratios of approximately 1.15, 1.54, and 1.85, which are within the limits given by AISC 341-10 [8].

The ELF method prescribed in ASCE 7-10 [45] is implemented using the risk-adjusted maximum considered earthquake (MCE_R) mapped spectral accelerations of 0.217g at short period and 0.069g at a period of 1s, where g is the gravitational acceleration [45]. The elastic response spectrum is constructed assuming the following parameters: (1) Risk category II, (2) a soil profile of Class D (stiff soil), and (3) an importance factor of 1.0 [45]. The selected parameters lead to Seismic Design Category B; accordingly, the redundancy factor is taken as 1.0 regardless of the configuration of B-SPSWs.

The buildings are designed following two design approaches: (1) using a response modification factor, R, of 3 without detailing the system specifically for seismic resistance, i.e., without conforming to the capacity design principles, and (2) using an R of 3.25 following the capacity design principles. The former and latter design approaches will be referred as the non-seismically detailed design (ND) and the seismically detailed

design (SD), respectively. Note that R=7 for special SPSWs and R=8 when special SPSWs are part of a dual system; however, R of 3.25 is selected for the SD of B-SPSWs in this study to be consistent with the R used for ordinary concentrically braced frames (OCBFs) that can be used in low-seismic applications [45]. CSA S16-09 [40] provides different response modification factors for Type LD and Type D SPSWs. Although, the terminology used in CSA S16-09 [40] is different than ASCE 7-10 [45]; the response modification factors equivalent to the R of ASCE 7-10 [45] are 3 and 8 for Type LD and Type D SPSWs, respectively, that align with the R factors given for the design without detailing the system specifically for seismic resistance and special SPSWs, respectively, by ASCE 7-10 [45].

While experimental testing of B-SPSWs with simple beam-column connections is limited, the basis of the R=3.25 assumption for SD B-SPSWs seems reasonable, and possibly conservative. While B-SPSWs are expected to have limited inelastic deformation capacity compared to special SPSWs as discussed in *Introduction and Background*, B-SPSWs are still expected to have higher ductility than comparable OCBFs. The cyclic testing of the 1/3-scaled three-story B-SPSW specimen with full-moment beam-column connections [34] showed that the specimen exhibited a ductile behavior until the third-floor beam fractured at 5.4% roof drift with limited tearing of the web plate. Similarly, the 1/3-scaled one-story B-SPSW specimen with partial moment-resisting beam-column connections tested under cyclic loads by Vatansever and Yardimci [26] displayed a ductile behavior until the test was terminated at 3% drift due to the limitations of the test set-up. For comparison, two full-scale cyclic tests of one-story one-bay special concentrically braced frames (that are expected to have better inelastic deformation capacity than OCBFs) presented in Hsiao et. al. [46] and designed in accordance with AISC 341-10 [8] exhibited brace fracture at drifts less than 2%.

Consequently, it can be concluded that B-SPSWs have higher inelastic deformation capacity than OCBFs and the R=3.25 assumption is conservative. Additional testing and numerical studies using the FEMA P-695 [47] approach are required to verify the performance and appropriate R-factor for design of B-SPSWs; however, the selection of R=3.25 for SD B-SPSWs is meant to provide a proof-of-concept for the low-seismic B-SPSW system.

The total seismic masses at the floor and the roof levels are estimated as 8263 and 8903kN, respectively. The buildings are assumed to have a total of four bays of B-SPSWs in the N-S direction; therefore, each B-SPSW bay resists one-quarter of inertial forces resulting from the total seismic mass. The base shear coefficients are determined in accordance with the approximate fundamental period calculated per ASCE 7-10 [45]. It is assumed that the wind load does not govern the design.

The average web plate stress in PTF, σ, that is used in *Eq.4* and *Eq.5* to calculate boundary element demands, is given by *Eq.15* for ND and SD. As discussed by Sabelli and Bruneau [42], for the design of non-seismically detailed SPSWs with R of 3, the design of boundary elements can be done assuming a uniform distribution of the average web plate stress whose tangential component in horizontal direction is equal to the story shear divided by the shear resisting area of the web plate (i.e., L_p times t_w for B-SPSWs). F_k in *Eq.15* is the portion of the base shear applied at the story level k determined directly from the ELF method for ND designs. For SD designs, σ is taken as R_yF_y of the web plate in accordance with the capacity design principles of AISC 341-10 [8].

$$\sigma_i = \begin{cases} \dfrac{2\sum_{k=i}^{N_S} F_k}{L_{p(i)} t_{w(i)} \sin 2\theta_{(i)}} & \text{for } ND \\ R_y F_y & \text{for } SD \end{cases} \tag{15}$$

In addition to strength requirements, the beams of B-SPSWs are checked against the minimum flexural stiffness requirement given by *Eq.16* [8] to assure that the beams provide sufficient anchorage for the web plates to develop their ultimate shear strength:

$$I_b \geq 0.0031 \frac{L^4}{H} \Delta t_w \tag{16}$$

where I_b is the moment of inertia of the beam in the plane of the web plates and Δt_w is the difference in the web plate thicknesses above and below the beam. Note that AISC 341-10 [8] requires the columns of SPSWs to satisfy a similar stiffness requirement; however, beam-connected web plates are not anchored by the columns of B-SPSWs. Thus, the minimum stiffness requirement is omitted for the design of the columns of B-SPSWs. One should also note that the beam-column connections, the lengths of TFA, and the inclination angles of TFA are different for SPSWs and B-SPSWs as discussed herein. Although, preliminary analysis has shown that the beam stiffness limit given in *Eq.16* provides satisfactory development of web plate PTF for B-SPSWs; further research is needed to establish a new minimum stiffness requirement for the beams of B-SPSWs.

The member sizes of the eighteen B-SPSW designs are given in Table 1. The naming scheme for the designs is as follows: (number of stories) - (bay width in feet) - (design approach: ND or SD). ASTM A36 and A992 steels are selected for web plates and boundary elements, respectively. The beams are selected from W shapes while the columns are selected from W14 sections and change at every three stories. It is assumed that the beams have adequate lateral bracing to reach the plastic moment capacity. The web plates are chosen from U.S. standard sheet metal gauges and steel plate thicknesses. The web plates are proportioned to the story shear as closely as possible to avoid

unnecessary overstrength and possible concentration of inelastic deformation in some stories as suggested by Berman and Bruneau [48].

Table 1. Member sizes

M	S	t_w(mm)	Column	Beam
3-15-ND	1	2.66	W14x53	W18x40
	2	2.28	W14x53	W21x44
	3	1.37	W14x53	W24x55
6-15-ND	1	4.76	W14x109	W21x50
	2	4.55	W14x109	W21x50
	3	4.18	W14x109	W21x50
	4	3.80	W14x61	W21x50
	5	2.66	W14x61	W21x50
	6	1.52	W14x61	W24x55
3-20-ND	1	1.71	W14x48	W21x50
	2	1.37	W14x48	W24x62
	3	0.84	W14x48	W27x84
6-20-ND	1	3.04	W14x90	W21x50
	2	3.04	W14x90	W21x50
	3	2.66	W14x90	W21x50
	4	2.28	W14x61	W24x62
	5	1.71	W14x61	W24x76
	6	0.91	W14x61	W27x84
3-24-ND	1	1.21	W14x48	W21x44
	2	1.06	W14x48	W24x76
	3	0.68	W14x48	W30x99
6-24-ND	1	2.28	W14x90	W24x55
	2	2.28	W14x90	W24x76
	3	1.90	W14x90	W24x55
	4	1.71	W14x53	W27x84
	5	1.21	W14x53	W27x84
	6	0.68	W14x53	W30x99
9-15-ND	1	5.31	W14x159	W21x50
	2	5.31	W14x159	W21x50
	3	4.94	W14x159	W21x50
	4	4.76	W14x99	W21x50
	5	4.18	W14x99	W21x50
	6	3.80	W14x99	W21x44
	7	3.04	W14x61	W21x44
	8	2.28	W14x61	W21x50
	9	1.21	W14x61	W24x55
9-20-ND	1	3.80	W14x132	W24x68
	2	3.18	W14x132	W24x55
	3	3.04	W14x132	W24x55
	4	3.04	W14x90	W21x50
	5	2.66	W14x90	W21x50
	6	2.28	W14x90	W21x50
	7	1.90	W14x53	W24x62
	8	1.37	W14x53	W24x68
	9	0.76	W14x53	W24x76
9-24-ND	1	2.66	W14x120	W24x55
	2	2.66	W14x120	W24x76
	3	2.28	W14x120	W24x55
	4	2.28	W14x90	W24x76
	5	1.90	W14x90	W24x55
	6	1.71	W14x90	W24x68
	7	1.37	W14x48	W24x68
	8	1.06	W14x48	W27x84
	9	0.53	W14x48	W27x84
3-15-SD	1	2.66	W14x74	W21x50
	2	2.28	W14x74	W24x55
	3	1.37	W14x74	W24x55
6-15-SD	1	4.55	W14x159	W27x84
	2	4.18	W14x159	W21x83
	3	3.90	W14x159	W24x62
	4	3.18	W14x109	W21x57
	5	2.66	W14x109	W24x62
	6	1.37	W14x109	W24x55
3-20SD	1	1.52	W14x61	W21x50
	2	1.37	W14x61	W24x68
	3	0.76	W14x61	W24x76
6-20-SD	1	2.66	W14x132	W24x62
	2	2.66	W14x132	W24x68
	3	2.28	W14x132	W24x55
	4	2.28	W14x82	W24x76
	5	1.52	W14x82	W24x68
	6	0.84	W14x82	W27x84
3-24-SD	1	1.21	W14x61	W24x55
	2	1.06	W14x61	W27x84
	3	0.61	W14x61	W30x90
6-24-SD	1	2.28	W14x120	W27x84
	2	1.90	W14x120	W24x62
	3	1.90	W14x120	W24x76
	4	1.52	W14x68	W27x84
	5	1.06	W14x68	W27x84
	6	0.61	W14x68	W30x90
9-15-SD	1	4.76	W14x257	W27x84
	2	4.76	W14x257	W27x84
	3	4.55	W14x257	W27x84
	4	4.18	W14x159	W24x62
	5	4.18	W14x159	W21x83
	6	3.80	W14x159	W24x76
	7	3.04	W14x82	W24x62
	8	1.90	W14x82	W21x50
	9	1.06	W14x82	W21x50
9-20-SD	1	3.04	W14x211	W24x68
	2	3.04	W14x211	W24x68
	3	3.04	W14x211	W24x76
	4	2.66	W14x132	W24x62
	5	2.66	W14x132	W24x68
	6	2.28	W14x132	W24x68
	7	1.71	W14x68	W24x62
	8	1.21	W14x68	W24x62
	9	0.68	W14x68	W24x68
9-24-SD	1	2.28	W14x176	W24x68
	2	2.28	W14x176	W24x68
	3	2.28	W14x176	W24x68
	4	2.28	W14x120	W27x84
	5	1.90	W14x120	W24x76
	6	1.52	W14x120	W24x62
	7	1.37	W14x61	W27x84
	8	0.91	W14x61	W24x76
	9	0.53	W14x61	W27x84

M: Model name; S: Story

FINITE ELEMENT MODELING AND VERIFICATION

The web plates of SPSWs are typically modeled using two modeling techniques, namely, the continuum model and the strip model. In the former approach, the web plate is represented by shell elements to capture the shear buckling behavior explicitly. However, this modeling approach is computationally expensive and is prone to numerical convergence or instability issues [49,50]. The latter approach, the strip model, is a simplified model proposed by Thorburn et al. [1] where the web plate is represented by a series of evenly-spaced inclined tension-only truss elements. This modeling technique has been used and modified/improved by several researchers [51-53] and validated against experimental results. Ozcelik and Clayton [33] have proposed a strip model for B-SPSWs that is implemented in this study.

Typically, the compressive strength of the strip is conservatively ignored for thin web plates as suggested by Sabelli and Bruneau [42]; however, recent research [31,54,55] has revealed that the tension-only assumption for thicker web plates might significantly underestimate the energy dissipation and unloading strength of SPSWs during cyclic analysis. As discussed herein and by Clayton et al. [31], B-SPSWs require thicker web plates than SPSWs; consequently, the compressive strength of B-SPSWs is more prominent and should be accounted for in the strip modeling approach. In Ozcelik and Clayton's strip model [33], a parametric study of shell finite element beam-connected web plate models of varying aspect ratios and thicknesses was conducted, and an empirical equation was proposed to estimate the compressive strength of the strip of B-SPSWs given as follow:

$$\beta = -0.04 + 0.02\frac{L_c}{H_c} + \frac{2.75}{\sqrt{H_c/t_w}} \geq 0 \tag{17}$$

where β is the ratio of the compressive strength of the strip to $R_y F_y$. The proposed strip model comprises a pinched tension-only material in parallel with a bilinear material that accounts for the compressive capacity of the web plate. Calculating β using *Eq.17* and combining the pinched tension-only material and bilinear material in parallel, the material model of the web plate (parallel material) accounting for the compressive strength can be obtained. The normalized stress-strain diagrams of these materials are given in Fig. 6.

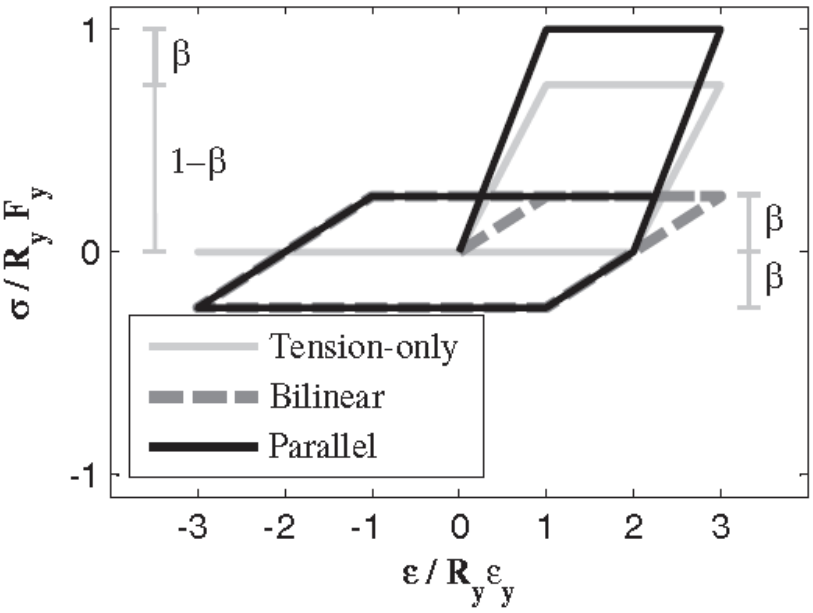

Figure 6. Normalized stress-strain diagrams of material models.

In addition to *Eq.17*, Ozcelik and Clayton [33] provided equations for θ and the area of a strip, A_s, that are given by *Eq.1* and *Eq.18*, respectively; where n_s is the number of strips in each direction. In this study, ten strips are used in each direction to represent the web plates as required by AISC 341-10 [8] and recommended by Ozcelik and Clayton [33].

$$A_s = \frac{t_w L_p \cos\theta}{n_s} \tag{18}$$

The two-dimensional analyses are performed in OpenSEES [56]. The web plates are modeled using corotational truss elements with the parallel materials as described. Built-in hysteretic and Steel02 materials are used for the pinched tension-only and bilinear materials, respectively. R_yF_y is taken as 323MPa (R_yF_y of A36 steel) with a 0.5% isotropic strain hardening based on the cyclic material tests conducted by Shen et al. [57]. The beams and columns are modeled using force-based distributed-plasticity nonlinear beam-column elements where the interaction between axial load and bending moment is achieved through the integration of the uniaxial stress-strain relations of fibers over the cross section. A Menegotto-Pinto (Steel02 in OpenSEES [56]) material with a yield strength of 345MPa (nominal yield strength of A992) and a 0.5% isotropic strain hardening is adopted for the boundary frames.

The beam-column connections and columns bases are assumed to be simple connections, modeled here as perfect pins. The gravity load carried by the B-SPSW bay is applied on the columns of the B-SPSW at each floor level as point loads. The remainder of the total gravity load is applied on two dummy columns with negligible flexural stiffness to account for P-Delta effects. Lumped masses are placed on two nodes (the intersections of beam and column centerlines) at each floor level. Two-percent mass and stiffness proportional Rayleigh damping is assumed in the first and last (i.e. mode number equal to the number of stories, N_s) modes of each model. A representative two-story B-SPSW model is shown schematically in Fig. 7.

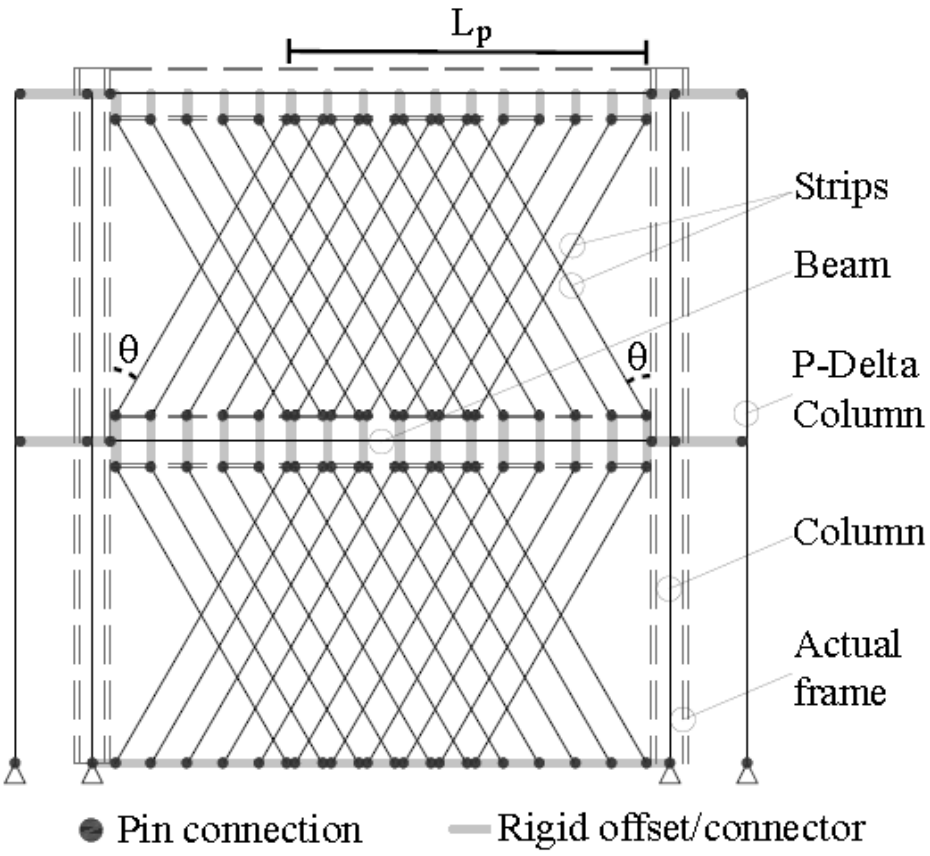

Figure 7. Typical strip model (applied gravity loads not shown for clarity)

The proposed strip model was used to model the cyclic response of a 1/3-scaled one-story B-SPSW specimen (denoted as S1) tested by Guo et al. [32]. The base shear vs. horizontal displacement responses of the experiment and the OpenSEES [56] analysis are given in Fig. 8. The results indicate that the proposed strip model captures the overall response adequately. The base shear capacity and the unloading strength of the B-SPSW are in agreement. For this particular experiment, the proposed strip model appears to overestimate the strength and stiffness at small drift levels less than approximately 0.008 radians (note that the height of the specimen S1 in the study of Guo et al. [32] is 1100mm); however, this difference is believed to be partially due to slip in the bolted

connections used at the beam-web plate interface which is not considered in the model [32]. Similarly, the amplitude of out-of-plane initial imperfections in the web plate affects the lateral stiffness, especially for lower drifts, [58,59] which is not captured by the truss element representation of the web plates.

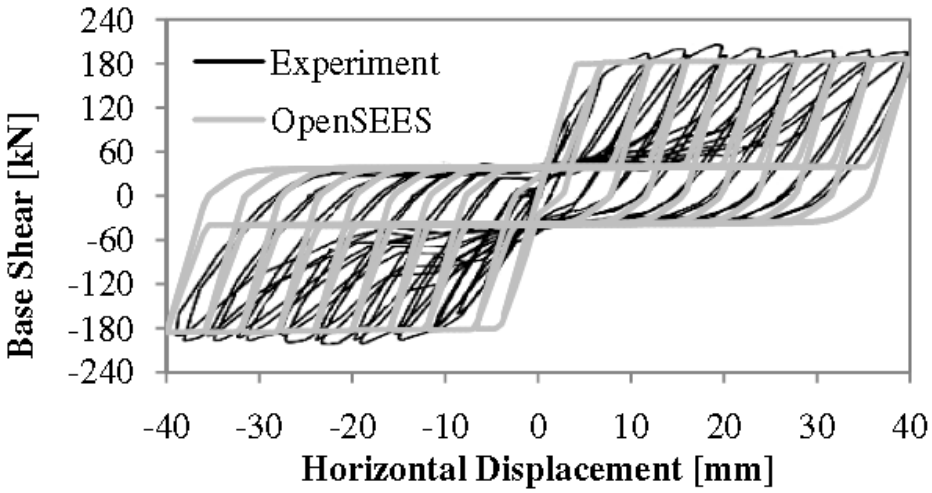

Figure 8. Base shear vs. displacement of the experiment (adapted from Guo et al. [32]) and the OpenSEES model.

RESULTS OF NONLINEAR RESPONSE-HISTORY ANALYSES

All eighteen models are analyzed under the ground motions (GM) developed by Somerville et al. [60] for the Boston site. The first suite includes twenty GMs scaled to a seismic hazard level of 10% probability of exceedence in 50 years (10/50). Similarly, the second set includes twenty GMs representing a seismic hazard level of 2% probability of exceedence in 50 years (2/50). Therefore, each building is subjected to forty GMs, and 720 nonlinear response-history analyses are performed in total. For the comparison with the MCE_R mapped spectral accelerations, the target spectra of the GM suites for 5% damping level [60] are given in Table 2.

Table 2. Target response spectra values.

Hazard Level	Period (s)			
	0.3	1.0	2.0	4.0
2/50	0.340	0.160	0.077	0.030
10/50	0.120	0.052	0.028	0.0108
MCE_R	0.217	0.069	-	-

To assess the seismic performance of B-SPSWs, the following response parameters are considered: (1) maximum peak interstory drift (ISD), (2) maximum beam DCR for axial load and moment interaction (PM_B), (3) maximum beam DCR for shear (V_B), (4) maximum column DCR for axial load and moment interaction (PM_C), (5) maximum beam-column connection rotation for intermediate stories (CR_I, in units of radians), and (6) maximum beam-column connection rotation for roof (CR_R, in units of radians). The DCRs are determined considering all sections along the length of all beams or columns throughout the entire response history assuming resistance factors of 1.0 and assuming that the beams can reach their full plastic moment capacity. The axial load and moment capacities of the columns are calculated per AISC 360-10 [43] considering both in-plane and out-of-plane unbraced lengths. Since the models are two-dimensional (i.e., out-of-plane deformations are not simulated), the in-plane and out-of-plane stabilities of columns are checked independently as per equations H1-1 and H1-2 in AISC 360-10 [43]. The mean and 84^{th} percentile response parameters for the seismic hazard levels of 10/50 and 2/50 are given in Table 3.

Table 3. Response parameters of nonlinear time-history analyses.

Model Name	10/50												2/50											
	ISD [%]		PM_B		V_B		PM_C		CR_I		CR_R		ISD [%]		PM_B		V_B		PM_C		CR_I		CR_R	
	Mean	84^{th} Pct	Mean	84^{th} Pct	Mean	84^{th} Pct	Mean	84^{th} Pct	Mean	84^{th} Pct	Mean	84^{th} Pct	Mean	84^{th} Pct	Mean	84^{th} Pct	Mean	84^{th} Pct	Mean	84^{th} Pct	Mean	84^{th} Pct	Mean	84^{th} Pct
3-15-ND	0.69	0.97	0.51	0.67	0.58	0.72	0.86	1.02	0.007	0.011	0.011	0.017	1.55	2.09	0.84	0.96	0.89	0.97	1.06	1.13	0.017	0.025	0.021	0.029
3-15-SD	0.68	0.99	0.50	0.68	0.48	0.60	0.62	0.79	0.007	0.010	0.012	0.019	1.42	1.99	0.66	0.72	0.66	0.72	0.84	0.90	0.014	0.020	0.021	0.028
3-20-ND	0.73	1.08	0.39	0.51	0.33	0.41	0.91	1.05	0.008	0.011	0.012	0.019	1.41	2.10	0.58	0.73	0.46	0.54	1.06	1.13	0.015	0.020	0.019	0.026
3-20-SD	0.70	1.07	0.37	0.48	0.31	0.40	0.66	0.78	0.007	0.010	0.012	0.019	1.52	2.13	0.54	0.61	0.43	0.47	0.86	0.95	0.015	0.021	0.022	0.029
3-24-ND	0.70	1.06	0.34	0.45	0.26	0.33	0.90	1.03	0.008	0.011	0.011	0.019	1.22	1.81	0.59	0.75	0.38	0.43	1.04	1.12	0.015	0.019	0.014	0.021
3-24-SD	0.72	1.14	0.31	0.43	0.24	0.32	0.72	0.95	0.007	0.011	0.012	0.021	1.27	1.74	0.47	0.56	0.35	0.39	0.84	0.93	0.014	0.020	0.019	0.026
6-15-ND	1.08	1.48	0.73	0.95	0.78	1.03	0.94	1.20	0.013	0.019	0.019	0.027	1.96	2.71	0.90	0.97	0.99	1.05	1.08	1.22	0.019	0.023	0.028	0.039
6-15-SD	1.09	1.66	0.68	0.93	0.66	0.88	0.76	1.02	0.012	0.019	0.020	0.030	2.08	2.97	0.81	0.93	0.81	0.89	0.89	1.05	0.020	0.025	0.030	0.040
6-20-ND	1.10	1.62	0.64	0.89	0.59	0.77	0.96	1.21	0.013	0.019	0.019	0.028	2.19	3.07	0.77	0.89	0.70	0.76	1.09	1.20	0.019	0.027	0.029	0.040
6-20-SD	1.32	1.94	0.59	0.81	0.51	0.68	0.87	1.16	0.014	0.020	0.021	0.031	2.05	2.93	0.72	0.87	0.61	0.66	0.99	1.15	0.021	0.028	0.029	0.040
6-24-ND	1.08	1.43	0.57	0.76	0.44	0.56	1.12	1.31	0.013	0.019	0.019	0.025	2.22	3.40	0.68	0.80	0.55	0.59	1.17	1.31	0.021	0.028	0.030	0.045
6-24-SD	1.26	1.94	0.49	0.67	0.39	0.49	0.94	1.18	0.012	0.018	0.021	0.029	2.36	3.39	0.59	0.69	0.45	0.50	1.00	1.20	0.021	0.028	0.033	0.044
9-15-ND	1.10	1.43	0.74	0.99	0.87	1.14	1.02	1.22	0.014	0.022	0.018	0.024	2.30	3.36	0.90	1.00	1.07	1.19	1.11	1.24	0.022	0.031	0.031	0.043
9-15-SD	1.12	1.52	0.71	0.92	0.70	0.96	0.87	1.17	0.013	0.018	0.020	0.027	2.29	3.05	0.82	0.95	0.82	0.94	0.99	1.16	0.022	0.029	0.034	0.043
9-20-ND	1.16	1.46	0.72	0.94	0.67	0.83	1.21	1.31	0.017	0.024	0.021	0.026	2.08	2.75	0.78	0.96	0.73	0.84	1.24	1.34	0.021	0.028	0.031	0.040
9-20-SD	1.26	1.65	0.68	0.85	0.58	0.71	1.10	1.23	0.017	0.023	0.023	0.028	2.10	2.93	0.72	0.89	0.63	0.75	1.06	1.23	0.021	0.027	0.030	0.038
9-24-ND	1.18	1.51	0.66	0.87	0.50	0.61	1.22	1.35	0.016	0.023	0.021	0.027	2.34	3.53	0.69	0.88	0.56	0.65	1.25	1.37	0.020	0.028	0.032	0.047
9-24-SD	1.33	1.65	0.59	0.77	0.47	0.55	1.14	1.26	0.017	0.024	0.023	0.028	2.34	2.94	0.62	0.73	0.51	0.57	1.10	1.24	0.023	0.028	0.033	0.042

The mean and 84th percentile ISDs of all buildings for the 10/50 hazard level are below 2%, and the mean ISDs for the 2/50 hazard level are between 1.2% and 2.4% which are smaller than the peak ISDs observed in special (i.e. high seismic) SPSWs at the 2/50 hazard level [11,61]. Fig. 9 and Fig. 10 show the comparison of the peak interstory drift demands for the SD and ND along the building height for the seismic hazard levels of 10/50 and 2/50, respectively. The medians of the peak interstory drifts show a similar trend for the ND and SD at both seismic hazard levels. As seen in Fig. 9, except for few cases such as the 6th story of 6-24-SD and the 9th story of 9-24-SD, the peak story drifts are below 2%. As shown in Fig. 10, at the 2/50 hazard level, the peak story drifts are below 3% except for the drift demands at the roof levels of six- and nine-story models.

In general, the different design approaches (SD vs. ND) do not have a significant effect on ISDs. This can be attributed to the fact that there is no frame action for B-SPSWs; consequently, the lateral stiffness of the system stems from the web plates only, assuming the beams have enough flexural stiffness to anchor the web plates. Since similar R factors are adopted for both design approaches (namely, ND and SD), the web plate thicknesses are very similar which yields similar lateral stiffnesses and strengths. Note that the peak ISD demands given in Table 3 increase as the building height increases. Although Table 3 does not explicitly reveal it (however, it is depicted in Fig. 9 and Fig. 10), the mean and 84th percentile ISDs for 6- and 9-story frames tabulated in Table 3 are mostly the peak interstory drifts recorded at the roof levels while the peak interstory drifts for lower levels are significantly smaller. This phenomenon can be attributed, in part, to the higher mode effects observed for taller structures designed using the ELF method [62,63].

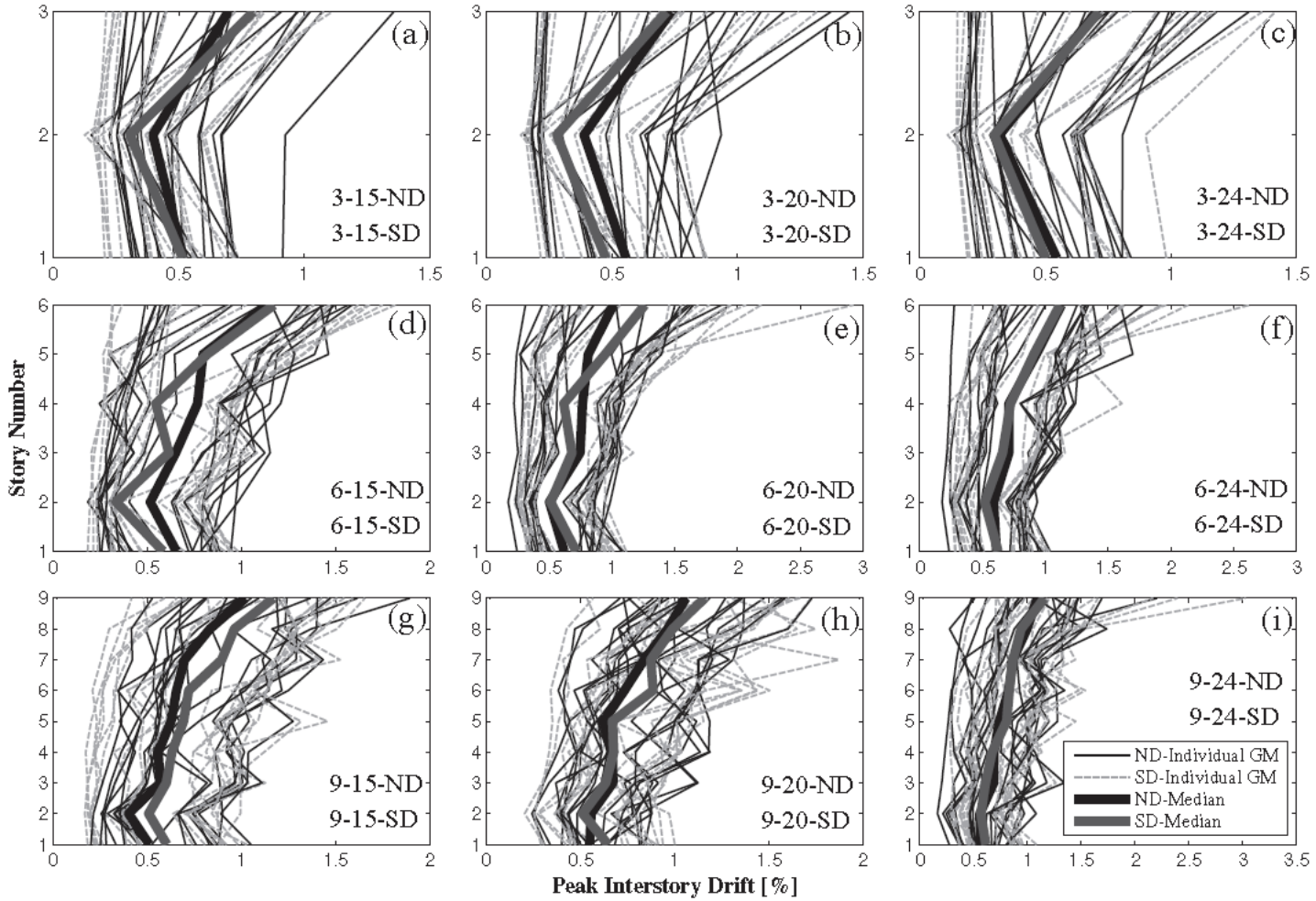

Figure 9. Peak interstory drifts at the 10/50 hazard level.

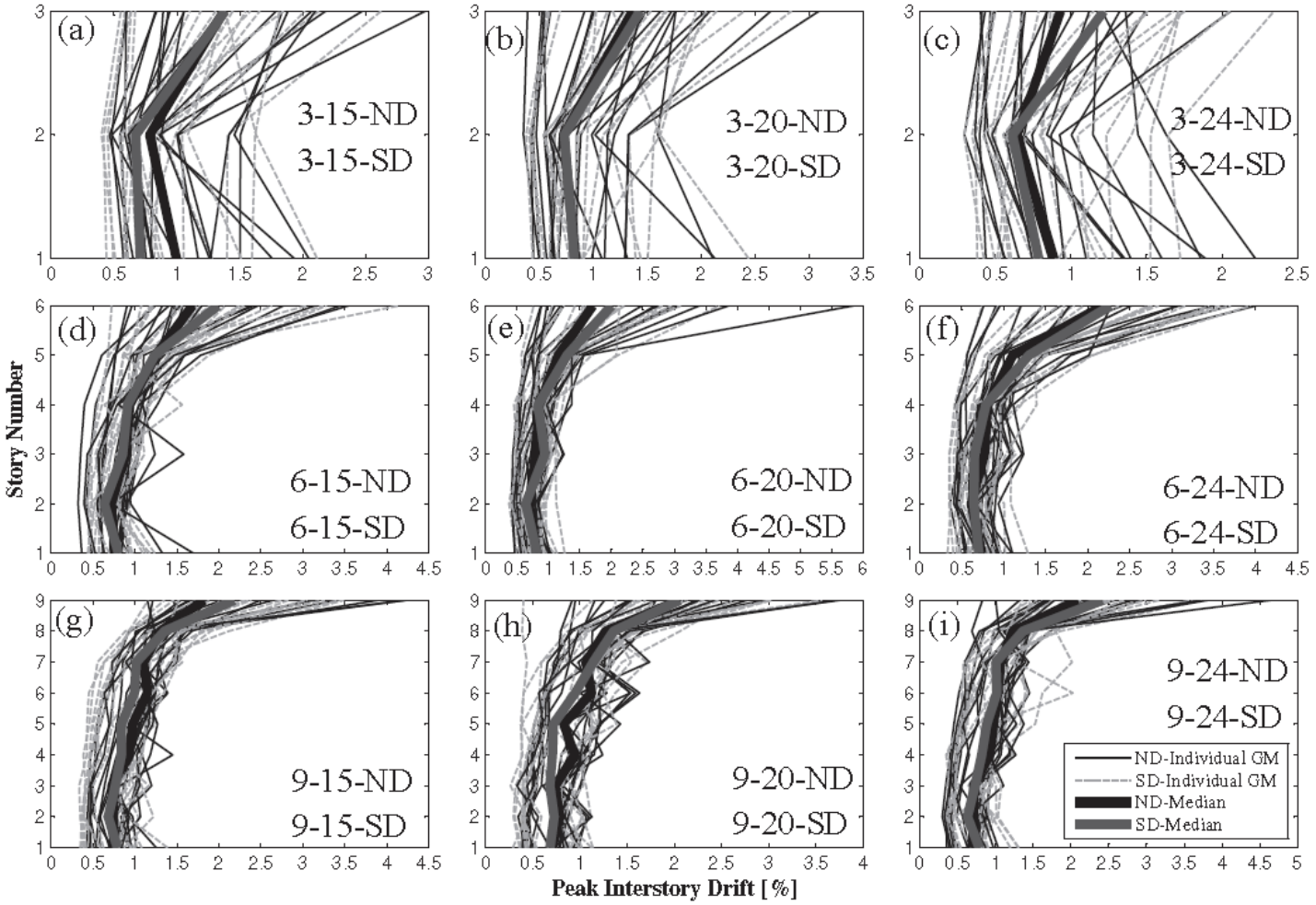

Figure 10. Peak interstory drifts at the 2/50 hazard level.

The 84th percentile PM_B values are less than 1.0 for all buildings at both hazard levels, which signifies the beams remain essentially elastic in terms of moment and axial load interaction. The SD yields lower PM_B values compared to the ND as expected since the beams of SD are capacity designed to resist higher flexural, axial, and shear demands than the beams of ND. Note that the differences in PM_B values for the ND and SD are more profound for the 2/50 hazard level.

The 84th percentile V_B is less than 1.0 for most of the models at both hazard levels. The buildings with narrower bay widths designed per the ND approach experience more significant shear demands at both hazard levels compared to the other buildings. Hence it can be concluded that the design approach and bay width significantly affect V_B. The ND leads to higher V_B values compared to the SD, which is consistent with the loads assumed in design. Similarly, as discussed in *Shear Reactions*, shear forces are dominant for beams in narrower B-SPSWs, which can be attributed to the steeper PTF inclination angle, θ. As a result, it can be inferred that shear yielding might be the failure mode for beams in narrow B-SPSWs designed per the ND; however, this yielding is localized at the ends of the beams.

Fig. 11(a) and Fig. 11(b) show the comparison of PM_B and V_B, respectively, along the building height for 9-15-ND and 9-15-SD, the buildings with the most severe beam demands. As can be seen from Fig. 11, the ND yields higher PM_B and V_B compared to the SD as expected. The beam shear demands in 9-15-ND exceed the yield strength under several GMs, especially for lower stories whereas 9-15-SD does not.

In spite of significant difference in PM_C values for the ND and SD design at the 10/50 hazard level, the mean PM_C values are less than 1.0 for most of the buildings. However, the columns designed in accordance with the ND experience significant

yielding at the 2/50 hazard level while the mean PM_C values of most of the SD columns are still less than 1.0.

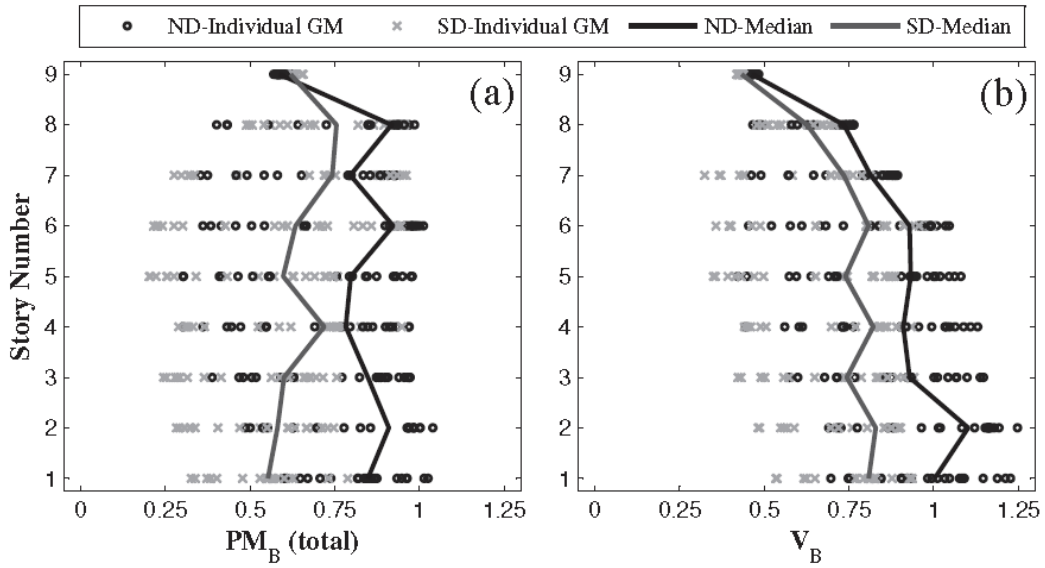

Figure 11. Demand-to-capacity ratios for the beams of 9-15-ND and 9-15-SD

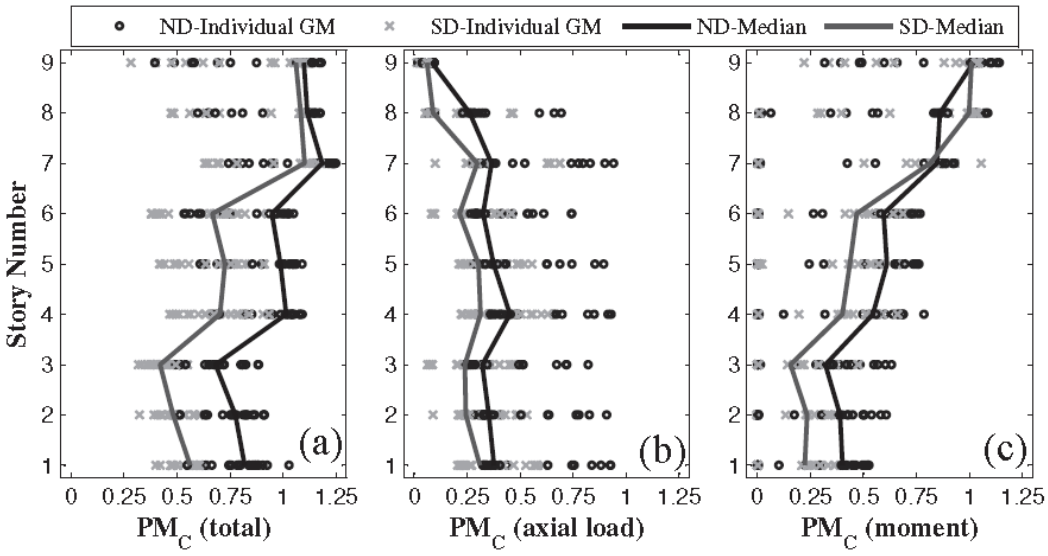

Figure 12. Demand-to-capacity ratios for the columns of 9-15-ND and 9-15-SD

Fig. 12 reveals the column demand-to-capacity values for 9-15-ND and 9-15-SD along the building height. Fig. 12(a), Fig. 12(b), and Fig. 12(c) show the total PM_C resulting from both the axial load and the bending moment, the contribution of the axial load to PM_C, and the contribution of the bending moment to PM_C, respectively. Recall that the axial load and moment capacities of the columns used in the PM interaction equations are calculated considering flexural buckling in the out-of-plane direction and lateral torsional buckling in the major bending direction of the wide flange section (in some cases which are much less than full plastic capacities) that are not captured in two-dimensional models. As depicted in Fig. 12, the vast portion of PM_C results from the bending moment. The contribution of the bending moment to the PM_C is more profound for upper stories. Recall that the column demands used in design are based on the axial loads from the gravity loads and the vertical web plate demands from the beam, V_L and V_R, and associated bending moments due to the beam end shears acting offset from the column centerline. The column bending moment demands considered in design account for only about 10% of the section P-M interaction ratio, implying that the columns are designed primarily for axial loads, which leads to light column sections vulnerable to additional moment demands. The column yielding (as demonstrated by PM_C values greater than or approaching 1.0) results from the additional bending moment demands associated with lateral drifts that are not considered in design. These bending moments are created due to unequal interstory drifts in the adjacent stories that affect the column section demands especially at floor levels. Newell and Uang [64] suggested that the bending moment demands in the columns at the floor levels can be accommodated by use of suitable lateral bracing at the floor levels for compact column sections susceptible to lateral torsional buckling under flexural demands, and column yielding at floor levels is deemed acceptable unless column instabilities occur (i.e., column buckling or column

hinging at mid-height of the column). Current research is focused on a column design procedure accounting for the bending moment demands resulting from nonuniform drifts.

CR_I and CR_R are also tabulated in Table 3. The reason of considering two connection rotation parameters is that the intermediate-story beams mostly undergo double curvature while roof beams always experience single curvature that affects the beam-column connection rotation demands. At the 10/50 hazard level, the 84^{th} percentile CR_I values and CR_R values are less than 0.024 and 0.031 rad, respectively. At the 2/50 hazard level, the 84^{th} percentile maximum CR_I is determined as 0.031 rad while the 84^{th} percentile maximum CR_R is 0.047 rad. Astaneh-Asl [65,66] reported that simple connections with single plate shear tabs can accommodate gravity rotations up to 0.103 rad (with rotation capacity increasing as the number bolts in the connection decreases) and cyclic rotations of 0.09 rad, and double angles supporting gravity loads can withstand rotations of 0.05 to 0.09 rad. Consequently, it can be concluded that simple connections can accommodate cyclic rotation demands in low-seismic regions and are suitable to be used as beam-column connections of B-SPSWs.

CONCLUSIONS

In this proof-of-concept study, the seismic performance of an alternative SPSW configuration called B-SPSWs designed for a low-seismic region is investigated. A series of 3-, 6-, and 9-story buildings located in Boston are designed as per the web plate strength and the boundary frame demand equations presented herein. Two different design approaches are considered: using R=3 without any seismic design considerations, and R=3.25 using a capacity design methodology consistent with other limited ductility (or "ordinary") steel seismic systems. Each building is subjected to forty ground motions scaled to the hazard levels of 10/50 and 2/50 for a low-seismic site in Boston. The

maximum peak interstory drifts from these analyses are below 2% at the 10/50 hazard level. For the designs in which the system is not specifically detailed for seismic resistance (R=3), some columns experience yielding at floor levels for the 2/50 hazard level; however, the beams remain essentially elastic. Note that the columns experience yielding primarily due to the moments induced by differential drifts that are not accounted for in design. The other design approach, in which the system is capacity designed for seismic resistance (R=3.25), leads to better performance where most of boundary elements remain elastic. The rotations in the simple beam-column connections are below the connection rotation capacities given for different simple connection types. The results appear to indicate that B-SPSWs show acceptable seismic performance for both design approaches (even though the seismically detailed (R=3.25) designs exhibit better performance than those non-seismically (R=3) detailed) and can be a viable option as a seismic force resisting system in low-seismic regions. Further experimental and numerical research is needed to verify or modify the response modification factor of 3.25 adopted for the SD designs, to evaluate the effects of and potential mitigation strategies for shear yielding in the ends of beams in narrow ND designs, and to develop column design methodologies accounting for the flexural demands resulting from differential drifts that are not considered by traditional design methodologies.

REFERENCES

[1] C.J. Thorburn, L.J. Kulak, G.L. Montgomery, Analysis of steel plate shear walls, Structural Engineering Report No. 107. University of Alberta. Edmonton, AB, 1983.

[2] T.M. Roberts, S. Sabouri-Ghomi, Hysteretic characteristics of unstiffened perforated steel plate shear panels, Thin-Walled Struct. 14 (1992) 139–151. doi:10.1016/0263- 8231(92)90047-Z.

[3] V. Caccese, M. Elgaaly, R. Chen, Experimental study of thin steel plate shear walls under cyclic load, J. Struct. Eng. 119 (1993) 573–587. doi:10.1061/(ASCE)0733-9445(1993)119:2(573).

[4] M. Elgaaly, Thin steel plate shear walls behavior and analysis, Thin-Walled Struct. 32 (1998) 151–180. doi:10.1016/S0263-8231(98)00031-7.

[5] A.S. Lubell, H.G.L. Prion, C.E. Ventura, M. Rezai, Unstiffened steel plate shear wall performance under cyclic loading, J. Struct. Eng. 126 (2000) 453–460. doi:10.1061/(ASCE)0733-9445(2000)126:4(453).

[6] B. Qu, M. Bruneau, Design of steel plate shear walls considering boundary frame moment resisting action, J. Struct. Eng. 135 (2009) 1511–1521. doi:10.1061/(ASCE)ST.1943-541X.0000069.

[7] K. Basler, Strength of plate girders in shear, Reprint No. 186 (61-13). Lehigh University Fritz Laboratory. Bethlehem, PA, 1961.

[8] ANSI/AISC 341-10 Seismic provisions for structural steel buildings, American Institute for Steel Construction (AISC), Chicago, IL, 2010.

[9] B. Qu, M. Bruneau, C.-H. Lin, K.-C. Tsai, Testing of Full-Scale Two-Story Steel Plate Shear Wall with Reduced Beam Section Connections and Composite Floors, J. Struct. Eng. 134 (2008) 364–373. doi:10.1061/(ASCE)0733-9445(2008)134:3(364).

[10] R. Purba, M. Bruneau, Case Study on the Impact of Horizontal Boundary Elements Design on Seismic Behavior of Steel Plate Shear Walls, J. Struct. Eng. 138 (2012) 645–657. doi:10.1061/(ASCE)ST.1943-541X.0000490.

[11] J.W. Berman, Seismic behavior of code designed steel plate shear walls, Eng. Struct. 33 (2011) 230–244. doi:10.1016/j.engstruct.2010.10.015.

[12] M. Gholipour, M.M. Alinia, Behavior of multi-story code-designed steel plate shear wall structures regarding bay width, J. Constr. Steel Res. 122 (2016) 40–56. doi:10.1016/j.jcsr.2016.01.020.

[13] J.W. Berman, M. Bruneau, Experimental investigation of light-gauge steel plate shear walls for the seismic retrofit of buildings, Technical Report MCEER-03-0001, Multidisciplinary Center for Earthquake Engineering Research, Buffalo, NY, 2003.

[14] J.W. Berman, M. Bruneau, Experimental Investigation of Light-Gauge Steel Plate Shear Walls, J. Struct. Eng. 131 (2005) 259–267. doi:10.1061/(ASCE)0733-9445(2005)131:2(259).

[15] A.K. Bhowmick, Seismic behavior of steel plate shear walls with centrally placed circular perforations, Thin-Walled Struct. 75 (2014) 30–42. doi:10.1016/j.tws.2013.09.027.

[16] D. Vian, M. Bruenau, Testing of special LYS steel plate shear walls, in: Proc. 13th World Conf. Earthq. Eng., Vancouver, BC, 2004.

[17] M. Bruneau, T. Bhagwagar, Seismic retrofit of flexible steel frames using thin infill panels, Eng. Struct. 24 (2002) 443–453. doi:10.1016/S0141-0296(01)00111-0.

[18] S.-J. Chen, C. Jhang, Experimental study of low-yield-point steel plate shear wall under inplane load, J. Constr. Steel Res. 67 (2011) 977–985. doi:10.1016/j.jcsr.2011.01.011.

[19] H. Moghimi, R.G. Driver, Column demands in steel plate shear walls with regular perforations using performance-based design methods, J. Constr. Steel Res. 103 (2014) 13–22. doi:10.1016/j.jcsr.2014.07.020.

[20] D. Vian, M. Bruneau, K.C. Tsai, Y.-C. Lin, Special Perforated Steel Plate Shear Walls with Reduced Beam Section Anchor Beams. I: Experimental Investigation, J. Struct. Eng. 135 (2009) 211–220. doi:10.1061/(ASCE)0733-9445(2009)135:3(211).

[21] D. Vian, M. Bruneau, R. Purba, Special Perforated Steel Plate Shear Walls with Reduced Beam Section Anchor Beams. II: Analysis and Design Recommendations, J. Struct. Eng. 135 (2009) 221–228. doi:10.1061/(ASCE)0733-9445(2009)135:3(221).

[22] T. Zirakian, J. Zhang, Structural performance of unstiffened low yield point steel plate shear walls, J. Constr. Steel Res. 112 (2015) 40–53. doi:10.1016/j.jcsr.2015.04.023.

[23] M. Xue, L.W. Lu, Interaction of infilled steel shear wall panels with surrounding frame members, in: Proc. Struct. Stab. Res. Counc. Annu. Tech. Sess., Bethlehem, PA, 1994: pp.339–354.

[24] G.L. Kulak, D.J.L. Kennedy, R. Driver, Discussion of "Experimental Study of Thin Steel Plate Shear Walls under Cyclic Load" by Vincent Caccese, Mohamed Elgaaly, and Ruobo Chen (February, 1993, Vol. 119, No. 2), J. Struct. Eng. 120 (1994) 3072–3073. doi:10.1061/(ASCE)0733-9445(1994)120:10(3072).

[25] E.W. Tromposch, G.L. Kulak, Cyclic and static behavior of thin panel steel plate shear walls, Structural Engineering Report No. 145. University of Alberta. Edmonton, AB, 1987.

[26] C. Vatansever, N. Yardimci, Experimental investigation of thin steel plate shear walls with different infill-to-boundary frame connections, Steel Compos. Struct. 11 (2011) 251–271. doi:10.12989/scs.2011.11.3.251.

[27] M. Xue, Behavior of steel shear wall panels and frame-wall systems (Ph.D. Dissertation), Lehigh University, 1995.

[28] R. Purba, M. Bruneau, Impact of Horizontal Boundary Elements Design on Seismic Behavior of Steel Plate Shear Walls, Technical Report MCEER-10-0007, MCEER, University at Buffalo, Buffalo, NY, 2010.

[29] H. Moghimi, R.G. Driver, Beam design force demands in steel plate shear walls with simple boundary frame connections, J. Struct. Eng. 140 (2014) 4014046. doi:10.1061/(ASCE)ST.1943-541X.0000993.

[30] A. Jahanpour, H. Moharrami, A. Aghakoochak, Evaluation of ultimate capacity of semi-supported steel shear walls, J. Constr. Steel Res. 67 (2011) 1022–1030. doi:10.1016/j.jcsr.2011.01.007.

[31] P.M. Clayton, J.W. Berman, L.N. Lowes, Seismic performance of self-centering steel plate shear walls with beam-only-connected web plates, J. Constr. Steel Res. 106 (2015) 198–208. doi:10.1016/j.jcsr.2014.12.017.

[32] L. Guo, Q. Rong, X. Ma, S. Zhang, Behavior of steel plate shear wall connected to frame beams only, Int. J. Steel Struct. 11 (2011) 467–479. doi:10.1007/s13296-011-4006-7.

[33] Y. Ozcelik, P.M. Clayton, Strip model for steel plate shear walls with beam-connected web plates, Eng. Struct. (2017) 369-379. doi: 10.1016/j.engstruct.2017.01.051

[34] I.-R. Choi, H.-G. Park, Steel plate shear walls with various infill plate designs, J. Struct. Eng. 135 (2009) 785–796. doi:10.1061/(ASCE)0733-9445(2009)135:7(785).

[35] ANSYS, ANSYS Documentation, 2016.

[36] P.M. Clayton, J.W. Berman, L.N. Lowes, Seismic Design and Performance of Self-Centering Steel Plate Shear Walls, J. Struct. Eng. 138 (2012) 22–30. doi:10.1061/(ASCE)ST.1943-541X.0000421.

[37] P.M. Clayton, T.B. Winkley, J.W. Berman, L.N. Lowes, Experimental Investigation of Self-Centering Steel Plate Shear Walls, J. Struct. Eng. 138 (2012) 952–960. doi:10.1061/(ASCE)ST.1943-541X.0000531.

[38] D.M. Dowden, P.M. Clayton, C.-H. Li, J.W. Berman, M. Bruneau, L.N. Lowes, K.-C. Tsai, Full-Scale Pseudodynamic Testing of Self-Centering Steel Plate Shear Walls, J. Struct. Eng. 142 (2016) 4015100. doi:10.1061/(ASCE)ST.1943-541X.0001367.

[39] J.W. Berman, M. Bruneau, Capacity design of vertical boundary elements in steel plate shear walls, Eng. Journal, AISC. 45 (2008) 55–71.

[40] CAN/CSA-S16-09 Design of steel structures, Canadian Standards Association, Mississauga, ON, 2009.

[41] P.A. Timber, G.L. Kulak, Experimental study of steel plate shear walls, Structural Engineering Report No. 114. University of Alberta, Edmonton, AB, 1983.

[42] R. Sabelli, M. Bruneau, Steel design guide: Steel plate shear walls, AISC, 2012.

[43] ANSI/AISC 360-10 Specification for structural steel buildings, American Institute for Steel Construction (AISC), Chicago, IL, 2010.

[44] State of art report on systems performance of steel moment frames subject to earthquake ground shaking, FEMA 355C, Federal Emergency Management Agency (FEMA), Washington D.C., 2000.

[45] Minimum design loads for buildings and other structures, ASCE/SEI 7-10, American Society of Civil Engineers and Structural Engineering Institute (ASCE/SEI), Reston, VA, 2010.

[46] P.-C. Hsiao, D.E. Lehman, J.W. Berman, C.W. Roeder, J. Powell, Seismic Vulnerability of Older Braced Frames, J. Perform. Constr. Facil. 28 (2014) 108–120. doi:10.1061/(ASCE)CF.1943-5509.0000394.

[47] Quantification of building seismic performance factors, FEMA P695, Federal Emergency Management Agency (FEMA), Washington D.C., 2009.

[48] J. Berman, M. Bruneau, Plastic analysis and design of steel plate shear walls, J. Struct. Eng. 129 (2003) 1448–1456. doi:10.1061/(ASCE)0733-9445(2003)129:11(1448).

[49] D.J. Webster, J.W. Berman, L.N. Lowes, Experimental investigation of SPSW web plate stress field development and vertical boundary element demand, J. Struct. Eng. 140 (2014) 4014011. doi:10.1061/(ASCE)ST.1943-541X.0000989.

[50] M. Behbahanifard, G. Grondin, A. Elwi, Analysis of steel plate shear wall using explicit finite element method, Proc., 13th World Conf. Earthq. Eng. Vancover, B.C., Canada. (2004).

[51] R.G. Driver, G.L. Kulak, A.E. Elwi, D.J.L. Kennedy, FE and simplified models of steel plate shear wall, J. Struct. Eng. 124 (1998) 121–130. doi:10.1061/(ASCE)0733-9445(1998)124:2(121).

[52] J.J. Shishkin, R.G. Driver, G.Y. Grondin, Analysis of steel plate shear walls using the modified strip model, J. Struct. Eng. 135 (2009) 1357–1366. doi:10.1061/(ASCE)ST.1943-541X.0000066.

[53] L. Guo, R. Li, S. Zhang, G. Yan, Hysteretic analysis of steel plate shear walls (SPSWs) and a modified strip model for SPSWs, Adv. Struct. Eng. 15 (2012) 1751–1764. doi:10.1260/1369-4332.15.10.1751.

[54] D.J. Webster, The inelastic seismic response of steel plate shear wall web plates and their interaction with the vertical boundary members (Ph.D. Dissertation), University of Washington, 2013.

[55] P.M. Clayton, C.-Y. Tsai, J.W. Berman, L.N. Lowes, Comparison of web plate numerical models for self-centering steel plate shear walls, Earthq. Eng. Struct. Dyn. 44 (2015) 2093–2110. doi:10.1002/eqe.2578.

[56] S. Mazzoni, F. Mckenna, M.H. Scott, G.L. Fenves, OpenSees command language manual, (2006).

[57] C. Shen, Y. Tanaka, E. Mizuno, T. Usami, A two-surface model for steels with yield plateau, Japan Soc. Civ. Eng. Struct. Eng. Earthq. Eng. 8 (1992) 179–188.

[58] B. Qu, F. Sanchez-Zamora, M. Pollino, Mitigation of inter-story drift concentration in multi-story steel concentrically braced frames through implementation of rocking cores, Eng. Struct. 70 (2014) 208–217. doi:10.1016/j.engstruct.2014.03.032.

[59] P. Uriz, F.C. Filippou, S.A. Mahin, Model for cyclic inelastic buckling of steel braces, J. Struct. Eng. 134 (2008) 619–628. doi:10.1061/(ASCE)0733-9445(2008)134:4(619).

[60] P. Somerville, N. Smith, S. Punyamurthula, J. Sun, Development of ground motion time histories for Phase 2 of the FEMA/SAC Steel Project, SAC Background Document, Report No. SAC/BD-97/04, 1997.

[61] R. Purba, M. Bruneau, Seismic performance of steel plate shear walls considering two different design philosophies of infill plates. II: Assessment of collapse potential, J. Struct. Eng. 141 (2015) 4014161. doi:10.1061/(ASCE)ST.1943-541X.0001097.

[62] P.M. Clayton, J.W. Berman, L.N. Lowes, Seismic design and performance of self-centering steel plate shear walls, J. Struct. Eng. 138 (2012) 22–30. doi:10.1061/(ASCE)ST.1943-541X.0000421.

[63] S.H. Chao, S.C. Goel, S.-S. Lee, A seismic design lateral force distribution based on inelastic state of structures, Earthq. Spectra. 23 (2007) 547–569.

[64] J.D. Newell, C.-M. Uang, Cyclic behavior of steel wide-flange columns subjected to large drift, J. Struct. Eng. 134 (2008) 1334–1342. doi:10.1061/(ASCE)0733-9445(2008)134:8(1334).

[65] A. Astaneh-Asl, Design of shear tab connections for gravity and seismic loads, Steel Tips, Struct. Steel Educ. Counc. (2005).

[66] A. Astaneh-Asl, Notes on design of double-angle and tee shear connections for gravity and seismic loads, Steel Tips, Struct. Steel Educ. Counc. (2005).

Appendix C

Paper 3. Behavior of columns of steel plate shear walls with beam-connected web plates

Yigit Ozcelik, Patricia M. Clayton

Submitted to *Engineering Structures*

ABSTRACT

Steel plate shear walls with beam-connected web plates (B-SPSWs) are an alternative configuration of steel plate shear walls (SPSWs) where web plates are connected to the beams only. Detaching web plates from columns and introducing simple beam-column connections in B-SPSWs eliminate flexural demands in the columns resulting from web plate tension field action; consequently, the columns of B-SPSWs are designed primarily for axial loads. A recent study, however, showed that the columns of B-SPSWs resist significant flexural demands during earthquake shaking due to differential interstory drifts that result in significant column rotations at floor levels. Typical design methods (i.e., the Equivalent Lateral Force method and Modal Response Spectrum analysis) do not capture these rotations associated with differential drifts that might lead to column instability. A two-phase numerical study is conducted to evaluate the behavior and stability of B-SPSW columns. In the first phase, three-dimensional nonlinear response-history analyses are conducted to investigate the column stability for eighteen B-SPSWs with different geometric characteristics designed following two design approaches. The results suggest that column buckling is a possible mode of failure for one of the design approaches. In the second phase, a parametric study is undertaken to further investigate potential column buckling failure modes in B-SPSW columns and to

establish an upper-bound estimate for the column buckling strength reduction due to column rotations at floor levels that are not considered in traditional design approaches.

KEYWORDS

Steel plate shear wall, beam-connected web plate, column behavior, column stability, unequal interstory drift, low-seismic design

INTRODUCTION AND BACKGROUND

Steel plate shear walls (SPSWs) are a reliable lateral load resisting system known for their high lateral stiffness, stable hysteresis characteristics, and high energy dissipation capacity [1-5]. Owing to moment-resisting beam-column connections in the boundary frame, the moment frame resists some portion of the lateral load; however, the primary lateral load resisting elements of SPSWs are web plates that are connected to beams and columns on all four edges. Due to a mechanism called tension field action (TFA) [6], thin web plates have a significant lateral load capacity and lateral stiffness after web plate buckling, provided that the surrounding boundary frame (i.e., beams and columns) has sufficient flexural stiffness and strength to anchor the inclined pull-in forces resulting from TFA. The inclined pull-in forces of the adjacent stories acting on an intermediate story beam create bending demands in opposite directions (i.e., the pull-in forces of the upper-story and lower-story web plates result in hogging and sagging in the beam, respectively). Unlike the beams of SPSWs, the pull-in forces act on only one side of the columns of SPSWs; consequently, the flexural demands resulting from TFA are more critical for columns. In addition to flexural demands, the columns of SPSWs resist significant axial loads due to both TFA and frame action, which leads to very large column sections for conventional SPSWs [7,8].

An alternative configuration of SPSWs called SPSWs with beam-connected web plates and simple beam-column connections (B-SPSWs) is proposed in the literature, where web plates are attached to the beams only [5,9-14]. Releasing web plates from the columns eliminates both flexural and axial demands in the columns due to the pull-in forces of the TFA acting on columns. Similarly, the simple beam-column connections prevent bending moment demands in columns resulting from frame action. Consequently, the columns of B-SPSWs show a similar behavior to gravity columns (leaner columns) and are expected to primarily resist axial loads, which might lead to lighter columns compared to the columns of conventional SPSWs.

Due to the difference in the boundary conditions of web plates, B-SPSWs show a different behavior in terms of the formation of TFA compared to conventional SPSWs. Fig.1(a) shows the formation of tension field action in the web plates of B-SPSWs when the B-SPSW undergoes a right lateral sway. Since the columns of B-SPSWs do not anchor the web plates, the formation of TFA is limited to some diagonal portion of the web plates, resulting in a partial tension field (PTF). The length of the PTF (L_p) and the inclination of the PTF measured from the vertical axis (θ) are given by Eq.1 and Eq.2, respectively, where L_c and H_c are the clear length and the clear height of the web plate, respectively [15]. The semi-empirical derivation of Eq.2 for the PTF inclination is described in detail by Ozcelik and Clayton [15]:

$$L_p = L_c - H_c \tan\theta \tag{1}$$

$$\theta = max\begin{pmatrix} 0.55-0.03\frac{L_c}{H_c} \\ 0.51 \end{pmatrix} \quad \tan^{-1}\frac{L_c}{H_c} \tag{2}$$

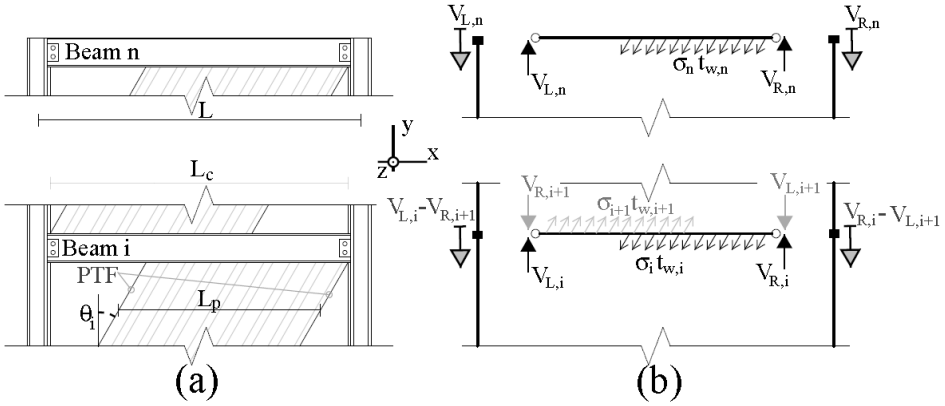

Figure 1. PTF in B-SPSWs (right sway): (a) formation of PTF and (b) column demands due to PTF.

Fig.1(b) shows the beam end vertical reactions and corresponding axial loads at the floor levels acting on the columns due to the PTF acting on the beams. The axial load transferred by the i^{th} floor beam (where i is the story index) to the right column is equal to the difference between the beam right end upward vertical reaction due to the PTF forces of the i^{th} story plate ($V_{R,i}$) and the beam right end downward vertical reaction due to the PTF forces of the $(i+1)^{th}$ story plate. Owing to the equilibrium of the web plate, the beam right downward vertical reaction of the i^{th} floor beam due to the PTF forces of the $(i+1)^{th}$ story plate is equal to the beam left end upward vertical reaction of the $(i+1)^{th}$ floor beam due to the PTF forces of the $(i+1)^{th}$ story plate ($V_{L,i+1}$). Similarly, the axial load transferred by the i^{th} floor beam to the left column is equal to the difference between the beam left end upward vertical reaction due to the PTF forces of the i^{th} story plate ($V_{L,i}$) and the beam left end downward vertical reaction due to the PTF forces of the $(i+1)^{th}$ story plate ($V_{R,i+1}$). Assuming the web plate stress in the PTF (σ) is uniform, the axial loads in left and right columns in the i^{th} story due to lateral loads ($P_{R,i}$ and $P_{L,i}$, respectively), $V_{R,i}$, and $V_{L,i}$ can be calculated using Eq.3, Eq.4, Eq.5, and Eq.6, respectively, where t_w is the web plate thickness and n is the number of stories.

$$P_{R_i} = \sum_{j=i}^{n} V_{R_j} - \sum_{k=i+1}^{n} V_{L_k} \quad (3)$$

$$P_{L_i} = \sum_{j=i}^{n} V_{L_j} - \sum_{k=i+1}^{n} V_{R_k} \quad (4)$$

$$V_{R_i} = \sigma\, t_{w_i}\, cos^2\theta_i\; L_{P_i}\left(1 - 0.5L_{p_i}/L_c\right) \quad (5)$$

$$V_{L_i} = \sigma\, t_{w_i}\, cos^2\theta_i\; L_{P_i}\left(0.5L_{p_i}/L_c\right) \quad (6)$$

A proof-of-concept study was undertaken by Ozcelik and Clayton [16] to assess the performance of B-SPSWs designed for low-seismic regions. Three-, six-, and nine-story B-SPSWs were designed for Boston adopting the dead and live loads and the floor plan of the three-story prototype building given in the SAC steel project [17]. Three aspect ratios (L_c/H_c) were considered in the parametric study to cover a wide range of applications. Ozcelik and Clayton [17] adopted two different design approaches, namely, the non-seismically-detailed design (ND) and the seismically-detailed design (SD); consequently, eighteen B-SPSWs were studied. The response modification factors (R) were chosen as 3 for the ND to be consistent with the R=3 assumed for non-seismically detailed steel systems, and R=3.25 was assumed for the SD to be consistent with the comparable Ordinary Concentrically Braced Frame steel system suitable for low-seismic design [19]. The web plate stress, σ, to be used in *Eq.5* and *Eq.6* to determine the column demands is given in Eq.7 for both design approaches. Note that σ for the ND is equal to the web plate stress resulting from the forces that are used to proportion the web plate; whereas, the SD adopts capacity design principles.

$$\sigma_i = \begin{cases} \frac{2\sum_{k=i}^{n} F_k}{L_{p_i} t_{w_i} \sin 2\theta_i} & \text{for } ND \\ R_y F_{yw} & \text{for } SD \end{cases} \quad (7)$$

where, F_k is the portion of the base shear applied at the story level k determined from the Equivalent Lateral Force method (ELF), and R_yF_{yw} is the expected yield strength of the web plate material.

Following the ND and SD approaches, Ozcelik and Clayton [16] designed the columns of the B-SPSWs for the axial loads given in Eq.3 and Eq.4 and the moments resulting from these loads acting at the beam end, which is offset from the column centerline (note that moment demands accounted for less than 10% of the design axial load-moment interaction ratio). Details of these designs, including geometry, beam and column member sizes, and web plate thicknesses are provided by Ozcelik and Clayton [16]. Two-dimensional nonlinear response-history analyses of the B-SPSWs were performed in OpenSEES [18], where the columns were represented by nonlinear beam-column elements without considering initial imperfections and residual stresses in the columns. The results of nonlinear response-history analyses revealed that the beams of SPSWs performed satisfactorily (i.e., the beams remained elastic); however, axial and moment demands in the columns suggested yielding and/or instabilities occurred in the columns of some buildings in spite of the fact that the axial load demands were less than the design axial loads. This result was attributed to the fact that unequal interstory drifts (ISD) causing rotations at floor levels resulted in significant moment demands in continuous multistory columns, having maximum demands at floor levels, which led to column failures. Note that the *AISC Seismic Provisions* (AISC 341-10) [19] states that ELF and the Modal Response Spectrum analysis have not been particularly developed to estimate the differences in story drifts that might cause flexural demands in the columns.

It is worth noting that since the models in this initial B-SPSW study were two-dimensional, Ozcelik and Clayton [16] evaluated the in-plane and out-of-plane stabilities of columns separately using the interaction equations H1-1 and H1-2 given in *AISC Specifications* (AISC 360-10) [20]. Hence, there is a need for investigating the bending moment demands in the columns of B-SPSWs resulting from the unequal ISDs that are not captured when the ELF is adopted for design, as well as the effects of these bending moment demands on the column performance. Such a study can be done by implementing a more detailed column model that explicitly captures in-plane and out-of-plane column buckling.

In this paper, a two-phase numerical study is undertaken to evaluate the column performance when there is bending moment demands in the columns resulting from unequal ISDs. Pursuant to this goal, in the first phase of the study, three-dimensional finite element models of the columns designed by Ozcelik and Clayton [16] are developed and analyzed adopting nonlinear analyses with seismic displacement histories. In the second phase, three-story isolated columns are analyzed considering various ISD patterns to establish an upper-bound estimate of the reduction in the axial load capacity of the columns due to unequal-ISD-induced moments.

FINITE ELEMENT MODEL OF COLUMNS

Three-dimensional finite element models of isolated columns (Fig.2(a)) are built in the commercially-available finite element software ABAQUS [21]. The columns are modeled using eight-node brick elements with reduced integration and hourglass control (C3D8R). ASTM A992 steel is selected for columns and the stress-strain diagram of ASTM A992 steel is adopted from the coupon test results of Stoakes and Fahnestock [22]

(Fig.3). Note that materials with different yield strengths are assigned to the flanges and webs of the columns. An isotropic strain hardening rule is assumed for both materials.

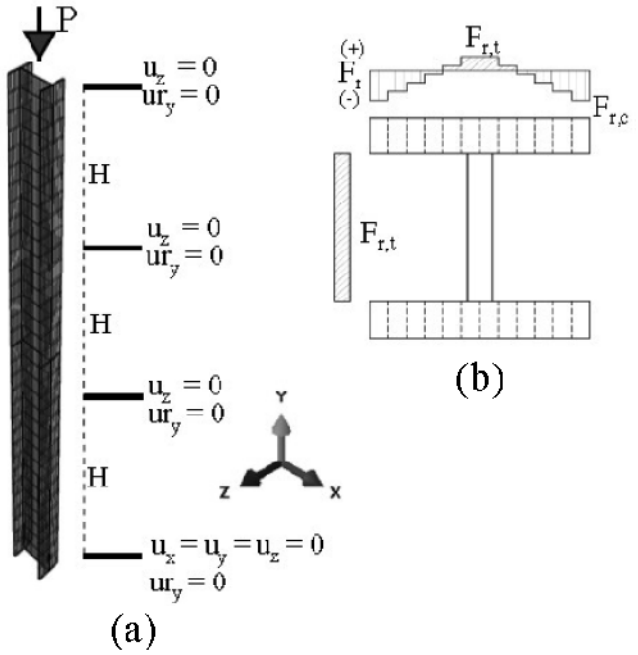

Figure 2. A typical three-story column model: (a) boundary conditions and (b) residual stress distribution in the cross-section.

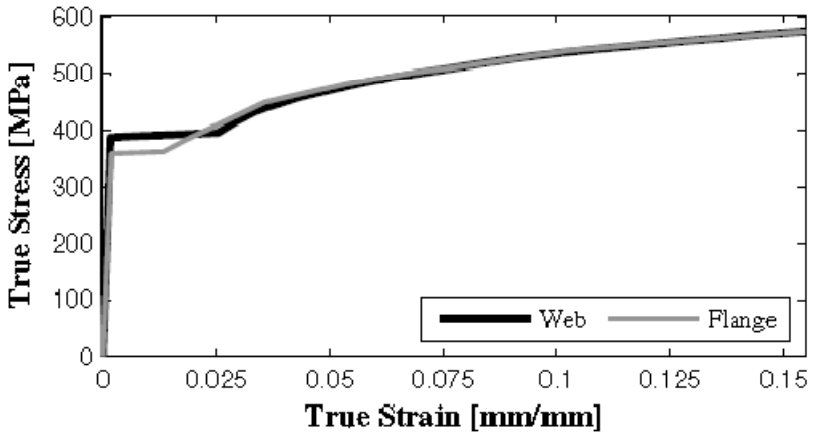

Figure 3. Stress-strain diagram of ASTM A992 steel adopted from Stoakes and Fahnestock [22]

Since the models consist of isolated columns, the interaction between the column and other elements (i.e., web plates and beams) is simulated by applying appropriate boundary conditions. Since the columns of B-SPSWs are typically oriented for strong-axis bending in the plane of the web plates, the Z-direction is selected as the out-of-plane direction and the translations in the Z-direction (u_z) are restrained at each floor level, i.e., the translations perpendicular to the B-SPSW bay are prevented at floor levels. The ISDs in the plane of web plates are simulated by applying translations at floor levels in the X-direction (u_x). The details and variations of u_x are explained in sections *Analysis of B-SPSWs columns* and *Parametric study of isolated columns* of this paper. The rotations about the column longitudinal axis (ur_y) at floor levels are restrained, assuming adequate torsional restraint is provided at each floor level and torsional deformation (twist) is negligible. A built-in constraint in ABAQUS called rigid body constraint is assigned to the sections at floor levels, which provides warping restraint. Note that the global coordinates of the system (X, Y, and Z) and the local coordinates of the cross-section (x, y, and z) are arranged so as to coincide with each other; consequently, the x- and z-axes are the minor (weak) and major (strong) bending axes of the column, respectively.

To simulate the inelastic buckling of columns, residual stresses (F_r) in the cross-section are modeled explicitly. The F_r distribution reported by Huber [23] for the wide flange section of W14x426 is adopted. The F_r pattern is approximated by a triangular distribution for flanges and a constant value is assumed for webs (Fig.2(b)). In the models, the flanges are split into twelve elements across the flange width in order to achieve the triangular F_r distribution. In accordance with the AISC 360-10 [20], the maximum magnitude of F_r (that is equal to the maximum compressive residual stress, F_{rc}) is assumed to be 30% of the column yield strength (F_y). The magnitude of the maximum tensile F_r, F_{rt}, is calculated by Eq.8.

$$F_{r_t} = F_{r_c} A_f / (A_f + A_w) \quad (8)$$

where, A_f and A_w are the flange and web areas, respectively.

The initial geometric imperfections are specified in both in-plane and out-of-plane directions assuming a *sine* shape distribution along the longitudinal direction (y-axis) of the column where the initial imperfections are maximum at mid-story heights and zero at floor levels in both directions. As per AISC 360-10 [20], the maximum out-of-straightness, Δ_o, is conservatively selected as $H/1000$, where H is the story height.

FINITE ELEMENT MODEL VALIDATION

To determine the validity of the finite element model, a parametric study is undertaken considering five W14 wide-flange sections covering a wide range of applications. Table 1 tabulates the cross-sectional area, the moment of inertia in the strong axis (I_z), the radius of gyration in the strong axis (r_z), the moment of inertia in the weak axis (I_x), and the radius of gyration in the weak axis (r_x) of the wide-flange sections considered in this study. Note that although I_x represents the strong-axis moment of inertia in AISC 360-10 [20], in this study, I_x and I_z align with the column local coordinate system. One-story pin-ended W14 sections are modeled following the aforementioned modeling approach and a concentric compressive axial load (P) is applied on the top end of the column in the y-direction. H is altered in order to obtain various column effective slenderness ratios, where the effective slenderness ratio in the out-of-plane (i.e., minor) direction is denoted as λ_x. Note that Δ_o is assumed to be $H/1500$ for the validation study since the column buckling strength curve provided by AISC 360-10 [20] is based on an Δ_o of $H/1500$.

Table 1. Cross-sectional dimensions of selected W14 wide flange sections

Section	Area (cm^2)	Major axis		Minor axis		
		I_z (10^4 cm^4)	r_z (cm)	I_x (10^4 cm^4)	r_x (cm)	r_z / r_x
W14x48	91.0	2.01	14.9	0.21	4.9	3.06
W14x61	115.5	2.66	15.2	0.45	6.2	2.44
W14x109	206.5	5.16	15.8	1.86	9.5	1.67
W14x176	334.2	8.91	16.3	3.49	10.2	1.60
W14x257	487.7	14.2	17.0	5.37	10.5	1.62

The plots of P normalized with respect to the axial yield strength, P_y, vs. maximum out-of-plane deflection at the mid-story height (Δ_z) normalized with respect to Δ_o are obtained. The maximum P obtained from each analysis is assumed to be the buckling strength (P_{cr}) of the corresponding λ_x. Fig.4 shows the determination of P_{cr} for W14x109 with various λ_x values.

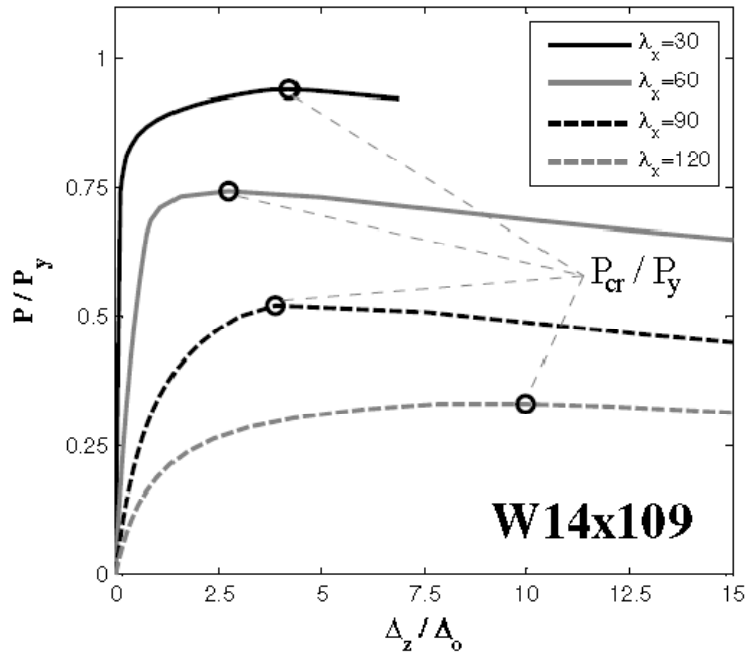

Figure 4. Determination of P_{cr} for W14x109 with various column effective slenderness ratios.

The comparison of P_{cr} determined from the analyses and the nominal compressive strength, P_n, given by AISC 360-10 as per equation E3-1 [20] is provided in Fig.5. F_y used in the P_n calculations is assumed to be the yield strength of the flange (358MPa) and the effective length factor in the minor direction (K_x) is assumed to be equal to 1.0. Fig.5 shows that P_{cr} and P_n are in reasonable agreement. For columns with λ_x in the vicinity of 80, the finite element model slightly underestimates the column buckling strength compared to the AISC column buckling strength curve; however, for the purpose of this study, it is deemed conservative and acceptable.

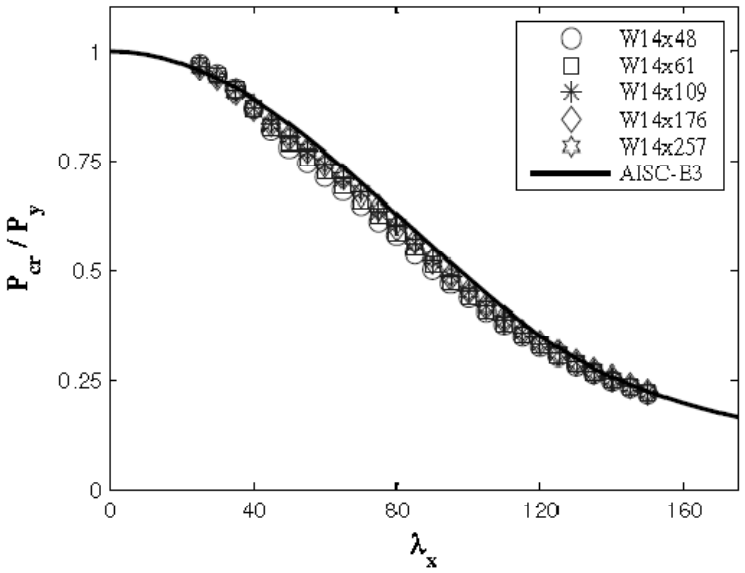

Figure 5. Comparison of column strengths of the finite element model and the AISC column buckling strength curve.

ANALYSIS OF B-SPSWS COLUMNS

The model Ozcelik and Clayton [16] adopted in the initial study of B-SPSW seismic behavior was not capable of properly simulating column buckling due to three main reasons: (1) Although the P-Δ effects were included in the system owing to the story drifts resulting from earthquake forces, the P-δ effects were not captured because no initial imperfections were specified in the columns between the floor levels, i.e., the stability of individual columns was not simulated in spite of the fact that the frame stability was considered in the models. (2) The residual stresses in the column were not simulated; consequently, the column stiffness in the inelastic range was not fully represented. (3) The models were two-dimensional; consequently, the out-of-plane deformations were not considered. Note that the strong axis of the columns of B-SPSWs is generally oriented in the plane of the B-SPSW; therefore, the out-of-plane stability of

columns, which was not simulated, is generally more critical compared to the in-plane stability of columns. Hence, a detailed study of columns is necessary.

Ozcelik and Clayton [16] analyzed eighteen B-SPSWs under two sets of ground motions (GM) developed by Somerville et al. [24] for Boston, each of which includes twenty GMs. The first suite was scaled to a seismic hazard level of 10% probability of exceedence in 50 years (10/50) while the second suite was scaled to a seismic hazard level of 2% probability of exceedence in 50 years (2/50). To evaluate the column performance based on the column demands obtained from these two-dimensional nonlinear time-history analyses, the maximum demand-capacity ratio of the columns (PM_c) were calculated. Pursuant to this goal, the interaction equations of AISC 360-10 [20] given in Eq.9 and Eq.10 were adopted which consider the in-plane and out-of-plane stabilities of the columns, respectively:

$$PM_c = \begin{cases} \frac{P_r}{P_{cz}} + \frac{8}{9}\left(\frac{M_{rx}}{M_{cx}} + \frac{M_{rz}}{M_{cz}}\right), & \frac{P_r}{P_{cz}} \geq 0.2 \\ \frac{P_r}{2P_{cz}} + \left(\frac{M_{rx}}{M_{cx}} + \frac{M_{rz}}{M_{cz}}\right), & \frac{P_r}{P_{cz}} < 0.2 \end{cases} \quad (9)$$

$$PM_c = \left(1.5 - 0.5\frac{P_r}{P_{cx}}\right) + \left(\frac{M_{rz}}{C_b M_{cz}}\right)^2 \quad (10)$$

where, P_r is the required axial strength (i.e., the axial demand), P_{cx} is the available compressive strength out of the plane of the B-SPSW, P_{cz} is the available compressive strength in the plane of B-SPSW, M_{rx} is the required flexural strength for weak axis flexure (i.e., the weak axis moment demand), M_{cx} is the design flexural strength for weak axis flexure, M_{rz} is the required flexural strength for strong axis flexure, M_{cz} is the design flexural strength for strong axis flexure (i.e., the strong axis moment demand), and C_b is the lateral-torsional buckling modification factor for strong axis flexure.

Table 2 tabulates the mean and 84th percentile of the $PM_{c,max}$ values for the suite of twenty GMs at the 2/50 hazard level as determined and discussed in detail by Ozcelik and Clayton [16], where $PM_{c,max}$ is the maximum PM_c calculated considering all of the sections along the length of all columns throughout the entire response history. The naming scheme for the models is as follows: (number of stories) - (bay width, L, in feet) - (design approach: ND or SD). The results show that the mean and 84th percentile of the $PM_{c,max}$ values of most of the B-SPSWs were larger than 1.0, especially for the ND. Note that while calculating the $PM_{c,max}$ values, the moment and axial load capacities of columns (M_{cx}, M_{cz}, P_{cx}, and P_{cz}) were determined as per AISC 360-10 [20] considering unbraced lengths of the columns in both axes and assuming resistance factors of 1.0. Ozcelik and Clayton [16] assumed that columns failed when $PM_{c,max}$ was approximately 1.0 or larger; however, this assumption might be conservative for the columns of B-SPSWs and the columns might have performed adequately in spite of having $PM_{c,max}$ larger than 1.0. As explained in *Introduction and background* section, the flexural demands resulting from differential ISDs are maximum at the floor levels; however, the second-order moments due to P-δ, which were not explicitly considered in the two-dimensional models, are more critical at the mid-height of the columns. The reduced axial capacity due to P-δ effects are incorporated in the interaction equations through use of column buckling strength instead of P_y. The use of the interaction equations (Eq.9 and Eq.10) of AISC 360-10 [20] to calculate PM_c at floor levels might have resulted in higher $PM_{c,max}$ compared to the real section demands for the columns of B-SPSWs since AISC 360-10 [20] necessitates the use of buckling strength for all sections along the length of columns even if the maximum bending demands resulting from the P-δ effects occur at the mid-height of the columns. Hence, having a $PM_{c,max}$ value at a floor level that is larger than 1.0 does not necessarily mean that column instability occurs. This observation

aligns with the results of the experimental study performed by Newell and Uang [25] which states that column yielding at floor levels is acceptable provided that suitable bracing is provided at floor levels and column instabilities do not occur. Note that the $PM_{c,max}$ values given in Table 2 are mostly the $PM_{c,max}$ values calculated at floor levels in upper stories where ISDs and the strong axis moment demands associated with differential ISDs are largest.

Table 2. Maximum demand-to-capacity ratios of B-SPSW columns at the 2/50 hazard level [16].

Model Name	$PM_{c,max}$		Model Name	$PM_{c,max}$	
	Mean	84th Pct		Mean	84th Pct
3-15-ND	1.06	1.13	3-15-SD	0.84	0.90
3-20-ND	1.06	1.13	3-20-SD	0.86	0.95
3-24-ND	1.04	1.12	3-24-SD	0.84	0.93
6-15-ND	1.08	1.22	6-15-SD	0.89	1.05
6-20-ND	1.09	1.20	6-20-SD	0.99	1.15
6-24-ND	1.17	1.31	6-24-SD	1.00	1.20
9-15-ND	1.11	1.24	9-15-SD	0.99	1.16
9-20-ND	1.24	1.34	9-20-SD	1.06	1.23
9-24-ND	1.25	1.37	9-24-SD	1.10	1.24

To investigate the behavior and stability of the column cases where column yielding occurs at floor levels due to the moments resulting from differential ISDs, three-dimensional models of the columns designed by Ozcelik and Clayton [16] are built in ABAQUS [21] as described in *Finite element model of columns* section. The column sizes are given in Table 3 [16]. As described in *Introduction and background* section, the

columns of B-SPSWs are released from web plates, the bases of the B-SPSW columns are assumed to be pinned, and simple connections are selected for beam-column connections; consequently, the contribution of the B-SPSW columns to the lateral stiffness of the B-SPSWs is theoretically assumed to be negligible. In other words, the flexural rigidity of the columns of B-SPSWs are assumed to not affect the ISD demands in B-SPSWs provided that column instabilities do not occur. Owing to this assumed behavior, the columns of B-SPSWs are modeled as isolated columns and the ISD demands and beam end shear reactions obtained from the nonlinear response-history analyses conducted by Ozcelik and Clayton [16] are applied to the system to simulate the ISDs and column axial load demands. All eighteen models with a constant H of 3.96 m were subjected to the ISD and beam end shear demands found in the twenty GMs representing the hazard level of 2/50 (i.e., GMs Bo21 through Bo40 given in Somerville et.al [24]). Using the amplitude function defined in ABAQUS [21], the discretized ISD demands at each floor level recorded throughout the time-history analyses of Ozcelik and Clayton [21] are applied as lateral translations in the x-direction (i.e., u_x). Similarly, the beam end shears are applied as point loads at floor levels using the amplitude function considering these loads act at the face of the column, offset from the column centerline. Note that each model consists of two isolated columns (left and right columns of the B-SPSWS) where they resist different axial loads while undergoing the same ISD demands. The splices are provided at the mid- height of the fourth story for six-story models and at the mid-height of the fourth and seventh stories for nine-story models. The base-to-column connections are assumed to be simple connections.

Table 3. Column sizes of B-SPSWs [16]

Model Name	Story			Model Name	Story		
	1-3	4-6	7-9		1-3	4-6	7-9
3-15-ND	W14x53	-	-	3-15-SD	W14x74	-	-
3-20-ND	W14x48	-	-	3-20-SD	W14x61	-	-
3-24-ND	W14x48	-	-	3-24-SD	W14x61	-	-
6-15-ND	W14x109	W14x61	-	6-15-SD	W14x159	W14x109	-
6-20-ND	W14x90	W14x61	-	6-20-SD	W14x132	W14x82	-
6-24-ND	W14x90	W14x53	-	6-24-SD	W14x120	W14x68	-
9-15-ND	W14x159	W14x99	W14x61	9-15-SD	W14x257	W14x159	W14x82
9-20-ND	W14x132	W14x90	W14x53	9-20-SD	W14x211	W14x132	W14x68
9-24-ND	W14x120	W14x90	W14x48	9-24-SD	W14x176	W14x120	W14x61

The results of these analyses that impose seismic response histories revealed that except for the columns of three-story B-SPSWs designed following the ND approach, the columns did not buckle under the GMs at the 2/50 hazard level. Note that $PM_{c,max}$ values given in Table 2 revealed that six- and nine-story columns had higher values, which suggested that six- and nine-story columns were more prone to column failures. This result, in part, can be attributed to the fact that the ISDs for the roof level of the taller models obtained from the two-dimensional nonlinear response-history analyses conducted by Ozcelik and Clayton [16] were larger compared to the lower stories due to higher mode effects, which led to higher strong-axis flexural demands at floor levels. However, the three-dimensional analyses undertaken in this study suggests that these flexural demands observed in six- and nine-story B-SPSWs do not lead to column stability problems even if column yielding is observed.

The $PM_{c,max}$ values calculated from the three-dimensional finite element analyses along the column height using Eq.9 are given in Fig.6, Fig.7 and Fig.8 for the three-, six-, and nine-story models with L of 20 feet (6.10m), respectively. The contributions of the flexural demands in the weak- and strong-axis to the total $PM_{c,max}$ are given in the figures. Note that while calculating $PM_{c,max}$, M_{cx} and M_{cz} are assumed as the plastic moment capacities in the weak axis and strong axis, respectively. Similarly, P_{cx} and P_{cz} are taken as P_y of the column section since the models are capable of capturing both P-Δ and P-δ effects.

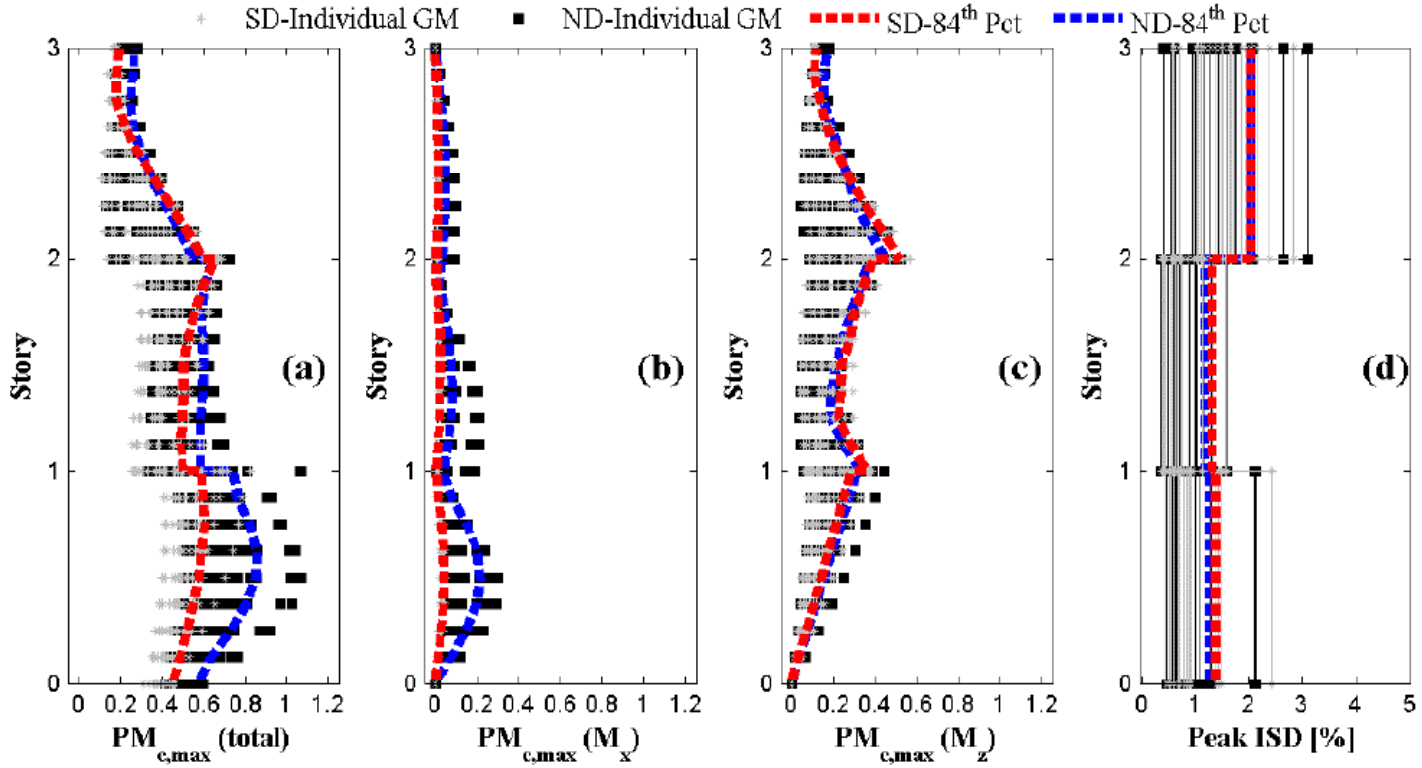

Figure 6. $PM_{c,max}$ for 3-20-ND and 3-20-SD: (a) total $PM_{c,max}$, (b) contribution of the weak-axis bending to $PM_{c,max}$, (c) contribution of the strong-axis bending to $PM_{c,max}$, and (d) peak interstory drift.

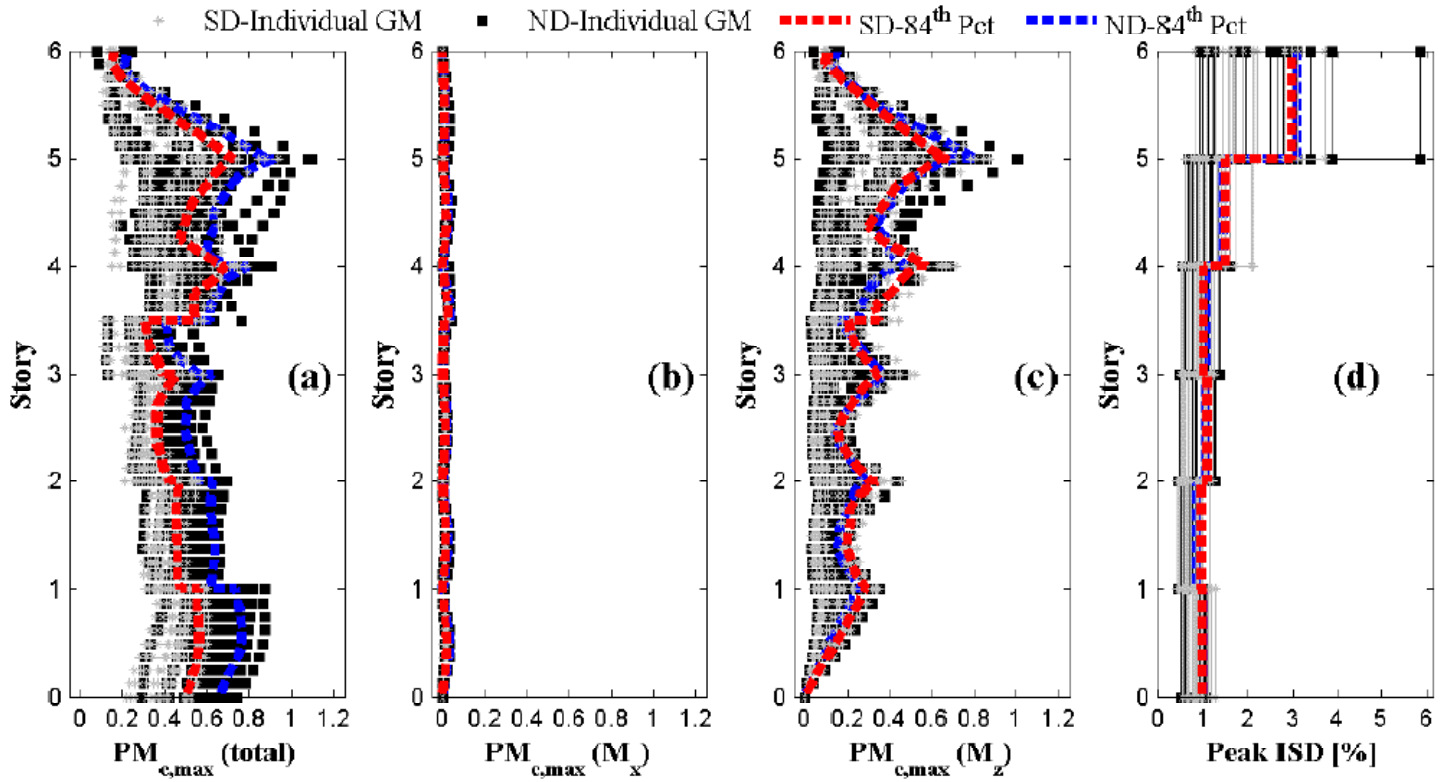

Figure 7. $PM_{c,max}$ for 6-20-ND and 6-20-SD: (a) total $PM_{c,max}$, (b) contribution of the weak-axis bending to $PM_{c,max}$, (c) contribution of the strong-axis bending to $PM_{c,max}$, and (d) peak interstory drift.

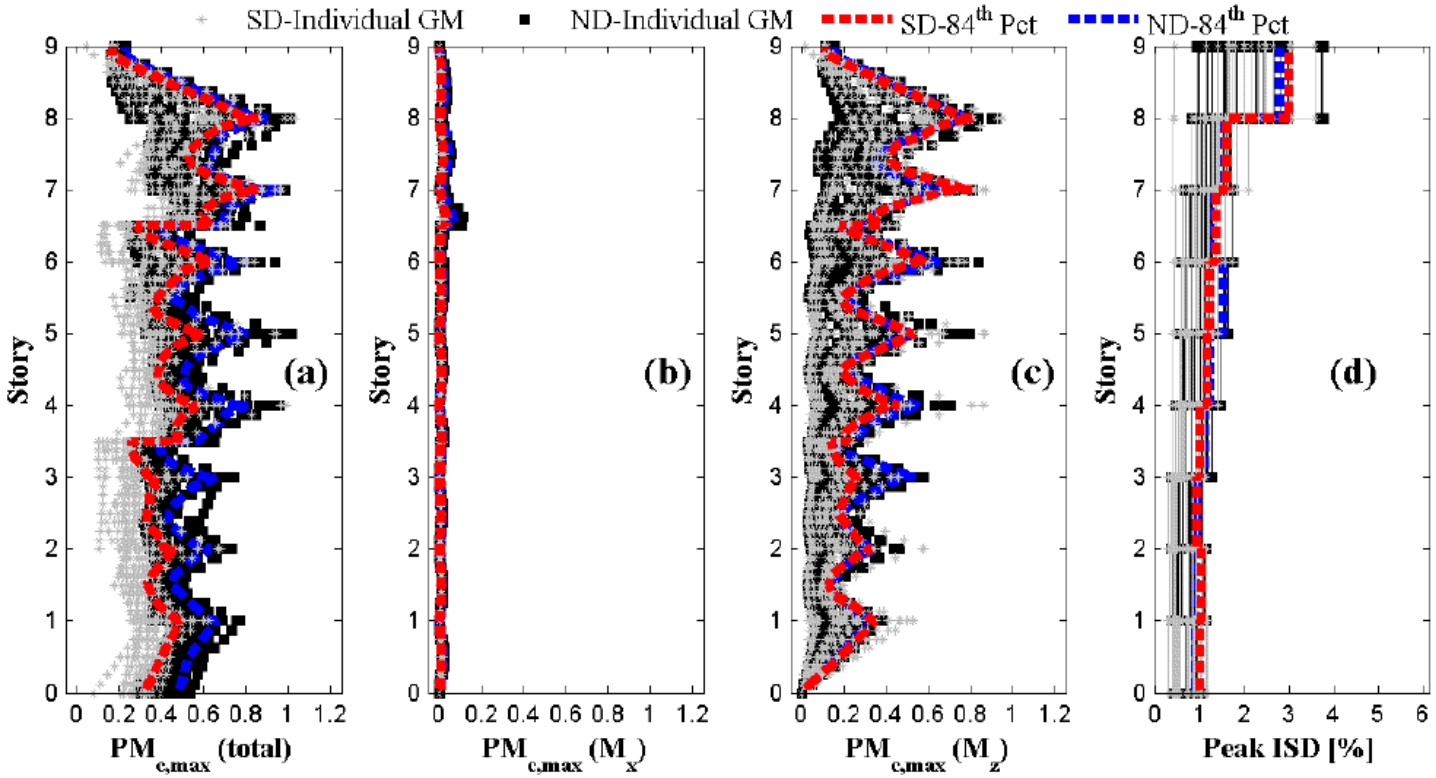

Figure 8. $PM_{c,max}$ for 9-20-ND and 9-20-SD: (a) total $PM_{c,max}$, (b) contribution of the weak-axis bending to $PM_{c,max}$, (c) contribution of the strong-axis bending to $PM_{c,max}$, and (d) peak interstory drift.

As depicted in Fig.6, column yielding at floor levels is not observed for both 3-20-ND and 3-20-SD except for one case (yielding at first floor of 3-20-ND under one of the GMs); however, column buckling occurs about the minor axis for 3-20-ND under several GMs as can be inferred from the significant flexural demands in the weak-axis at the mid-height of the first-story column (Fig.6(b)). Fig.7(c) and Fig.8(c) reveal that the columns of both six- and nine-story B-SPSWs designed for both ND and SD resist flexural demands close to the plastic moment capacities in the strong axis for upper floor levels. Note that the design approach does not have a significant effect on the strong-axis flexural demands at the floor levels. This can be attributed to the fact that both design approaches adopt similar R factors, which leads to almost identical web plate thicknesses; consequently, the lateral stiffnesses of B-SPSWs are similar, which results in comparable ISDs and column rotations at floor levels. As seen from Fig.7 and Fig.8, the column strengths are mostly exhausted by the strong-axis flexural demands, and the total $PM_{c,max}$ values are approaching to or larger than 1.0; however, column stability is maintained for both six- and nine-story columns regardless of the design approach. It is worthwhile noting that the columns of the SD show a better performance compared to the ND in terms of total $PM_{c,max}$.

The P_{max}/P_n ratios are calculated and tabulated in *Table 4*. P_{max}/P_n is defined as the maximum axial load carried by the column normalized with respect to P_n (details of the P_n calculation are given in *Finite element validation* section). Recall that column buckling is observed only for the columns of 3-15-ND, 3-20-ND, and 3-24-ND. Note that the SD frame members were designed assuming higher σ values due to capacity design principles, which leads to higher column design loads in the SD compared to the ND when the plate thickness are almost identical. Also note that both design approaches yield similar plate thicknesses as previously mentioned. As can be seen from Table 4, the B-

SPSWs designed per the ND approach have higher P_{max}/P_n ratios, which aligns with the expectations considering the smaller column sizes. As the P_{max}/P_n ratios for B-SPSWs adopting the NDs are close to 1.0 (especially for three-story B-SPSWs), it can be concluded that the SD leads to designs less vulnerable to stability problems.

Table 4. Maximum column axial load demand-to-capacity ratios for response-history analyses

Model Name	P_{max}/P_n			Model Name	P_{max}/P_n		
	Min	84th Pct	Max		Min	84th Pct	Max
3-15-ND	0.58	0.92	0.98	3-15-SD	0.34	0.63	0.64
3-20-ND	0.70	0.96	1.00	3-20-SD	0.42	0.62	0.64
3-24-ND	0.65	0.92	0.98	3-24-SD	0.44	0.62	0.63
6-15-ND	0.37	0.69	0.84	6-15-SD	0.30	0.53	0.64
6-20-ND	0.35	0.77	0.86	6-20-SD	0.28	0.58	0.61
6-24-ND	0.44	0.77	0.86	6-24-SD	0.31	0.60	0.64
9-15-ND	0.35	0.57	0.74	9-15-SD	0.28	0.40	0.42
9-20-ND	0.37	0.60	0.64	9-20-SD	0.09	0.45	0.46
9-24-ND	0.46	0.62	0.80	9-24-SD	0.10	0.47	0.56

Fig.9 shows the P_{max}/P_n ratios under each ground motion for three-story models. Column buckling is observed for 8, 7, and 6 of the 20 GMs for 3-15-ND, 3-20-ND, and 3-24-ND, respectively. Note that it is judged that column buckling occurs when the column is not capable of carrying the beam end shear reactions at a particular time step of the response-history analysis, since the beam end shear demands applied on the column are force-controlled. For models 3-15-ND, 3-20-ND, and 3-24-ND, the P_{max}/P_n ratios of the columns for which column buckling is observed are between 0.87 and 0.98, 0.88 and

1.00, and 0.89 and 0.97, respectively. Note that the P_{max}/P_n ratios calculated under some of the GMs (e.g, Bo26 and Bo29 for 3-15-ND) fall in the P_{max}/P_n ratio ranges where column buckling is observed; however, columns do not buckle. Consequently, it can be inferred that a higher P_{max}/P_n ratio does not necessarily lead to column stability problems for particular GMs. For purposes of design, it would be beneficial to establish a lower-bound limit for the P_{max}/P_n ratio over which column stability may be a concern. This P_{max}/P_n limit for column instability is investigated in *Parametric study of isolated columns* section.

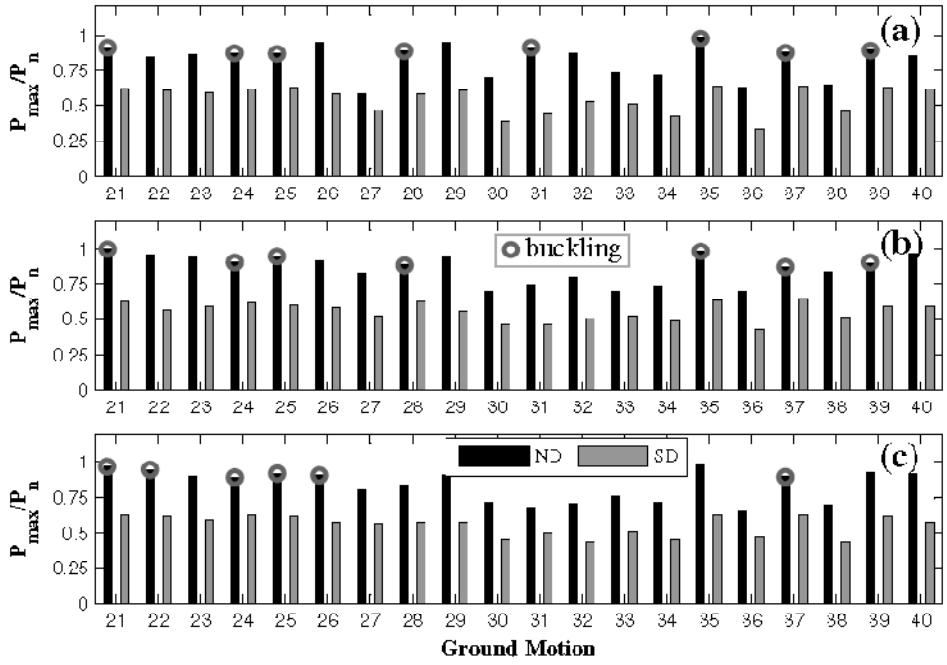

Figure 9. P_{max} / P_n for under each GM: (a) 3-15-ND and 3-15-SD, (b) 3-20-ND and 3-20-SD, and (c) 3-24-ND and 3-24-SD.

PARAMETRIC STUDY OF ISOLATED COLUMNS

As mentioned in *Introduction and background* section, the ELF procedure for determining seismic demands was not particularly developed to estimate differences in

ISD, and estimating differences in ISD using the Modal Response Spectrum analysis is problematic [19]. Nonlinear response-history analysis would be the viable option to estimate column rotations at floor levels and corresponding moment demands; however, it is not always practical in design and as mentioned in *Analysis of B-SPSWs columns* section the obtained demands from nonlinear response-history analyses are dependent on the suite of GMs selected. To propose a simplified column design approach based on the demands obtained from the ELF method, a parametric study of isolated columns is undertaken to evaluate the effect of the column bending moment demands resulting from differential ISDs on column buckling strength.

Three-story isolated column finite element models (as described in *Finite element model of columns* section) of five W14 sections (Table 1) are considered in this study. Two different *H*s are selected (3.96m and 6.10m) and *H* is assumed to be the same for all three stories. The ISDs are simulated by inducing translations in the x-direction at floor levels (u_x). Since the model consists of an isolated column and the ISDs observed in real buildings under dynamic loading are dependent on several parameters such as the geometrical characteristics and material properties of web plate and the GM-related parameters, a conservative approach is adopted for simulating ISDs. Thirteen variations of ISDs normalized with respect to the peak interstory drift (PD) given in Fig.10 are considered so that a wide range of possible ISD distributions creating differential drifts within three-story columns are evaluated. Four PDs are considered in this study (1, 2, 3, and 4%). Note that the maximum ISD Ozcelik and Clayton [16] obtained from nonlinear response-history analyses of B-SPSWs was about 4%. To simulate the restraining effect of the base plate or the column below the isolated three-story column model, two different boundary conditions, namely, pinned and fixed, are considered for the base boundary condition of the bottom-story column; consequently, lower and upper bounds

of the restraining effect are investigated. Note that although the fixed boundary condition restrains the bottom-story column better compared to the pinned boundary condition, it might increase the strong-axis flexural demands in the upper-story columns. Hence, it is difficult to predict in advance which boundary condition provides the worst-case scenario in terms of evaluating column buckling capacities.

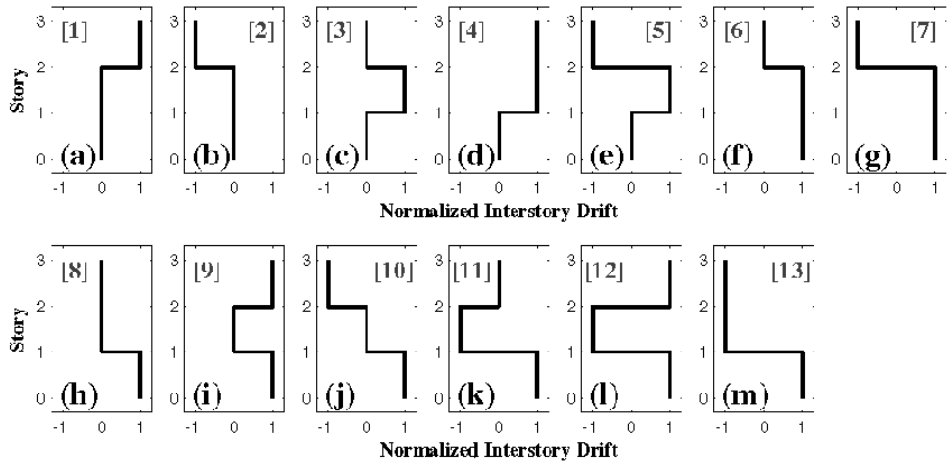

Figure 10. Variations of interstory drifts.

For each model, floor displacements are applied first considering one of the ISD distributions given in Fig.10 until reaching the prescribed PD (note that the ISD of each story is equal to 0. or +PD or -PD), then P is applied on the top-story column as depicted in Fig.2(a). P_{cr} is determined from the analysis results as explained in *Finite element model validation* section and shown in Fig.4; consequently, the relationship between P_{cr} and PD is obtained. Note that applying P only on the top-story column does not fully represent the axial load distribution in the columns of B-SPSWs; however, this approach provides a conservative baseline scenario for examining the column behavior since the restraining effect provided by the adjacent story columns that carry the same P is less

than columns resisting different axial loads. Similarly, the same P might cause buckling in the second or third stories if the strong-axis flexural demands are higher in these stories. This model in which P is the same in each of the three stories can be extended to columns with more than three-stories that are susceptible to buckling in their upper stories, because it is able to capture buckling in any of the three stories considering upper and lower bound limits on rotational restraint at the bottom of the three-story column segment.

For Hs of 3.96m and 6.10m, Fig.11 and Fig.12, respectively, show the applied load, P, normalized with respect to the nominal compression capacity calculated per AISC 360-10 [20], P_n, vs. the column mid-height displacement, Δ, normalized with respect to the maximum initial imperfection, Δ_o. The column response is shown for various PDs for the most critical ISD configuration (given in Fig.10) that leads to the lowest P_{cr} at a given PD. The naming scheme of each curve is as follows: boundary condition at the base (P for pin and F for fix) - the ISD configuration given in Fig.10 - the story at which column buckling occurs - the direction of the column mid-height displacement (i.e., x and z represent the in-plane and the out-of-plane buckling, respectively). As seen from Fig.11 and Fig.12, column buckling occurs in the weak-axis direction and the pinned base connection is more critical than fixed connection regardless of the ISD distribution or the column section. The ISD configuration 12 (Fig.10(l)) is the most critical ISD configuration for most of the cases, which can be attributed to the fact that the ISD configuration 12 induces displacements in the x-direction that are in the same direction with the specified initial imperfections in the x-direction (Fig.13); consequently, the P-δ effects become more prominent. The effect of PD on the reduction in the axial load capacity diminishes with the increase in PD. For example, for W14x48 with 3.96m story heights (Fig.11(a)), the P_{cr} when PD is 1% is about 16% less than the

P_{cr} when PD is zero (i.e., no flexural demands due to ISDs), while the reduction in P_{cr} when PD is 2% is about 19% compared to when PD is zero. This behavior can be attributed to the fact that flexural demands in the strong axis due to ISDs almost reach the plastic moment capacity when PD exceeds 1%. Another interesting observation is that column rotations at floor levels due to differential ISD demands do not have a significant effect on the columns with λ_x less than 50.

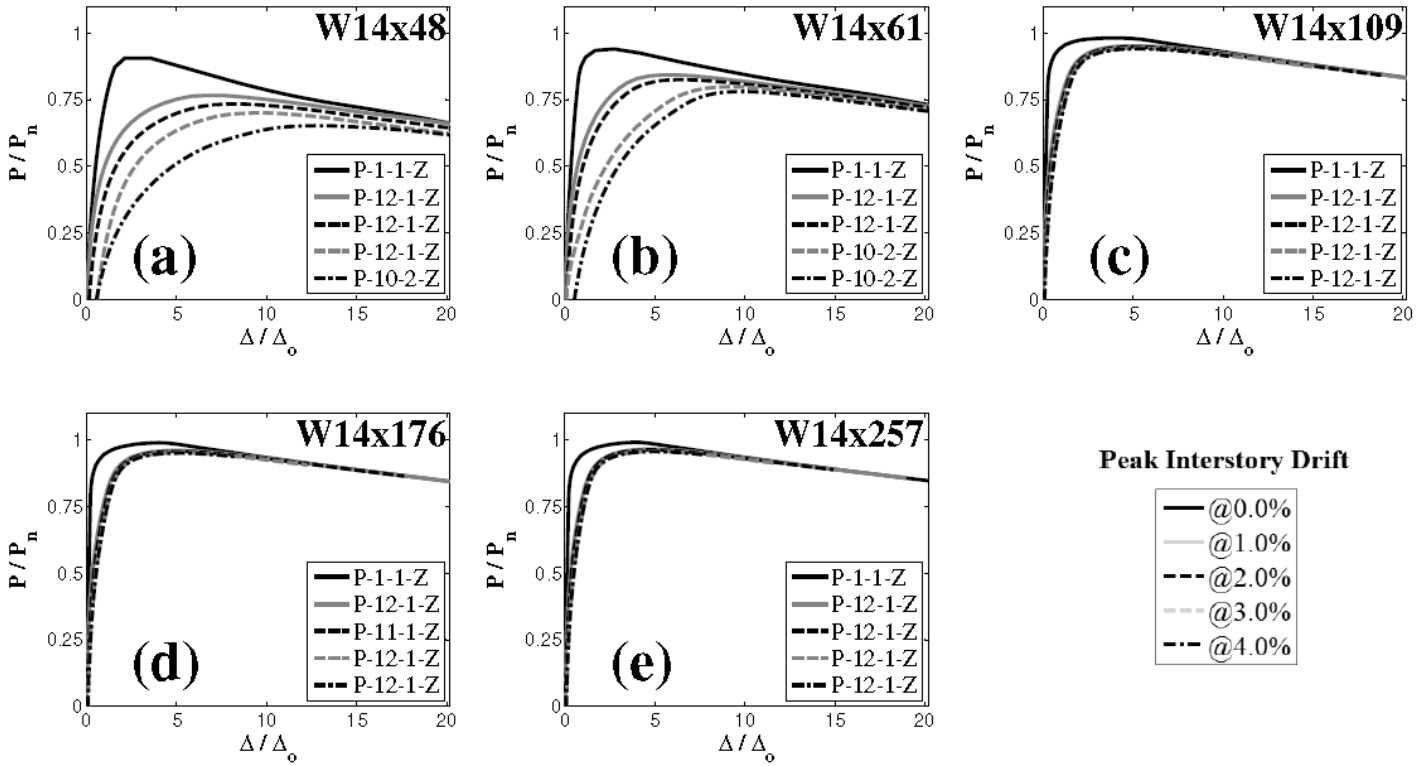

Figure 11. Normalized axial load vs. normalized column mid-height displacement at various peak interstory drifts (story height of 3.96m): (a) W14x48 (λ_x = 81), (b) W14x61(λ_x = 63), (c) W14x109 (λ_x = 42), (d) W14x176 (λ_x = 39), and (e) W14x257 (λ_x = 38).

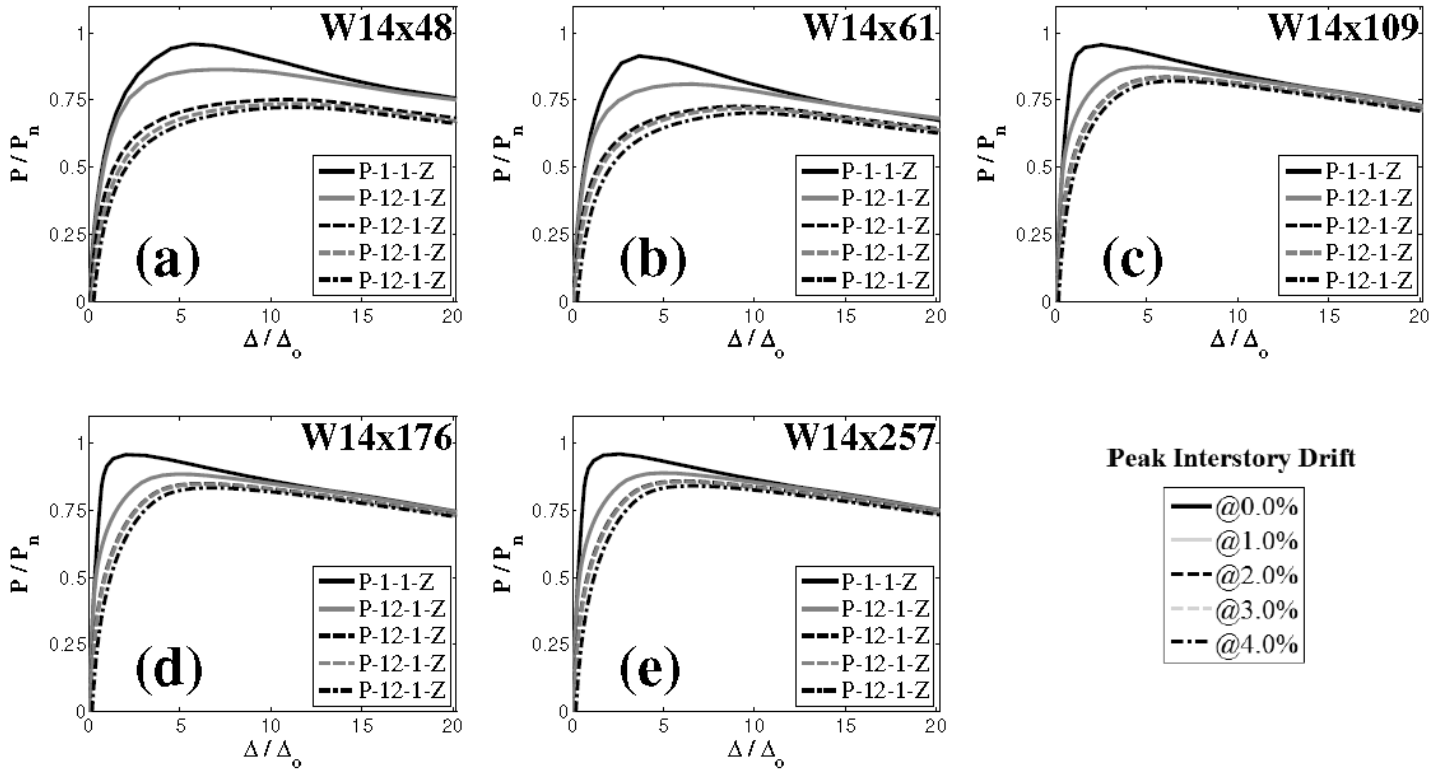

Figure 12. Normalized axial load vs. normalized column mid-height displacement at various peak interstory drifts (story height of 6.10m): (a) W14x48 (λ_x = 125), (b) W14x61 (λ_x = 97), (c) W14x109 (λ_x = 64), (d) W14x176 (λ_x = 59), and (e) W14x257 (λ_x = 58).

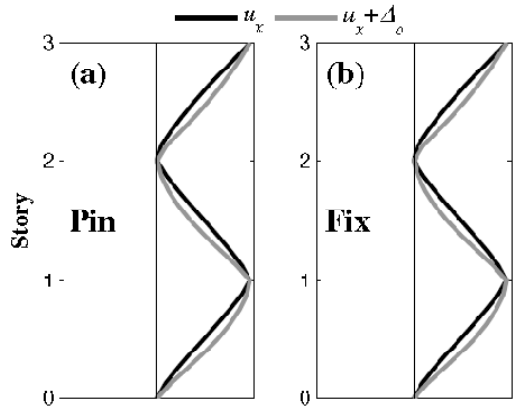

Figure 13. Column centerline in the x-direction for the ISD configuration 12 before applying *P*: (a) pinned base and (b) fixed base

For *H*s of 3.96m and 6.10m, Fig.14 and Fig.15, respectively, show the normalized P_{cr} vs. PD for all thirteen ISD configurations given in Fig.10 and the two boundary conditions (i.e., pinned and fixed) at the column base. The results show that as the slenderness of the column increases, the dependency of the reduction in P_{cr} on the ISD configuration increases, i.e., the buckling capacity of stockier columns are less prone to the changes in the ISD distribution. Another observation is that the rate of the reduction in P_{cr} for PDs larger than 2% is less profound, which aligns with the trends observed in Fig.11 and Fig.12. Owing to this trend and the fact that the 2% ISD is a typical drift limit used for seismic design, an empirical column strength reduction factor, ζ, that is dependent on geometrical and cross-sectional column properties and independent of the maximum expected drift demand, PD, is proposed. This ζ factor is proposed to reduce the nominal column compressive capacity, P_n, to conservatively account for potential instabilities associated with differential ISD demands when the ELF is adopted for seismic design. The equation for ζ is given in Eq.11. Note that this equation is calibrated for only W14 sections with typical *H* values found in buildings. *Eq.11* yields a ζ value of 0.70 for both of the W14x48 and W14x53 column sections with 3.96 m story heights that

are used for the three-story ND designs that experience column buckling as shown in Fig.9. Recall that the minimum P_{max}/P_n ratios that result in column buckling in the three-dimensional B-SPSW column models were 0.87, 0.88, and 0.89 for 3-15-ND, 3-20-ND, and 3-24-ND, respectively, which are larger than the ζ values given for W14x48 and W14x53 (i.e., the reduced column capacity determined using the proposed ζ is conservatively lower than the axial demands that were observed to result in column instability during seismic analysis). Consequently, it can be concluded that Eq.11 provides a lower-bound approximation accounting for the reduction in P_n due to the column rotations at floor levels.

$$\zeta = -0.42 + \frac{4.05}{r_z/r_x} - \frac{2.36}{(r_z/r_x)^2} + 0.008\frac{H}{r_x} - 0.023\frac{H}{r_z} \quad (11)$$

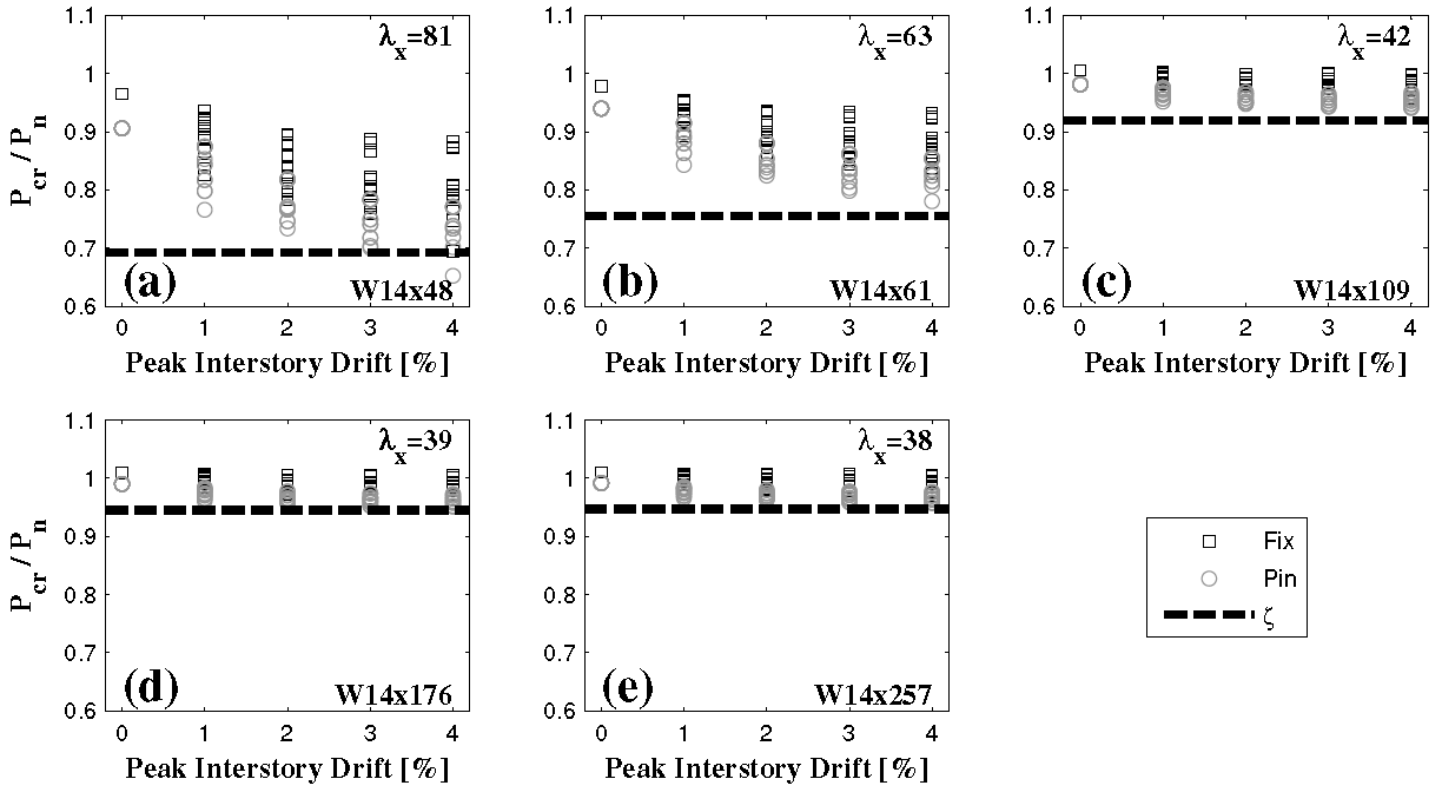

Figure 14. Normalized buckling strength vs. peak interstory drift for different ISD configurations and boundary conditions (story height of 3.96m): (a) W14x48, (b) W14x61, (c) W14x109, (d) W14x176, and (e) W14x257.

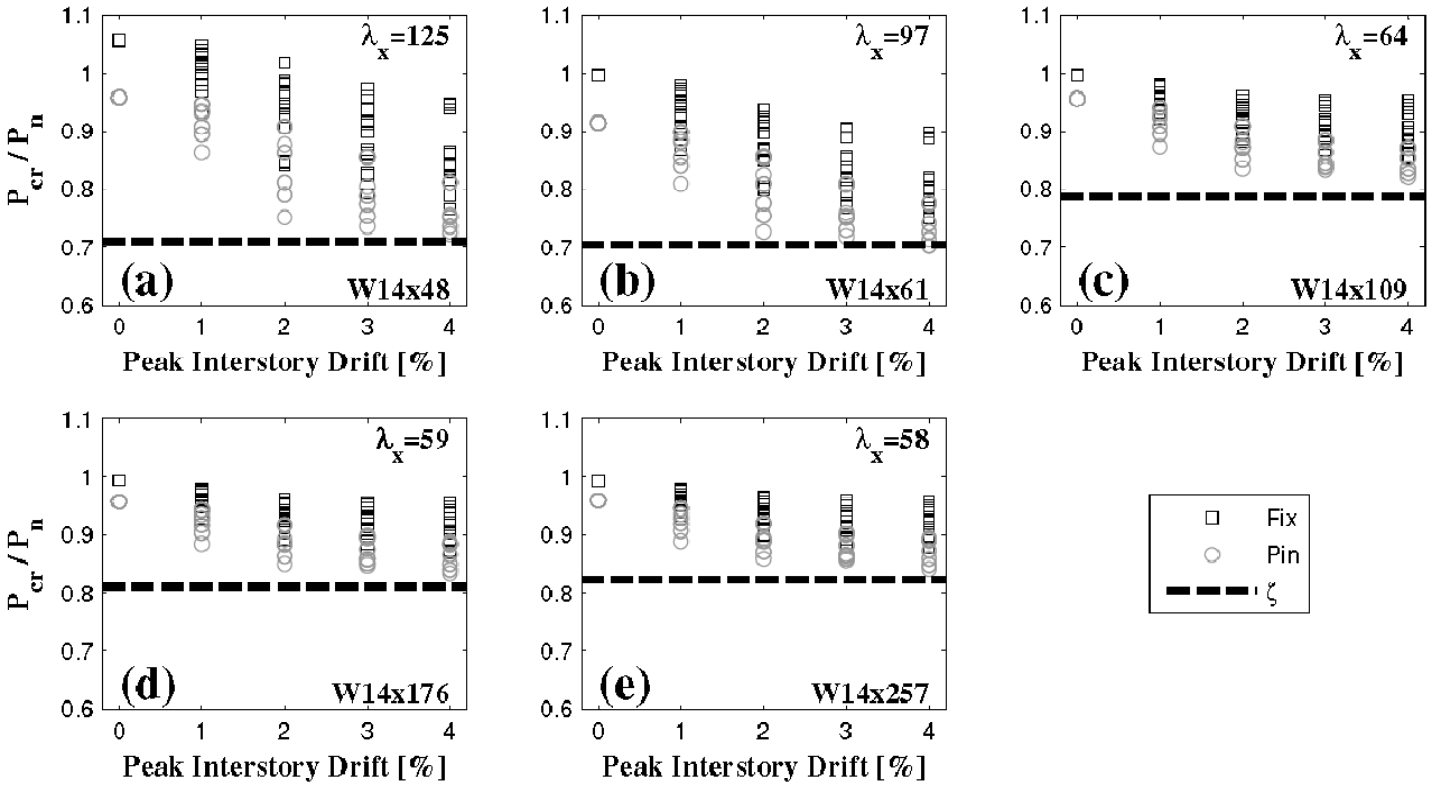

Figure 15. Normalized buckling strength vs. peak interstory drift for different ISD configurations and boundary conditions (story height of 6.10m): (a) W14x48, (b) W14x61, (c) W14x109, (d) W14x176, and (e) W14x257.

CONCLUSION

Compared to conventional SPSWs, the columns of B-SPSWs are designed primarily for axial loads due to the web plates being released from the columns and the simple beam-column connections used in the B-SPSW system. A recent study [16] revealed that unequal interstory drifts observed during a seismic event lead to column rotations at the floor level that are not captured by conventional seismic design methods, namely, the Equivalent Lateral Force method and the Modal Response Spectrum analysis. These rotations result in significant flexural demands in the strong axis of the column that reduce the buckling strength of the column and can cause column stability problems. A two-phase numerical study has been undertaken to investigate the effect of column flexural demands resulting from column rotations at floor levels due to the differential interstory drifts. Three-dimensional finite element models of isolated columns are built using brick elements, specifying initial imperfections, and introducing residual stresses to properly capture the column buckling behavior.

In the first phase, the columns of B-SPSWs design per two design approaches are analyzed under the loads and displacements obtained from nonlinear response-history analyses. The results suggest that the columns of B-SPSWs designed using the seismically-detailed design (i.e., the capacity design) perform better and do not buckle under twenty ground motions scaled to a seismic hazard level of 2% in 50 years. Column buckling is observed for 3-story B-SPSWs where the non-seismically-detailed design is adopted (i.e., the column loads are calculated as per the web plate stresses resulting from forces that are used to size the web plates).

In the second phase, a parametric study is undertaken to propose a simplified column design method that uses column axial load demands obtained from ELF and

accounts for the column buckling strength reduction due to the flexural demands resulting from column rotations at floor levels. Considering a wide range of W14 sections and possible interstory drift distributions along the building height, an empirical equation is proposed as a column buckling strength reduction factor that can be easily implemented in ELF design procedures. Further research is needed to verify the validity of the proposed equation for deeper wide flange sections with different story heights.

ACKNOWLEDGMENTS

This research was conducted at the University of Texas at Austin, and the first author was supported in part by the Fulbright Foreign Student Program. Any opinions, findings, conclusions, and recommendations presented in this paper are those of the authors and do not necessarily reflect the views of the sponsors.

REFERENCES

[1] V. Caccese, M. Elgaaly, R. Chen, Experimental study of thin steel plate shear walls under cyclic load, J. Struct. Eng. 119 (1993) 573–587. doi:10.1061/(ASCE)0733-9445(1993)119:2(573).

[2] M. Elgaaly, Thin steel plate shear walls behavior and analysis, Thin-Walled Struct. 32 (1998) 151–180. doi:10.1016/S0263-8231(98)00031-7.

[3] A.S. Lubell, H.G.L. Prion, C.E. Ventura, M. Rezai, Unstiffened steel plate shear wall performance under cyclic loading, J. Struct. Eng. 126 (2000) 453–460. doi:10.1061/(ASCE)0733-9445(2000)126:4(453).

[4] T.M. Roberts, S. Sabouri-Ghomi, Hysteretic characteristics of unstiffened perforated steel plate shear panels, Thin-Walled Struct. 14 (1992) 139–151. doi:10.1016/0263-8231(92)90047-Z.

[5] C.J. Thorburn, L.J. Kulak, G.L. Montgomery, Analysis of steel plate shear walls, Structural Engineering Report No. 107. University of Alberta. Edmonton, AB, 1983.

[6] K. Basler, Strength of plate girders in shear, Reprint No. 186 (61-13). Lehigh University Fritz Laboratory. Bethlehem, PA, 1961.

[7] M. Gholipour, M.M. Alinia, Behavior of multi-story code-designed steel plate shear wall structures regarding bay width, J. Constr. Steel Res. 122 (2016) 40–56. doi:10.1016/j.jcsr.2016.01.020.

[8] J.W. Berman, Seismic behavior of code designed steel plate shear walls, Eng. Struct. 33 (2011) 230–244. doi:10.1016/j.engstruct.2010.10.015.

[9] A. Jahanpour, H. Moharrami, A. Aghakoochak, Evaluation of ultimate capacity of semi-supported steel shear walls, J. Constr. Steel Res. 67 (2011) 1022–1030. doi:10.1016/j.jcsr.2011.01.007.

[10] M. Xue, Behavior of steel shear wall panels and frame-wall systems (Ph.D. Dissertation), Lehigh University, 1995.

[11] C. Vatansever, N. Yardimci, Experimental investigation of thin steel plate shear walls with different infill-to-boundary frame connections, Steel Compos. Struct. 11 (2011) 251–271. doi:10.12989/scs.2011.11.3.251.

[12] L. Guo, Q. Rong, X. Ma, S. Zhang, Behavior of steel plate shear wall connected to frame beams only, Int. J. Steel Struct. 11 (2011) 467–479. doi:10.1007/s13296-011-4006-7.

[13] I.-R. Choi, H.-G. Park, Steel plate shear walls with various infill plate designs, J. Struct. Eng. 135 (2009) 785–796. doi:10.1061/(ASCE)0733-9445(2009)135:7(785).

[14] P.M. Clayton, J.W. Berman, L.N. Lowes, Seismic performance of self-centering steel plate shear walls with beam-only-connected web plates, J. Constr. Steel Res. 106 (2015) 198–208. doi:10.1016/j.jcsr.2014.12.017.

[15] Y. Ozcelik, P.M. Clayton, Strip model for steel plate shear walls with beam-connected web plates, Eng. Struct. 136 (2017) 369–379. doi:10.1016/j.engstruct.2017.01.051.

[16] Y. Ozcelik, P.M. Clayton, Seismic design and performance of SPSWs with beam-connected web plates, J. Constr. Steel Res. (under review).

[17] State of art report on systems performance of steel moment frames subject to earthquake ground shaking, FEMA 355C, Federal Emergency Management Agency (FEMA), Washington D.C., 2000.

[18] S. Mazzoni, F. Mckenna, M.H. Scott, G.L. Fenves, OpenSees command language manual, (2006).

[19] ANSI/AISC 341-10 Seismic provisions for structural steel buildings, American Institute for Steel Construction (AISC), Chicago, IL, 2010.

[20] ANSI/AISC 360-10 Specification for structural steel buildings, American Institute for Steel Construction (AISC), Chicago, IL, 2010.

[21] ABAQUS, ABAQUS version 6.10 documentation, Simulia, 2010.

[22] C.D. Stoakes, L.A. Fahnestock, Strong-Axis Stability of Wide Flange Steel Columns in the Presence of Weak-Axis Flexure, J. Struct. Eng. 142 (2016) 1–13. doi:10.1061/(ASCE)ST.1943-541X.0001448.

[23] A.W. Huber, Residual stresses in wide flange beams and columns, Paper 1498. Lehigh University Fritz Laboratory. Bethlehem, PA, 1958.

[24] P. Somerville, N. Smith, S. Punyamurthula, J. Sun, Development of ground motion time histories for Phase 2 of the FEMA/SAC Steel Project, SAC Background Document, Report No. SAC/BD-97/04, 1997.

[25] J.D. Newell, C.-M. Uang, Cyclic behavior of steel wide-flange columns subjected to large drift, J. Struct. Eng. 134 (2008) 1334–1342. doi:10.1061/(ASCE)0733-9445(2008)134:8(1334).

Bibliography

ABAQUS. 2010. *ABAQUS Version 6.10 Documentation*. Simulia.

AISC. 2010a. *ANSI/AISC 341-10 Seismic Provisions for Structural Steel Buildings*. Chicago, IL: American Institute for Steel Construction (AISC).

AISC. 2010b. *ANSI/AISC 360-10 Specification for Structural Steel Buildings*. Chicago, IL: American Institute for Steel Construction (AISC).

Applied Technology Council (ATC). 1992. *Guidelines for Cyclic Seismic Testing of Components of Steel Structures*. Report No. 24. Applied Technology Council. Redwood City, CA.

ASCE. 2010. *Minimum Design Loads for Buildings and Other Structures, ASCE/SEI 7-10*. Reston, VA: American Society of Civil Engineers and Structural Engineering Institute (ASCE/SEI).

Astaneh-Asl, A. 2005a. "Notes on Design of Double-Angle and Tee Shear Connections for Gravity and Seismic Loads." *Steel Tips, Structural Steel Educational Council*.

Astaneh-Asl, A. 2005b. "Design of Shear Tab Connections for Gravity and Seismic Loads." *Steel Tips, Structural Steel Educational Council*.

Behbahanifard, MR, GY Grondin, and AE Elwi. 2004. "Analysis of Steel Plate Shear Wall Using Explicit Finite Element Method." *Proc., 13th World Conference of Earthquake Engineering, Vancover, B.C., Canada*.

Berman, J.W., and M. Bruneau. 2008. "Capacity Design of Vertical Boundary Elements in Steel Plate Shear Walls." *Engineering Journal, AISC* 45(1): 55–71.

Berman, Jeffrey W. 2011. "Seismic Behavior of Code Designed Steel Plate Shear Walls." *Engineering Structures* 33(1): 230–44.

Caccese, Vincent, Mohamed Elgaaly, and Ruobo Chen. 1993. "Experimental Study of Thin Steel Plate Shear Walls under Cyclic Load." *Journal of Structural Engineering* 119(2): 573–87.

CAN/CSA. 2009. *CAN/CSA-S16-09 Design of Steel Structures*. Mississauga, ON: Canadian Standards Association.

Chen, Sheng-Jin, and Chyuan Jhang. 2011. "Experimental Study of Low-Yield-Point Steel Plate Shear Wall under in-Plane Load." *Journal of Constructional Steel Research* 67(6): 977–85.

Clayton, Patricia M. 2013. "Self-Centering Steel Plate Shear Walls. Subassembly and Full-Scale Testing (Ph.D. Dissertation)." University of Washington.

Clayton, Patricia M., Jeffrey W. Berman, and Laura N. Lowes. 2013. "Subassembly Testing and Modeling of Self-Centering Steel Plate Shear Walls." *Engineering Structures* 56: 1848–57.

Clayton, Patricia M., Jeffrey W. Berman, and Laura N. Lowes. 2015. "Seismic Performance of Self-Centering Steel Plate Shear Walls with Beam-Only-Connected Web Plates." *Journal of Constructional Steel Research* 106: 198–208.

Clayton, Patricia M., Ching-Yi Tsai, Jeffrey W. Berman, and Laura N. Lowes. 2015. "Comparison of Web Plate Numerical Models for Self-Centering Steel Plate Shear Walls." *Earthquake Engineering & Structural Dynamics* 44(12): 2093–2110. http://doi.wiley.com/10.1002/eqe.2578 (June 18, 2016).

Driver, Robert G., Geoffrey L. Kulak, Alaa E. Elwi, and D. J. Laurie Kennedy. 1998. "FE and Simplified Models of Steel Plate Shear Wall." *Journal of Structural Engineering* 124(2): 121–30.

Driver, Robert G., Geoffrey L. Kulak, D. J. Laurie Kennedy, and Alaa E. Elwi. 1997. *Seismic Behavior of Steel Plate Shear Walls*. Structural Engineering Report No. 298. University of Alberta. Edmonton, AB.

FEMA. 2009. *Quantification of Building Seismic Performance Factors, FEMA P695*. Washington D.C.: Federal Emergency Management Agency (FEMA).

Gholipour, Masoumeh, and Mohamad Mehdi Alinia. 2016. "Behavior of Multi-Story Code-Designed Steel Plate Shear Wall Structures Regarding Bay Width." *Journal of Constructional Steel Research* 122: 40–56.

Guo, Lanhui, Ran Li, Sumei Zhang, and Guirong Yan. 2012. "Hysteretic Analysis of Steel Plate Shear Walls (SPSWs) and a Modified Strip Model for SPSWs." *Advances in Structural Engineering* 15(10): 1751–64.

Guo, Lanhui, Qin Rong, Xinbo Ma, and Sumei Zhang. 2011. "Behavior of Steel Plate Shear Wall Connected to Frame Beams Only." *International Journal of Steel Structures* 11(4): 467–79.

JGJ 101-96. 1996. *Specification of Testing Methods for Earthquake Resistant Building (in Chinese)*. Beijing, China: Ministry of Construction of the people's Republic of China.

Mazzoni, Silvia, Frank Mckenna, Michael H Scott, and Gregory L Fenves. 2006. "OpenSees Command Language Manual."

Moghimi, Hassan, and RG Driver. 2013. "Economical Steel Plate Shear Walls for Low-Seismic Regions." *Journal of Structural Engineering* 139(March): 379–88.

Purba, Ronny, and Michel Bruneau. 2015. "Seismic Performance of Steel Plate Shear Walls Considering Two Different Design Philosophies of Infill Plates. II: Assessment of Collapse Potential." *Journal of Structural Engineering* 141(6): 4014161.

Sabelli, Rafael, and Michel Bruneau. 2012. *Steel Design Guide: Steel Plate Shear Walls*. AISC.

Shishkin, Jonah J., Robert G. Driver, and Gilbert Y. Grondin. 2009. "Analysis of Steel Plate Shear Walls Using the Modified Strip Model." *Journal of Structural Engineering* 135(11): 1357–66. http://ascelibrary.org/doi/10.1061/%28ASCE%29ST.1943-541X.0000066.

Somerville, P., N. Smith, S. Punyamurthula, and J. Sun. 1997. *Development of Ground Motion Time Histories for Phase 2 of the FEMA/SAC Steel Project*. SAC Background Document, Report No. SAC/BD-97/04.

Thorburn, L.J. Kulak, G.L. Montgomery, C.J. 1983. *Analysis of Steel Plate Shear Walls*. Structural Engineering Report No. 107. University of Alberta. Edmonton, AB.

Vatansever, Cüneyt, and Jeffrey W Berman. 2015. "Analytical Investigation of Thin Steel Plate Shear Walls with Screwed Infill Plate." *Steel and Composite Structures* 5: 1145–65.

Vatansever, Cüneyt, and Nesrin Yardimci. 2011. "Experimental Investigation of Thin Steel Plate Shear Walls with Different Infill-to-Boundary Frame Connections." *Steel and Composite Structures* 11(3): 251–71.

Webster, David J. 2013. "The Inelastic Seismic Response of Steel Plate Shear Wall Web Plates and Their Interaction with the Vertical Boundary Members (Ph.D. Dissertation)." University of Washington.

Webster, David J., Jeffrey W. Berman, and Laura N. Lowes. 2014. "Experimental Investigation of SPSW Web Plate Stress Field Development and Vertical Boundary Element Demand." *Journal of Structural Engineering* 140(6): 4014011. http://ascelibrary.org/doi/10.1061/%28ASCE%29ST.1943-541X.0000989.

Xue, Ming. 1995. "Behavior of Steel Shear Wall Panels and Frame-Wall Systems (Ph.D. Dissertation)." Lehigh University.

Vita

Yigit Ozcelik was born in Istanbul, Turkey in 1986. He graduated from Middle East Technical University in Ankara, Turkey in 2010. After working for structural design firms, he entered the Graduate School of the University of Texas at Austin in 2013.

Email address: yigit (at) utexas (dot) edu
This dissertation was typed by Ahmet Yigit Ozcelik.